NOAA Technical Memorandum ERL AOML-91

COMPARISON OF THERMAL STATISTICS DERIVED FROM OBSERVATIONAL DATA SETS IN THE TROPICAL ATLANTIC AND PACIFIC OCEANS

J.F. Festa
R.L. Molinari

Atlantic Oceanographic and Meteorological Laboratory
Miami, Florida
August 1997

noaa NATIONAL OCEANIC AND ATMOSPHERIC ADMINISTRATION / Environmental Research Laboratories

NOAA Technical Memorandum ERL AOML-91

COMPARISON OF THERMAL STATISTICS DERIVED FROM OBSERVATIONAL DATA SETS IN THE TROPICAL ATLANTIC AND PACIFIC OCEANS

John F. Festa
Robert L. Molinari

Atlantic Oceanographic and Meteorological Laboratory
Miami, Florida
August 1997

UNITED STATES DEPARTMENT OF COMMERCE

William M. Daley
Secretary

NATIONAL OCEANIC AND ATMOSPHERIC ADMINISTRATION

D. JAMES BAKER
Under Secretary for Oceans and Atmosphere/Administrator

Environmental Research Laboratories

James L. Rasmussen
Director

NOTICE

Mention of a commercial company or product does not constitute an endorsement by the NOAA Environmental Research Laboratories. Use of information from this publication concerning proprietary products or the test of such products for publicity or advertising purposes is not authorized.

For sale by the National Technical Information Service, 5285 Port Royal Road
Springfield, VA 22061

CONTENTS

Page

Comparison of Thermal Statistics Derived from Observational Data Sets in the Tropical Atlantic and Pacific Oceans

John F. Festa
Robert L. Molinari

ABSTRACT. Statistical analysis of surface and subsurface temperature data in the tropical Atlantic and Pacific Oceans is presented. The statistics were estimated from the Comprehensive Ocean-Atmospheric Data Set (COADS) and the historical expendable bathythermograph (XBT) observations. Spatial structure functions (semivariograms) for the anomaly fields of sea surface temperature and the temperature at 200 m and 400 m were estimated for a 2 degree by 2 degree grid in the tropical oceans. Dominant scales of spatial variability are identified and compared with other investigations.

1. INTRODUCTION

Upper ocean temperature (UOT) data are an important component of many oceanographic studies directed at determining the role of the ocean in global climate. In the World Ocean Circulation Experiment (WOCE), "there is a need for measurements of the change in heat content in the upper ocean, primarily as a way to improve the reliability of estimates of the heat flux" (WMO, 1986). In the post-TOGA (Tropical Ocean Global Atmosphere) era, UOT data are "central to the successful initialization of coupled atmosphere-ocean models" directed at "supporting short-term climate predictions" (NRC, 1994). In the Atlantic Climate Change Program (ACCP), UOT data collection and analysis are supported to study the role of subsurface oceanic processes on decadal sea surface temperature (SST) variability (Molinari *et al.,* 1994). All three programs recognize the need for continued UOT observations and have as an important objective the establishment of long-lived networks that will constitute the Global Ocean Observing System (OOSDP, 1995). Sampling requirements, however, vary between the three programs, consistent with their somewhat different objectives. The majority of the data collected for these programs is from a volunteer observing ship (VOS) network, comprised of merchant ships that typically have fixed routes on which ship's crew members deploy expendable bathythermographs (XBTs) at specified intervals.

Sampling strategies for the VOS have primarily been based on a series of statistical studies in which the time and space scales of upper ocean thermal variability were estimated (Bretherton *et al.,* 1976; White and Bernstein, 1979; White *et al.,* 1982; Meyers *et al.,* 1991; Sprintall and Meyers, 1991; Festa and Molinari, 1992, for example). Based on some of these estimates, bimonthly profiles on a 1.5 degree of latitude by 7.5 degree of longitude grid represent the ideal TOGA network. WOCE and ACCP have modified this resolution somewhat, with four probes per day deployed on a monthly basis along VOS lines.

More recently, White (1995) reported on the results of an oceanographic global design study where covariance statistics were computed from temperature profiles at each 5 degree latitude by 10 degree longitude quadrangle in the ocean at depths of 0, 200, and 400 m. White's global analysis

shows significant non-uniformity in the resulting distributions, and he indicates that this "non-uniformity in the covariance statistics can cause inconsistencies in the analysis and interpretation of gridded fields and upper ocean temperature anomalies." White addressed this difficulty, following Sprintall and Meyers (1991), by basing the global design on a "uniform set of covariance statistics that defines the minimum space and time scales to be detected by the proposed global observing system at all depths." The minimum covariance scales selected by White were 2.5 degrees of latitude, 5 degrees of longitude, and three months.

Many of the statistical studies used to establish sampling requirements for both meteorological and oceanographic fields were based, in one form or another, on the optimum interpolation (OI) method described by Gandin (1963). One of the most important steps in this analysis is the accurate specification of the statistical characteristics of the field in question, which is often assumed to be homogeneous and isotropic. Typically, these assumptions are considered to be met if the longer term mean field is removed and the analysis is done on anomaly fields. However, problems can arise when knowledge of the long term mean is uncertain or unknown (Bretherton *et al.,* 1976) and often, even, the anomaly fields are neither isotropic or homogeneous.

The statistical characteristics for Gandin's method are usually given in the form of either a correlation or covariance function which serves as the basis for interpolation and error analysis. More recently, specification of the statistics has been in the form of structure functions, with the interpolation and error analysis techniques based on those used extensively in the geostatistical technique commonly called "kriging" (Matheron, 1963; Journel and Huijbregts, 1989; Cressie, 1990). Structure function analysis has been applied to both oceanographic and meteorological data (Hansen and Herman, 1988, 1989; Festa and Molinari, 1992; Gunst, 1995; Frankignoul *et al.,* 1996; Hansen and Poulain, 1996). Statistical and spatial data analysis based on the kriging method are now available in commercial statistical analysis packages.

One major problem in applying OI to any data set and, in particular, to the subsurface ocean observations is the absence of sufficient data. It becomes extremely difficult to determine the spatial structure required in network design and objective mapping analysis when there are too few data or data of mixed quality. Often this process becomes very subjective and sometimes underestimated in its importance. Nevertheless, this is the most important step in the application of objective analysis.

Even when sufficient data are available, the statistical forms used are sometimes assumed rather than supported by the data. For example, the most common functional form used in oceanographic objective analysis is the Gaussian function (White *et al.,* 1982; Meyers *et al.,* 1991; Clancy *et al.,* 1992; Reynolds and Smith, 1994). In many cases the data do not support this functional form and the spatial statistics are often better represented by an exponential function (see, for example, Festa and Molinari, 1992; White, 1995; Frankignoul *et al.,* 1996; Kessler *et al.,* 1996). As will be seen, the choice of the statistical representation of the data can also have a great effect on the results, especially in determining the estimated error of the mapped fields.

Four types of analyses are presented in this report. First, is the analysis of the SST statistics derived from the Comprehensive Ocean-Atmospheric Data Set (COADS; Woodruff *et al.,* 1987) and the XBT data sets. COADS provides global SST coverage that, when compared to XBT data, is

relatively dense in time and space. We believe that the surface statistics, using structure function analysis obtained from the COADS data, will provide a measure of the representativeness of the surface statistics derived from XBT data. Furthermore, confidence in the estimates of subsurface statistics determined from XBT data will be gained (eroded) if the surface statistics are similar (dissimilar).

Second, subsurface statistics obtained from the XBT data set are compared to those derived from the National Centers for Environmental Prediction (NCEP) numerical model simulations of the Atlantic and Pacific Oceans (Behringer, 1994; Ji *et al.,* 1995). These models assimilate XBT and other data to provide basinwide representations of the upper ocean thermal field. Although the model does assimilate the XBT data and the simulated and observed temperature fields are thus not independent, comparisons may provide a measure of the effect of assimilation procedures on the observed fields.

Third, data voids in the COADS SST fields have been recently filled (for example, Dasilva *et al.,* 1995, hereafter Dasilva; Smith *et al.,* 1996, hereafter Smith) using different statistical techniques. These reconstructed data sets are being used for numerical model initialization and global heat flux studies. By applying the spatial statistics that are derived directly from the COADS data sets, we have reconstructed 40 years of COADS data (1950-1989). The resulting climatology and anomaly fields for selected months and time periods are compared to those of Dasilva, Smith, and the NCEP models.

Fourth, the statistical analyses of the COADS and XBT SST anomaly fields are applied to the current and proposed WOCE tracklines to determine the error fields that would result depending on the number of lines occupied and the sampling frequencies along the tracklines. These analyses are focused on two regions that are extremely important in climate studies and predictions but, unfortunately, have been sparsely sampled: the tropical Atlantic and Pacific Oceans. The latitude limits for both basins are taken as 30°S and 30°N. The longitude limits for the Atlantic are 70°W and 15°E and for the Pacific are 150°E and 90°W. Examples of the data distribution in these regions for the decade of the 1980's are given in Figures 1 and 2. Analysis was also preformed in the eastern tropical Pacific (longitude limits of 180°W and 120°W; the Niño 34 region). We begin with a description of the data and the statistical analysis technique. Results are presented and a discussion of the implications of the analysis of these data sets to design studies completes this report.

2. DATA SOURCES

The two data sets used in this report are the highly sampled historical COADS SST global data and the XBT historical data collected in the Atlantic and Pacific Oceans. The COADS SST data are collected by merchant ships. We use the monthly summary data on a 2 degree latitude by 2 degree longitude grid for the time period of January 1950 through December 1989 (see Woodruff *et al.,* 1987 for details of the data and binning procedures). The summary SST data contains both mean and median values. We have chosen to present the 40-year (1950-1989) median values analysis, since the median is less likely to be affected by questionable data values. Analysis has also been preformed using mean values over shorter decadal time periods (*i.e.,* 1950-1959,...,1980-1989).

There is no significant difference in the results using either the mean or median values. Results are also similar between the 40 year and decadal time periods; in the Pacific Ocean this results from a uniform distribution of El Niño and La Niña events during the decadal time periods.

The historical XBT data have been compiled at the Atlantic Oceanographic and Meteorological Laboratory (AOML) for the Atlantic and Pacific Oceans. In the Atlantic, historical XBT data have been quality controlled (QC) for the period of June 1966 through December 1991 (Daneshzadeh *et al.*, 1994) and in the Pacific for the period of January 1979 through December 1993 (Donoso *et al.*, 1994). The XBT data are averaged by month and year on the COADS 2 degree by 2 degree data grid. Examples of the XBT and COADS data distribution on this grid for the months of January and July are given in Figures 1 and 2.

Data from the output of two NCEP data assimilation model runs are used for the time period January 1980 through December 1989. The Pacific data consists of monthly gridded temperature profiles taken from the sixth reanalysis model run (see Ji *et al.*, 1995 for details). The Pacific model grid covers the region between 122.25°E-71.25°W; 35.5°S-44.5°N. It is a non-uniform grid of approximately 1.5 degree of longitude by 1.0 degree of latitude. Monthly averages for each year are gridded onto the 2 degree by 2 degree COADS grid. Anomaly fields, based on the 10 year monthly averages of model data, are calculated from the reanalysis data set. Similar calculations are performed using the Atlantic model data set from the third reanalysis model run (see Behringer, 1994 for details) for the same time period, January 1980 through December 1989, and the region 97.5°W-19.5°E and 48.5°S-63.5°N .

3. METHOD OF ANALYSIS

Optimum interpolation (OI) schemes are commonly used to map the anomalies of temperature and other field variables onto a gridded network or to design an "optimal" sampling design network. These methods are also referred to as "objective analysis" or "objective mapping." An accurate representation of the statistics of the data to be mapped is a critical and essential requirement of OI schemes. These statistics are required to define the coefficients for an optimal linear predictor such that the mean square error between the unknown true value and the estimated value is minimized. Once this is determined, gridded values can be predicted and a measure of the reliability, in the form of an error map, can also be obtained.

For example, if a variable Z is to be predicted at some spatial location x_0 surrounded by N observations of the variable, then

$$\hat{Z}(x_0) = \sum_{i=1}^{N} W_i [Z(x_i) + \epsilon(x_i)], \tag{1}$$

where W are the weights determined to minimize the mean-square error

$$\left\langle [Z(x_0) - \hat{Z}(x_0)]^2 \right\rangle, \tag{2}$$

ϵ is the rms error associated with the observations, and the angle brackets denote ensemble averages. Since the true value of a variable is usually unknown, it is necessary to adopt a probabilistic approach to the problem, where the interpolated value $\hat{Z}(x_0)$ is assumed to be the outcome of a random process whose statistics are known.

Gandin (1963), a pioneer of objective analysis techniques, initially developed the statistics of the variable to be mapped in terms of the structure function S_{ij} defined as

$$S_{ij} = S(x_i, x_j) = \left\langle [Z(x_i) - Z(x_j)]^2 \right\rangle, \tag{3}$$

the mean-square difference between the values of Z at x_i and x_j. The value S_{ij} can be represented by $S(h)$ where h is the lag, a measure of the distance between variable pairs. Gandin showed that for a homogeneous and isotropic field there is a relationship between the structure function $S(h)$ and the autocorrelation function C_{ij} defined as

$$C_{ij} = C(x_i, x_j) = \left\langle Z(x_i)\, Z(x_j) \right\rangle = C(h), \tag{4}$$

such that

$$C(h) = \frac{1}{2}[S(\infty) - S(h)]. \tag{5}$$

The advantage of using the structure function is that the analysis can be done on either the field variable or the anomaly of the variable, if the mean and its error are well know. In addition, the structure function, typically referred to as the variogram in geostatistical applications, can always be estimated in contrast to the autocorrelation function, which under certain conditions cannot be estimated or is not well defined. Recently, Gunst (1995), in an analysis of U.S. temperature anomalies, recommends structure function fitting as the preferred method for estimating spatial correlations. Gunst states that the common occurrence of temporal trends and autocorrelations in meteorological data can induce substantial bias and an overestimation of spatial correlations when using correlation function fitting, and that the potential for temporal bias in the estimated spatial correlations from structure function model fits can be reduced, if not altogether eliminated.

Perhaps the most important step in this analysis is selecting the analytical form of the semivariogram to approximate the raw data. The semivariogram (γ) is equal to one half of the structure function and is used to determine the value of a variable as well as its error. Functional forms of several of the classical model semivariograms used in geostatistics (see Figure 3) are:

(a) Linear: $\gamma = C_0 + C_1 \times h$,

(b) Exponential: $\gamma = C_0 + C_1 \times (1\text{-exp}\ (-h/C_2))$,

(c) Gaussian: $\gamma = C_0 + C_1 \times (1\text{-exp}\ (-h/C_2)^2)$,

(d) Power: $\gamma = C_0 + C_1 \times (h^{C_2})$.

The value of the semivariogram at lag zero, C_0, is referred to as the nugget, which is a measure of both the instrument and subgrid geophysical noise. In the exponential and Gaussian functional forms, the asymptotic value of the semivariogram, $C_0 + C_1$ (which is not present in either the linear or power function models) is known as the sill and represents the variance of the field. The exponential model shows a linear behavior near the origin, while the Gaussian model shows a parabolic behavior. For both the exponential and Gaussian models, C_2 is a measure of the range over which correlation exists and is equivalent to the e-folding scale of the covariance function. The practical range, *i.e.,* the distance at which the correlation function effectively has reached zero, is given as $3 \times C_2$ for the exponential function and $\sqrt{3} \times C_2$ for the Gaussian function.

When the variability of the component semivariograms, for two-dimensional spatial variables, depends only on the magnitude of the lag h, the structural statistics are considered to be isotropic. However, when the variability depends on both magnitude and direction, a more common geophysical occurrence than the simple isotropic case, the statistics are said to be anisotropic. Anisotropies typically result from the underlying physical processes evolving differently in space. If the semivariograms can be reduced to isotropic functions by a simple linear transformation of coordinates, the anisotropy is referred to as geometric; otherwise, it is know as zonal.

Figure 4 shows examples of east-west and north-south isotropic and anisotropic semivariogram functions. The semivariograms in each direction are the same in the isotropic example. In the geometric anisotropic example, the sill, *i.e.,* total variance, is the same in each direction and the range in the north-south direction is half of that in the east-west direction. In the zonal anisotropic example, the variance in the north-south direction is 50% higher than in the east-west direction.

In most oceanographic design or objective mapping studies to date, isotropic or geometric anisotropic behavior has been assumed (Meyers *et al.,* 1991; Reynolds and Smith, 1994; Dasilva *et al.,* 1995; White, 1995, for example); however, as will be seen, the statistical structure of the COADS and XBT data, especially for the tropical Pacific, indicate zonal anisotropy. The effect of geometric and zonal anisotropy on the field variable and its error will be discussed in the next section.

A detailed review of the use of structure functions, as applied in geostatistics, is given by David (1977), Journel and Huijbregts (1978), Isaaks and Srivastava (1989), and Cressie (1991). A detailed look at the similarities and differences between Gandin's OI technique and geostatistical kriging techniques is given by Cressie (1990) and Herzfeld (1996).

4. DISCUSSION

In this report, we compute and compare semivariograms estimated from the surface COADS and XBT anomaly data on the 2 degree by 2 degree COADS grid in the tropical Atlantic and Pacific Oceans. The semivariograms, based on monthly anomaly fields, are examined in both the east-west and north-south directions. We also have identified the dominant scales of spatial variability in each direction and compare these values with those of other investigations. As will be shown, there is a major difference in the determination of spatial scales when the statistical representations are found to be either geometrically anisotropic or zonally anisotropic in their functional form.

Monthly anomaly maps of the COADS data are obtained by using the statistical interpolation method know as ordinary kriging (see Festa and Molinari, 1992 for details). Anomaly fields are compared to the reconstructed data sets of Smith and Dasilva for the months of January and July, during the decade of the 1980's, using different functional representations for the semivariograms. Finally, error maps are generated for the proposed WOCE tracklines in the tropical Atlantic and Pacific Oceans.

A. SST Anomaly Semivariograms

For the COADS data, during the period of January 1950 through December 1989, long term monthly means are calculated at each 2 degree by 2 degree grid node where there are at least five years of data. Monthly anomaly fields are obtained by subtracting the long term monthly mean climatology from the yearly values at each grid node. The same procedure is used to calculate the long term monthly mean climatology and anomaly fields for the XBT, which are gridded onto the 2 degree by 2 degree COADS data grid.

It should be noted that the COADS grid has been chosen as the base grid for binning data, since COADS data sets are widely used for numerous oceanographic and meteorological analyses. Use of this grid should preserve shorter scales, relative to other binning approaches which may bias the statistical results. For example, data have been averaged onto a coarse rectangular grid, *i.e.,* a 10 degree (or 5 degree) longitude by 2 degree (or 1 degree) latitude grid or anomaly fields have been calculated on a fine grid (2 degree longitude by 2 degree latitude grid) using a climatology defined for a coarser grid (5 degree longitude by 2 degree latitude) and then statistical inferences are made about the data to determine the spatial scales. We feel that these types of pre-conditioning of the raw data imply, *a priori*, the dominant spatial scale and direction, can result in a bias in the spatial scales to be determined, and should be avoided.

Mean squared difference values (*i.e.,* structure functions or semivariograms) in the north-south and east-west direction were computed for each 2 degree lag bin for each month and each year with data. Because of data limitations, values beyond 20 degrees of lag are suspect and not used in the analysis. Monthly composites were formed by taking the average value at any bin over the entire time period of record. Seasonal and annual composites were calculated in a similar manner. The four seasons were chosen as December-February (DJF), March-May (MAM), June-August (JJA), and September-November (SON).

The SST seasonal and annual composite semivariogram values for the COADS and XBT data sets for the tropical Atlantic are shown in Figure 5 and for the tropical Pacific in Figure 6a (the Niño 34 subset region with longitude limits of 180°W and 120°W is shown in Figure 6b). There is little seasonal variability for the COADS semivariograms in either tropical ocean except at the higher lags. More variability, especially in the Atlantic, is evident for the XBT semivariograms at all lags, which is the result of the lack of sufficient data during any seasonal time period. Little difference is observed between the semivariograms for the two Pacific regions.

As is typically done in most objective analysis applications, functional forms are fit to the binned values and used to determine decorrelation scales, map anomalies, and estimate errors.

However, it should be noted that geostatisticans (see Journel and Huijbregts, 1978 for example) strongly caution against the blind automatic fitting of parameters to semivariograms, such as least squares methods, since the values within any bin can often be subject to wide fluctuations and errors. As an example, the composite and individual yearly binned values of the east-west and north-south semivariograms, for the tropical Pacific XBT (SST) data from 1980-1989, are shown for the months of January and July (Figure 7). Note the wide variations about the composite value for each lag value. It is exactly this type of variability that, unfortunately, makes this reportedly objective analysis so subjective. Objective analyses routines are often applied to data without considering the variability of the lag values and the confidence of the functional forms and fits chosen, which can affect the uncertainty of the results.

For our analysis, we have chosen to use the annual composite semivariograms as a basis for determining the statistical structure of the data. It is our opinion that the COADS and XBT semivariograms exhibit exponential behavior. However, while this is consistent with some investigations, it is also inconsistent with others. Therefore, we have identified three types of functions (linear, exponential, and Gaussian) that can be fit (cautiously and subjectively) to the annual composites of the COADS and XBT SST anomaly semivariogram bin values.

We avoid the temptation of using automated programs to determine the fitting parameters. Instead, we interactively examine each of the semivariograms in each direction and after varying, as an example, the number of points to use in a fit and the value of the nugget based on extrapolation to zero lag of both the east-west and north-south semivariograms, obtain coefficients that are representative of the binned data. Spatial scales of these fits are determined; however, caution is given, in general, to the values of spatial scales since results can differ, sometimes by a factor of two, depending on, for example, just the number of points that are used in the fitting process.

Table 1 lists the fitting parameters that were obtained for the analytical SST semivariograms for the tropical Atlantic and Pacific Oceans for the three different functional forms. The statistical structure of the annual composite for the Atlantic is shown in Figure 8 and for the Pacific in Figure 9. The geophysical noise, *i.e.,* nugget, is given by C_0. For the linear functional fits, C_{1e} and C_{1n} represent the slope in the east-west (+) and north-south (o) directions, respectively. The ratio of these slopes gives some indication as to the degree of anisotropy; larger ratios indicate greater anisotrophy. For the exponential and Gaussian functional fits, the sum of C_{1e} (C_{1n}) to the nugget, C_0, represents a measure of the total variance in the east-west (north-south) direction. The statistics are considered geometrically anisotropic when the variances are the same in each direction and zonally anisotropic when they differ. The values C_{2e} and C_{2n} represent the e-folding scale lengths (*i.e.,* the decorrelation scales) in each direction and similarly, R_e and R_n represent the rms errors of the functional fits.

Comparing the XBT and COADS results provides a measure of the robustness of the results from the former. The nugget, as determined by the XBT data set, is nearly half of that obtained from COADS in both tropical ocean basins. Spatial scales in the Atlantic, as determined by the COADS data, are nearly twice as large as those of the XBT data, while those in the Pacific are approximately the same. In the Atlantic, the average e-folding scales, taking into consideration all of the exponential and Gaussian fits, are 8.7 degrees in longitude and 5.5 degrees in latitude for the COADS anomalies and 3.7 degrees in both longitude and latitude for the XBT data. In the Pacific

Table 1: Semivariogram functional fits.

	C_0	C_{1e}	C_{1n}	C_{2e}	C_{2n}	R_e	R_n
			Atlantic				
COADS:							
Linear	.28	.010	.016	---	---	.017	.052
Exponential (Z)	.22	.24	.28	7.8	5.7	.005	.006
Exponential (G)	.22	.26	.26	9.4	4.9	.007	.010
Gaussian (Z)	.27	.16	.21	8.1	6.3	.012	.009
Gaussian (G)	.27	.18	.18	9.4	5.2	.014	.022
XBT:							
Linear	.18	.009	.013	---	---	.059	.077
Exponential (Z)	.12	.15	.21	2.4	3.7	.019	.028
Exponential (G)	.12	.18	.18	4.3	2.7	.033	.024
Gaussian (Z)	.16	.11	.16	3.2	4.4	.019	.024
Gaussian (G)	.16	.14	.14	4.9	3.8	.036	.021
			Pacific				
COADS:							
Linear	.39	.014	.027	---	---	.025	.061
Exponential (Z)	.30	.37	.56	8.0	6.3	.010	.014
Exponential (G)	.30	.47	.47	12.9	4.1	.020	.042
Gaussian (Z)	.39	.24	.42	8.6	6.6	.020	.034
Gaussian (G)	.39	.33	.33	13.2	4.6	.034	.069
XBT:							
Linear	.22	.007	.015	---	---	.017	.022
Exponential (Z)	.18	.15	.35	5.3	10.3	.004	.007
Exponential (G)	.18	.25	.25	15.8	5.0	.020	.030
Gaussian (Z)	.22	.10	.24	6.1	8.0	.008	.017
Gaussian (G)	.22	.17	.17	14.3	5.2	.025	.048

Note: Z = zonal anisotropic
G = geometric anisotropic

Units are in $(°C)^2$ for C_0, C_{1e}, C_{1n}, R_e, and R_n and degrees of longitude/latitude for C_{2e} and C_{2n}.

the average longitude and latitude e-folding scales are 10.7 degrees and 5.4 degrees for COADS and 10.4 degrees and 7.1 degrees for XBT data. The more accurate XBT measurements (*i.e.,* compared to SST observations from VOS), lower geophysical noise, and larger variations in semivariogram bin values, as a result of the sparsity of XBT data, are likely to have contributed to these results.

Input to design strategies and the results of OI mapping are strongly dependent on the choices of analytical functions used to fit the raw semivariograms. For example, spatial resolution is often given in terms of the scales derived from the fitting (*e.g.,* two or three observations are needed per decorrelation scale). However, the results given in Table 1 demonstrate that these scales are critically dependent on the subjective choice of the analytical fitting function.

In the Pacific, for both the Gaussian and exponential fits, the zonal and geometric scales are dramatically different (Table 1). The effect on sampling requirements can be demonstrated by considering a criteria that three observations per decorrelation scale are needed to resolve variability along a 60 degree long east-west VOS line. For a zonal exponential fit from the COADS data, 23 XBTs would be required to resolve the 8 degree spatial scales given in Table 1 and for a geometrical exponential fit, only 14 XBTs would be needed. Over a one-year period of monthly sampling a difference of over 100 probes would result.

Differences in the spatial scales in each direction and the rms errors are smallest for the zonal anisotropic fits. In general, the exponential functions have smaller rms errors than the Gaussian functions. The average e-folding scales obtained by using the geometric anisotropic functions are quite different in each direction and agree more with those found by other investigators (Table 2). In the Atlantic these spatial scales are 9.4 (4.6) degrees in longitude and 5.0 (3.3) degrees in latitude and in the Pacific 13.1 (15.0) degrees in longitude and 4.3 (5.1) degrees in latitude for the COADS (XBT) data.

White (1995), for example, indicates SST longitude and latitude decay scales of 7 degrees and 3 degrees for the tropical Atlantic and 9 degrees and 4.5 degrees for the tropical Pacific. We calculated these scales by averaging the zero-crossing scales reported by White over the tropical latitude bands and taking into account that the e-folding scales, according to White, are approximately equal to one half of the reported zero-crossing scales. In the tropical Pacific, Meyers *et al.* (1991) report longitude and latitude scales of approximately 30 degrees and 6 degrees for SST anomaly fields (excluding El Niño data). Including El Niño data will result in longer scales (Meyers *et al.* have shown a doubling of the scales); however, so will the inclusion of La Niña data. If El Niño and La Niña data were to be both removed from these calculations, there would be very little, if any, data left. It is for this reason that we have not chosen to do separate analysis based on the presence of an El Niño.

The scales reported by White are based on geometric anisotropic correlation functions using exponential fits and those by Meyers *et al.* (1991) using Gaussian fits. Although the spatial scales that we obtain using geometric anisotropic functions are closer to those of other investigators, we feel that geometric anisotropic functional forms, especially in the Pacific, are not supported by either the COADS or XBT data. In addition, if we use the results of the NCEP model and the reconstructed fields of Smith and Dasilva as data sets, and calculate the semivariograms of their

Table 2: Spatial scale lengths (in degrees).

	Atlantic		Pacific	
	Longitude	Latitude	Longitude	Latitude
COADS (1)	8.7	5.5	10.7	5.4
COADS (2)	8.0	6.0	8.3	6.5
COADS (3)	9.4	5.0	13.1	4.3
XBT (1)	3.7	3.7	10.4	7.1
XBT (2)	2.8	4.0	5.7	9.1
XBT (3)	4.6	3.3	15.0	5.1
White (1995) (a)	7.0	3.0	9.0	4.5
Meyers *et al.* (1991) (b)	---	---	30.0	6.0
Festa and Molinari (1992)	4.7	4.7	---	---

(1) Average of zonal and geometric anisotropic cases.
(2) Average of zonal anisotropic cases.
(3) Average of geometric anisotropic cases.
(a) Including El Niño data.
(b) Excluding El Niño data.

anomaly fields, all three semivariograms support the zonal anisotropic nature of the COADS and XBT data in the tropical Pacific basin.

To repeat, the spatial scales that we find for SST (Table 1) differ significantly for the zonal and geometric anisotropic functions. While knowledge of the spatial scales is important for some design studies, as described above, geostatistical studies only use spatial scales as a guide to determining how far out to reach for data (*i.e.,* the practical range) when computing the values and errors of a variable. In some cases the semivariogram (*i.e.,* the linear model) has no spatial scale.

B. Subsurface Anomaly Semivariograms

The seasonal and annual composite tropical Atlantic and Pacific semivariogram binned values for XBT data at depths of 200 m and 400 m are shown in Figures 10 and 11. Binned values are suspect, especially in the tropical Atlantic, because of the sparsity of the data. This lack of data will effect both the calculation of the climatology and, subsequently, the anomaly fields.

Exponential zonal anisotropic fits to the annual composite semivariograms for the surface and subsurface are shown in Figure 12. In general, the spatial scales observed at 200 m and 400 m are smaller than those at the surface. This is in agreement with the results of White (1995) and Festa and Molinari (1992).

If we view the NCEP model output as a data set, comparisons can be made between XBT and NCEP model annual composite semivariograms at various depths (Figures 13 and 14). The NCEP semivariogram binned values are somewhat similar in shape to the XBT values for the tropical Pacific. However, the same can not be said of the tropical Atlantic, especially at 200 m, where the seasonal composite XBT semivariogram for June-August (Figure 10, JJA) looks more like the NCEP annual composite. The NCEP results support the type of anisotropic behavior seen for the XBT semivariograms in each ocean basin. It should be noted that the lower values of both the nugget and total variance observed for NCEP is indicative of the smoothing that occurs in the model calculations.

C. SST Anomaly Errors

In this section we compare anomaly fields that have been constructed based on the statistical analysis of the COADS and XBT data to fields obtained from Dasilva, Smith, and the NCEP numerical models. The anomaly fields are based upon the corresponding COADS, Dasilva, and Smith climatologies, calculated over a 40-year time period (1950-1989), and the NCEP model climatology, over a 10-year time period (1980-1989). Maps of the climatologies are shown in Figures 15 and 16 for the Atlantic and Pacific Oceans, respectively. Climatology fields appear quite similar.

SST anomaly fields and associated error maps have been computed for the COADS data based upon the various semivariograms reported in the previous section. Gandin (1963) indicated that, in general, the mapping of fields should not be overly sensitive to the choice of the covariance

functions (*i.e.,* spatial statistics) when there is moderately good data coverage. However, despite the warning of Bretherton *et al.* (1976) that this is not appropriate when data coverage is sparse, it is our belief that Gandin's general concept is typically applied independent of the data coverage and minimal effort is spent determining the statistical representation of the data. We feel this is likely to occur, for instance, when contour fields are reported to be "objectively mapped" and there is no evidence of a study showing the underlying statistical representation of the fields to be mapped.

Herein, we have examined the effect of using either the exponential zonal (EZ) or Gaussian geometric (GG) anisotropic semivariograms to compute the anomaly fields and associated error maps in the tropical Atlantic and Pacific. These specific semivariograms have been chosen because they represent the most contrasting anomaly statistics that we have found. Following the procedures described in Festa and Molinari (1992), values of the COADS anomaly field have been computed on the 2 degree COADS grid when there are at least six data points within a 15 degree search radius.

We show, as one example, COADS anomaly fields for January and July of 1983 (Figure 17) generated by using the fitting parameters listed in Table 1 as determined by the analysis of the COADS (EZC, GGC) and XBT (EZX, GGX) data sets. It is evident that there are differences in both the anomaly and error fields for the exponential and Gaussian fits. In general, the traditional Gaussian fit produces smoother anomaly fields and smaller error fields. Shorter scale features are preserved using the exponential fit. The effect of smaller geophysical noise (*i.e.,* a lower nugget) is to produce lower errors and even shorter scale features. This can be seen by examining the difference between using the COADS and XBT exponential zonal fits (EZC and EZX).

The error fields are also different by between .1 °C and .2 °C, especially in the areas of sparse data (refer to Figures 1 and 2). These results point out the importance of the choice of the statistical representation of the fields to be mapped, especially when the focus of design studies is the error fields and where the sample spacing is based on the size of the expected errors. These differences can become significant and once again reflect the highly subjective nature of this otherwise reported objective process. Similar results were obtained when applying the different statistical functions to the entire data set.

COADS anomaly fields have been computed for January and July for the time period of 1980-1989 using the exponential zonal anisotropic semivariograms. These fields are compared to the results of Dasilva, Smith, and the NCEP model. Shown in Figure 18 are comparisons for January and July of 1983 and 1987. The 1980-1989 COADS, Dasilva, Smith, and NCEP anomaly fields are shown in Figures 19-22. Differences between these various anomaly fields are clearly evident. There can be no comparison between the error fields, since no error analysis was done by Dasilva, Smith, and NCEP. The COADS error fields (Figure 23) show the largest error in areas where there are data voids; the area where some of the largest differences between the various anomaly fields have been observed.

Both the NCEP and Smith analysis have all but eliminated the small scale spatial structure as compared to the Dasilva and the COADS analysis. Dasilva's fields show even smaller scale variability than COADS. The most significant differences that exist are in the equatorial Pacific, where there is very little data. The Smith and NCEP anomaly maps indicate a much larger zonal correlation than either Dasilva or the COADS maps. The COADS and Dasilva fields are more

similar in the Atlantic, where the spatial statistics indicate a lower degree of zonal anisotropy than in the Pacific.

These results are not surprising since Smith's analysis removes the short scale processes, and the NCEP model in the Pacific is initialized by Smith's data. Smith, for example, used 30 EOF functions, based on the OI analysis of satellite data, Reynolds and Smith (1994), to determine the spatial structure of the global oceans. Their OI analysis was based on Gaussian correlation functions with geometric anisotropic scales of approximately 800 km in the east-west and 600 km in the north-south directions. If more EOF functions had been used, it is likely that the shorter scales, indicative of the original COADS data, would have been preserved.

Dasilva's analysis, while preserving the shorter scales, is not based on an OI method. Dasilva uses a Cressman method similar to Levitus (1982) to reconstruct the COADS data and does not account for differences in the east-west and north-south spatial statistics. There also may be problems with some of the mean values, as is evident by some of the bull's eyes in the anomaly maps and, therefore, Dasilva's analysis may, in fact, be creating additional short spatial scale variability.

D. Anomaly Error Analysis Along WOCE Tracklines

Shown for illustrative purposes (Figure 24) are the proposed WOCE tracklines that cross the tropical Atlantic and Pacific regions chosen for this study. It should be noted that some of the tracklines are currently being sampled on a regular basis; however, many are either being sampled on a less frequent basis or not at all.

Error maps were obtained by applying the spatial statistics for the anomaly field to hypothetical sampling strategies along the WOCE tracklines. Festa and Molinari (1992) have, for example, shown that there is very little change in error maps when sampling along tracklines at a rate of either 1 probe per 120 nmi or 1 probe per 60 nmi. However, they show that there is a significant increase in the error fields when the sampling rate is decreased to 1 probe per 240 nmi. Error analysis calculations for the tropical Atlantic and Pacific confirm this; therefore, we only show results for the sampling rate of 1 probe per 120 nmi. Since most VOS ships steam at speeds between 15 and 20 knots, this implies a drop rate of 3-4 probes per day.

Figures 25 and 26 show the error maps in the tropical Atlantic and Pacific using both the exponential zonal (EZ) and Gaussian geometric (GG) SST semivariogram models based on XBT and COADS analysis (see Table 1). In addition, the Gaussian geometric semivariograms are modified slightly by changing the spatial scales C_{2e} and C_{2n} to reflect those reported by White (1995) (GGW) and Festa and Molinari (1992) (GGFM) for the Atlantic and White (1995) (GGW) and Meyers *et al.* (1991) (GGM) for the Pacific (see Table 2).

Little differences are observed between the error maps obtained using the various semivariogram models for the Atlantic. This is not surprising since the analysis has shown that the anomaly statistics are generally geometrically anisotropic and the spatial scales are short. However, this is not the case for the Pacific where the scales are larger and more zonally anisotropic. In

general, the errors are larger for the COADS semivariogram models than the XBT models. The COADS semivariograms have the largest nugget and variances. There are also significant differences between the results based on the exponential and Gaussian models, where the Gaussian semivariograms indicate smaller errors, on the order of between .1 °C and .2 °C. Increasing the spatial scales to reflect the large values reported by White (1995) and Meyers *et al.* (1991) shows a marked decrease in the error fields. Thus, the choice of the functional form and the spatial scales have a profound effect on the error fields in the Pacific.

5. REFERENCES

Behringer, D.W., 1994: Sea surface height variations in the Atlantic Ocean: A comparison of TOPEX altimeter data with results from an ocean data assimilation system. *Journal of Geophysical Research,* **99**, 24,685-24,690.

Bretherton, F.P., R.E. Davis, and C.B. Fandry, 1976: A technique for objective analysis and design of oceanographic experiments applied to MODE-73. *Deep-Sea Research,* **23**, 559-582.

Clancy, R.M., J.M. Harding, K.D. Pollak, and P. May, 1992: Quantification of improvements in an operational global-scale ocean thermal analysis system. *Journal of Oceanic Technology,* **9**, 55-66.

Cressie, N., 1990: The origins of kriging. *Mathematical Geology,* **22**, 239-252.

Cressie, N., 1991: *Statistics for Spatial Data.* John Wiley and Sons, Inc., New York.

David, M., 1977: *Geostatistical Ore Reserve Estimation.* Elsevier Scientific Publishing Company, 364 pp.

Daneshzadeh, Y.-H., J.F. Festa, and S.M. Minton, 1994: Procedures used at NOAA-AOML to quality control real time XBT data collected in the Atlantic Ocean. NOAA Technical Memorandum, ERL AOML-78, 44 pp.

Dasilva, A.M., C.C. Young, and S. Levitus, 1995: Atlas of surface marine data. 1994 NOAA Atlas, NESDIS.

Donoso, M.C., J.E. Harris, and D.B. Enfield, 1994: Upper ocean thermal structure of the eastern tropical Pacific. NOAA Technical Report, ERL 450-AOML 36, 221 pp.

Festa, J.F., and R.L. Molinari, 1992: An evaluation of the WOCE volunteer observing ship XBT network in the Atlantic Ocean. *Journal of Atmospheric and Oceanic Technology,* **9**, 305-317.

Frankignoul, C., F. Bonjean, and G. Reverdin, 1996: Interannual variability of surface currents in the tropical Pacific during 1987-1993. *Journal of Geophysical Research,* **101**, 3629-3647.

Gandin, L.S., 1963: *Objective Analysis of Meteorological Fields.* Gidrometeorizdat, 266 pp. (reprinted in 1965 by the Israel Program for Scientific Translations, Jerusalem, 238 pp.)

Gunst, R.F., 1995: Estimating spatial correlations from spatial-temporal meteorological data. *Journal of Climate,* **8**, 2454-2470.

Hansen, D.V., and A. Herman, 1988: A seasonal isotherm depth climatology for the eastern tropical Pacific. NOAA Technical Report, ERL 434-AOML 33 (Revised), 35 pp.

Hansen, D.V., and A. Herman, 1989: Evolution of isotherm depth anomalies in the eastern tropical Pacific Ocean during the El Niño event of 1982-1983. *Journal of Geophysical Research,* **94,** 14,461-14,473.

Hansen, D.V., and P.-M. Poulain, 1996: Quality control and interpolations of WOCE-TOGA drifter data. *Journal of Atmospheric and Oceanic Technology,* **13,** 900-909.

Herzfeld, U.C., 1996: Inverse theory in the earth sciences: An introductory overview with emphasis on Gandin's method of optimum interpolation. *Mathematical Geology,* **28,** 137-160.

Isaaks, E.H., and R.M. Srivastava, 1989: *Applied Geostatistics.* Oxford University Press, 561 pp.

Ji, M., A. Leetmaa, and J. Derber, 1995: An ocean analysis system for seasonal to interannual climate studies. *Monthly Weather Review,* **123,** 460-481.

Journel, A.G., and C.J. Huijbregts, 1978: *Mining Geostatistics.* Academic Press, 600 pp.

Kessler, W.S., M.C. Spillane, M.J. McPhadden, and D.E. Harrison, 1996: Scales of variability in the equatorial Pacific inferred from the tropical ocean buoy array. *Journal of Climate,* **9,** 2999-3024.

Levitus, S., 1982: Climatology atlas of the world ocean. NOAA Professional Paper 13, U.S. Government Printing Office, Washington, D.C., 173 pp.

Matheron, G., 1963: Principles of geostatistics. *Economical Geology,* **58,** 1246-1266.

Meyers, G., H. Phillips, N. Smith, and J. Sprintall, 1991: Space and time scales for optimal interpolation of temperature: tropical Pacific Ocean. *Progress in Oceanography,* **28,** 198-218.

Molinari, R.L., D. Battisti, K. Bryan, and J. Walsh, 1994: The Atlantic Climate Change Program. *Bulletin of the American Meteorological Society,* **75,** 1191-1199.

NRC, 1994: *Ocean-Atmosphere Observations Supporting Short-Term Climate Predictions: Panel on Near-Term Development of Operational Ocean Observations.* National Academy Press, Washington, D.C., 31 pp.

OOSDP, 1995: Scientific design of the common module of the global ocean observing system and the global climate observing system: An ocean observing system for climate. Final Report, Ocean Observing System Development Panel, Department of Oceanography, Texas A&M University, College Station, Texas, 265 pp.

Reynolds, R.W., and T.M. Smith, 1994: Improved global sea surface temperature analysis using optimum interpolation. *Journal of Climate,* **7,** 929-948.

Smith, T.M., R.W. Reynolds, R.E. Livezey, and D.C. Stokes, 1996: Reconstruction of historical sea surface temperatures using empirical orthogonal functions. *Journal of Climate,* **9,** 1403-1420.

Sprintall, J., and G. Meyers, 1991: An optimal XBT sampling network for the eastern Pacific Ocean. *Journal of Geophysical Research,* **96**, 10,539-10,552.

White, W.B., 1995: Design of a global observing system for gyre-scale upper ocean temperature variability. *Progress in Oceanography,* **36**, 169-217.

White, W.B., and R.L. Bernstein, 1979: Design of an oceanographic network in the mid-latitude North Pacific. *Journal of Physical Oceanography,* **9**, 592-606.

White, W.B., G. Meyers, and K. Hasunma, 1982: Space/time scale statistics of short-term climate variability in the western North Pacific. *Journal of Geophysical Research,* **87**, 1979-1989.

Woodruff, S.D., R.J. Slutz, R.L. Jenne, and P.M. Steuer, 1987: A comprehensive ocean atmosphere data set (COADS). *Bulletin of the American Meteorological Society,* **68**, 1239-1250.

WMO, 1986: World Ocean Circulation Experiment, Implementation plan: Detailed requirements (volume 1). WMO/TD-No. 242, World Meteorological Organization, Geneva.

6. LIST OF FIGURES

Figure 11. Exponential zonal anisotropic semivariogram model fits to the annual composite 200 m and 400 m XBT anomaly data in the tropical Pacific.

Figure 12. Exponential zonal anisotropic semivariogram model fits to the annual composite SST, 200 m and 400 m XBT anomaly data in the tropical Atlantic and Pacific.

Figure 13. Annual composite semivariogram values for the NCEP and XBT anomaly SST, 200 m and 400 m data in the tropical Atlantic.

Figure 14. Annual composite semivariogram values for the NCEP and XBT anomaly SST, 200 m and 400 m data in the tropical Pacific.

Figure 15. January and July SST climatology based on COADS (1950-1989), Dasilva (1950-1989), Smith (1950-1989), and NCEP (1980-1989) data in the tropical Atlantic.

Figure 16. January and July SST climatology based on COADS (1950-1989), Dasilva (1950-1989), Smith (1950-1989), and NCEP (1980-1989) data in the tropical Pacific.

Figure 17a. January 1983 COADS anomaly and error maps for the tropical Atlantic based on the exponential zonal COADS (EZC) and XBT (EZX) semivariogram models and the Gaussian geometric COADS (GGC) and XBT (GGX) models in the tropical Atlantic.

Figure 17b. Same as 17a for July.

Figure 17c. Same as 17a in the tropical Pacific.

Figure 17d. Same as 17b in the tropical Pacific.

Figure 18a. COADS, Dasilva, Smith, and NCEP anomaly fields in the tropical Atlantic for January and July of 1983.

Figure 18b. Same as 18a for 1987.

Figure 18c. Same as 18a in the tropical Pacific.

Figure 18d. Same as 18b in the tropical Pacific.

Figure 19a. January tropical Atlantic anomaly maps for the COADS data during the time period 1980-1989.

Figure 19b. Same as 19a for the Dasilva data.

Figure 19c. Same as 19a for the Smith data.

Figure 19d. Same as 19a for the NCEP data.

Figure 20a. July tropical Atlantic anomaly maps for the COADS data during the time period 1980-1989.

Figure 20b. Same as 20a for the Dasilva data.

Figure 20c. Same as 20a for the Smith data.

Figure 20d. Same as 20a for the NCEP data.

Figure 21a. January tropical Pacific anomaly maps for the COADS data during the time period 1980-1989.

Figure 21b. Same as 21a for the Dasilva data.

Figure 21c. Same as 21a for the Smith data.

Figure 21d. Same as 21a for the NCEP data.

Figure 22a. July tropical Pacific anomaly maps for the COADS data during the time period 1980-1989.

Figure 22b. Same as 22a for the Dasilva data.

Figure 22c. Same as 22a for the Smith data.

Figure 22d. Same as 22a for the NCEP data.

Figure 23a. January tropical Atlantic error maps for the COADS data during the time period 1980-1989.

Figure 23b. Same as 23a for July.

Figure 23c. Same as 23a for the tropical Pacific.

Figure 23d. Same as 23b for the tropical Pacific.

Figure 24. Proposed WOCE XBT tracklines in the tropical Atlantic and Pacific.

Figure 25. Error maps for the tropical Atlantic based upon several XBT and COADS semivariogram models and hypothetical sampling along the proposed WOCE tracklines.

Figure 26. Error maps for the tropical Pacific based upon several XBT and COADS semivariogram models and hypothetical sampling along the proposed WOCE tracklines.

January XBT Data Distribution

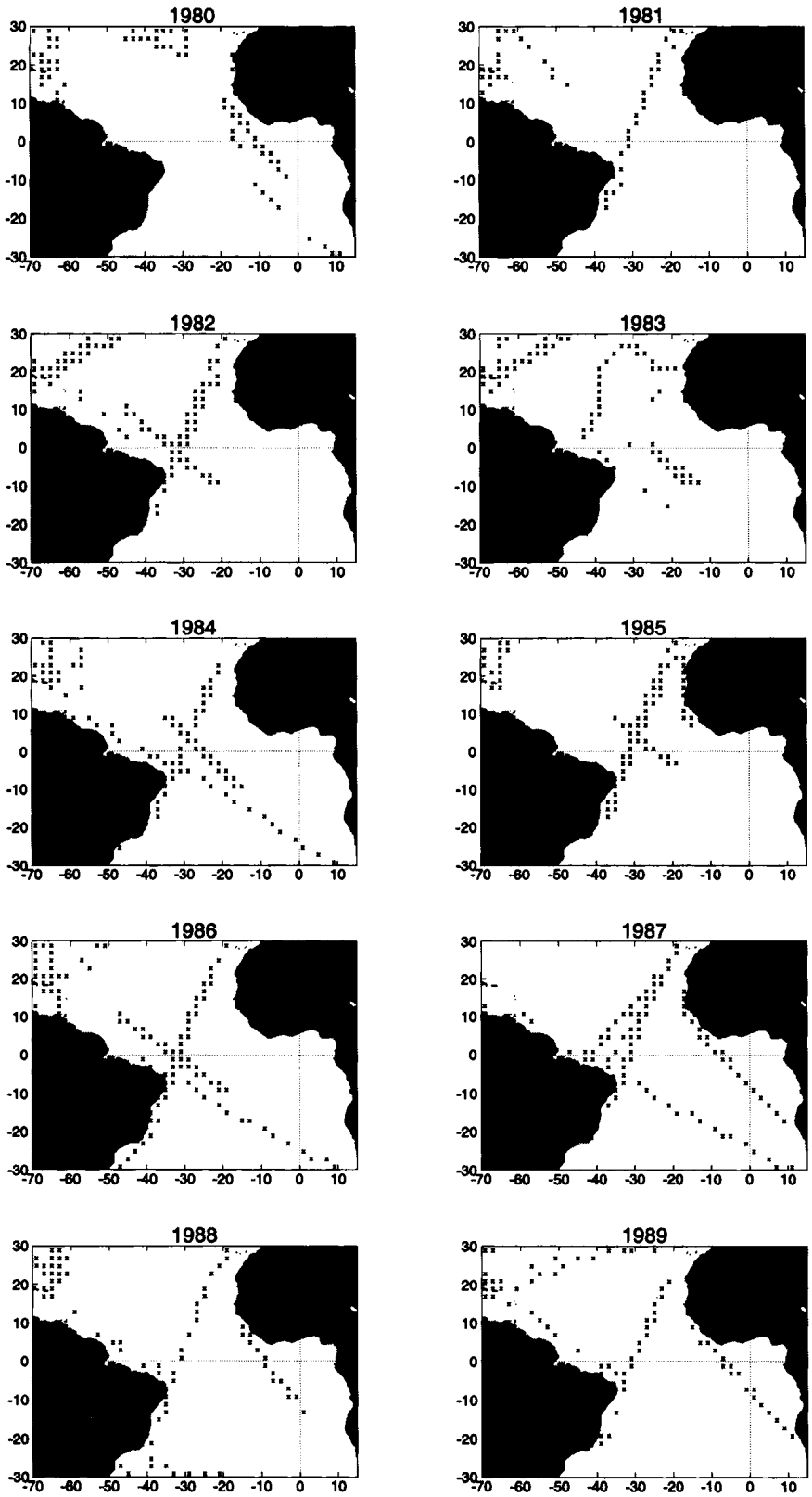

Figure 1a

January COADS Data Distribution

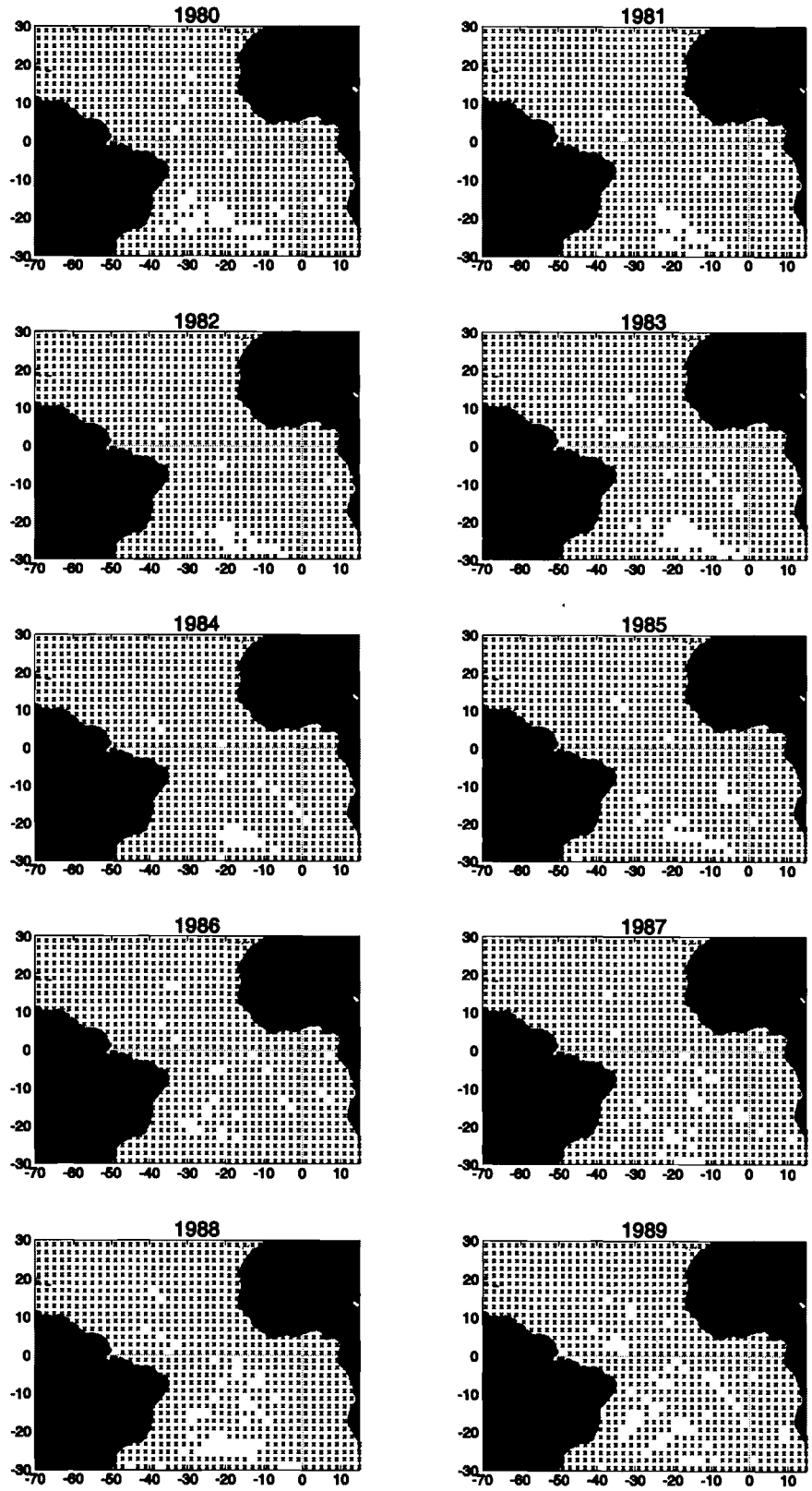

Figure 1b

July XBT Data Distribution

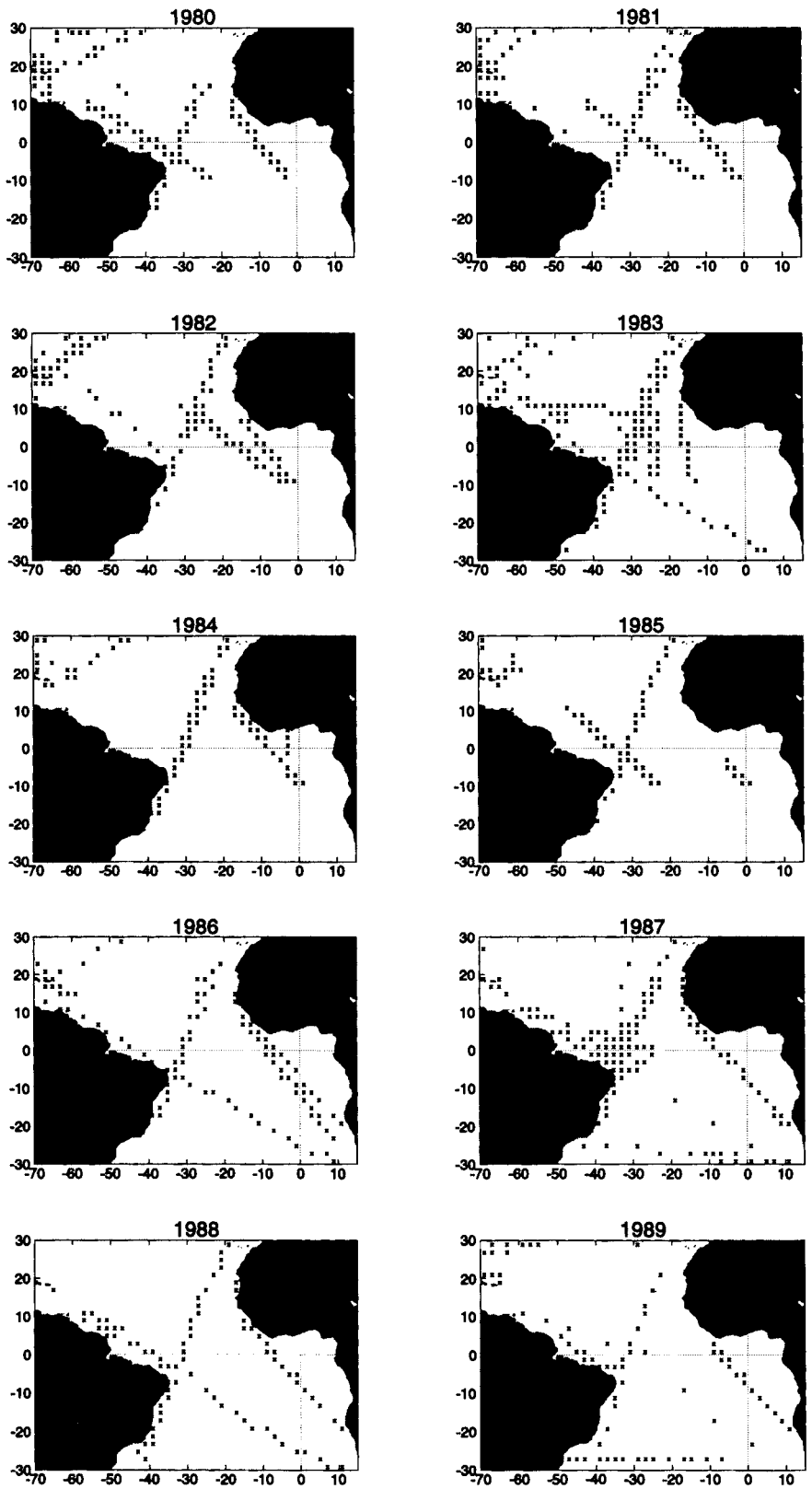

Figure 1c

July COADS Data Distribution

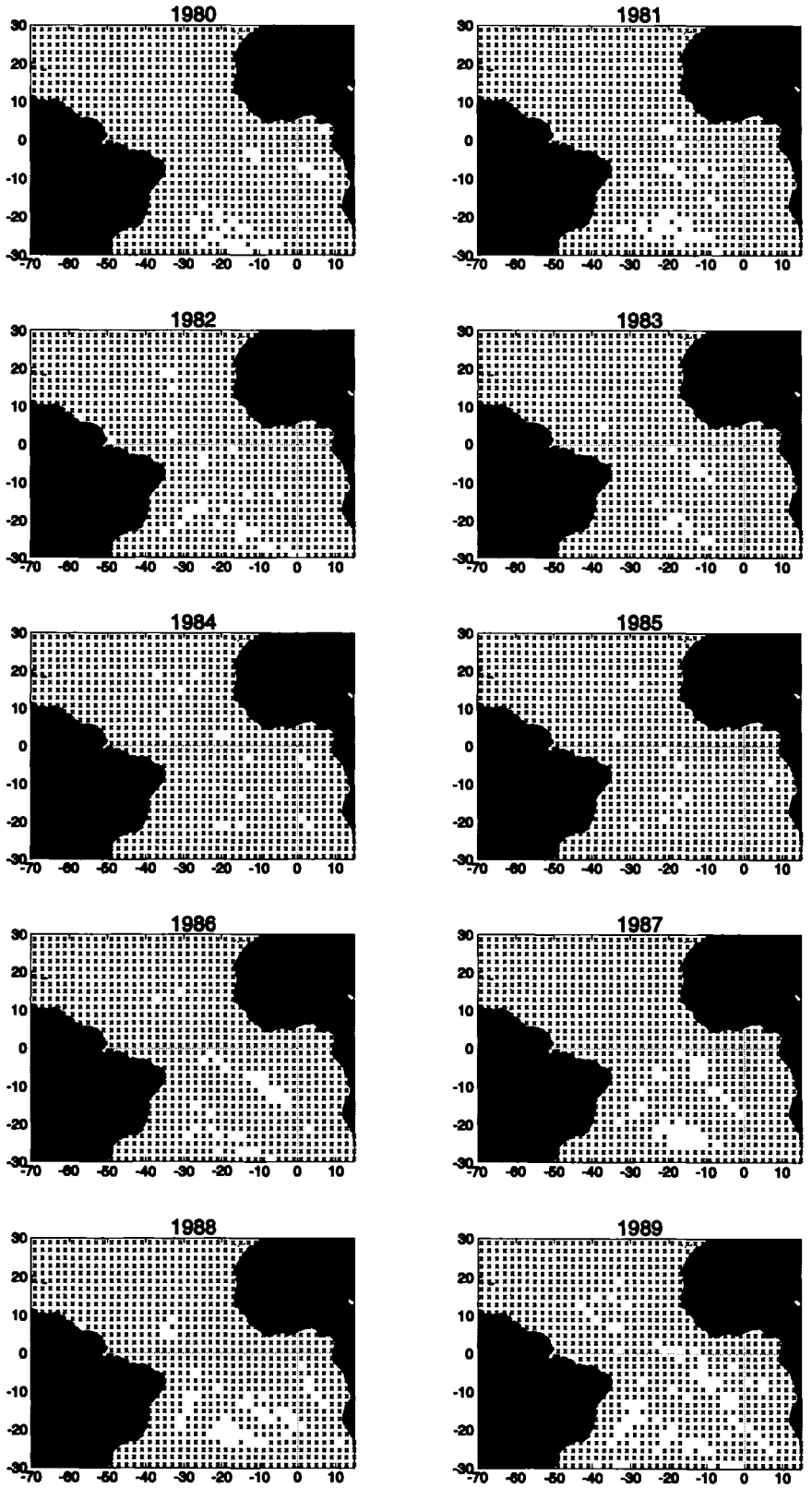

Figure 1d

January XBT Data Distribution

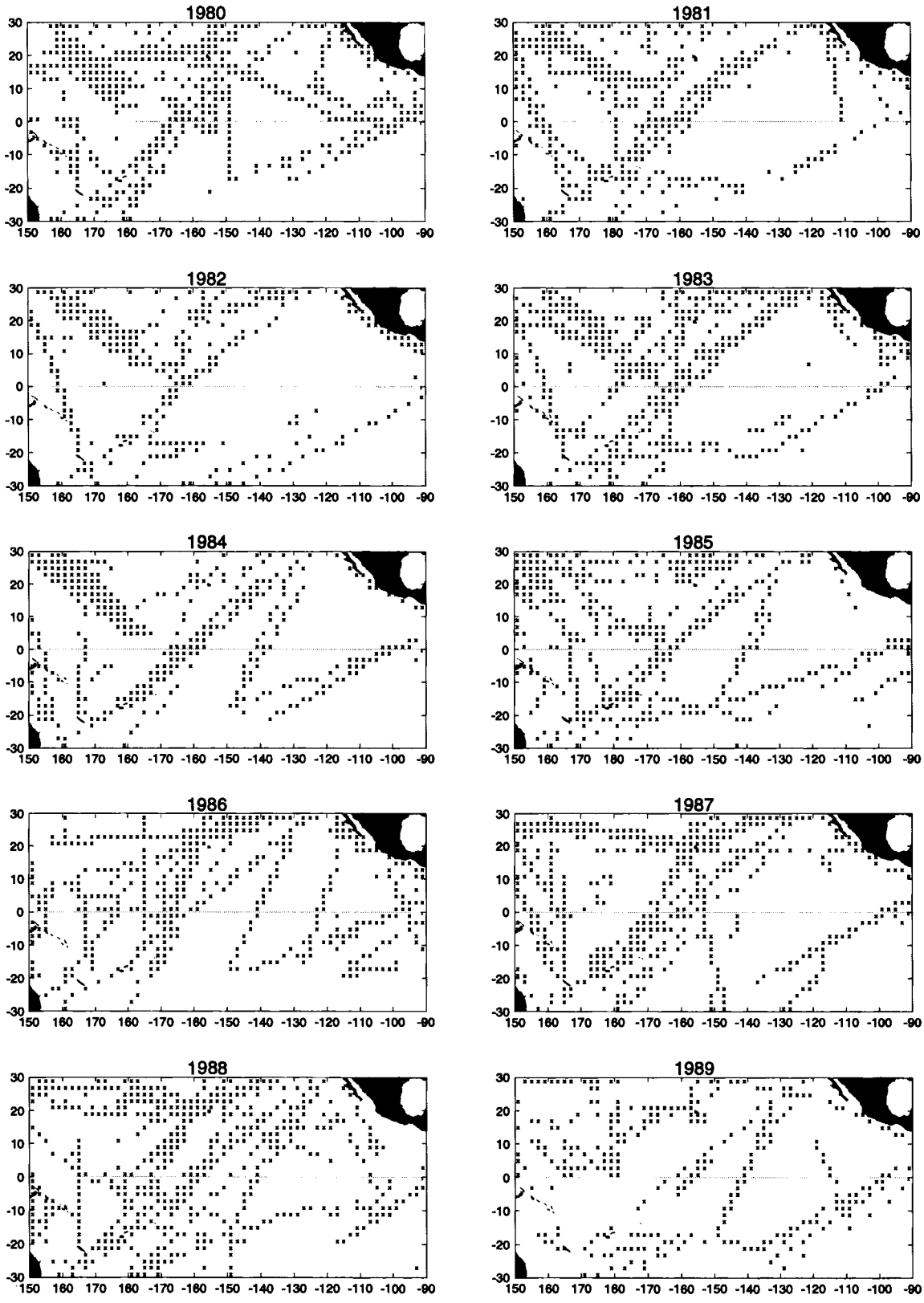

Figure 2a

January COADS Data Distribution

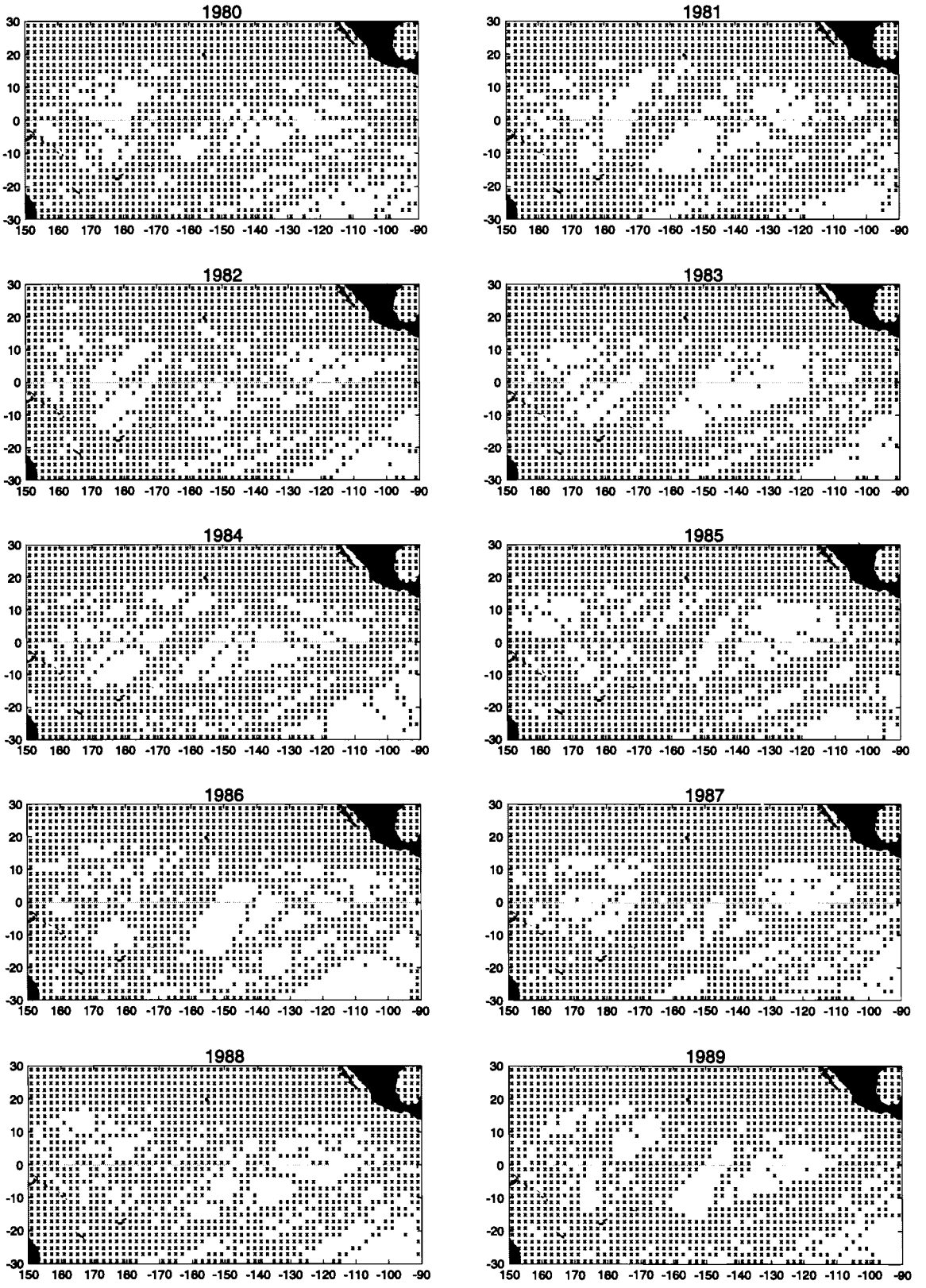

Figure 2b

July XBT Data Distribution

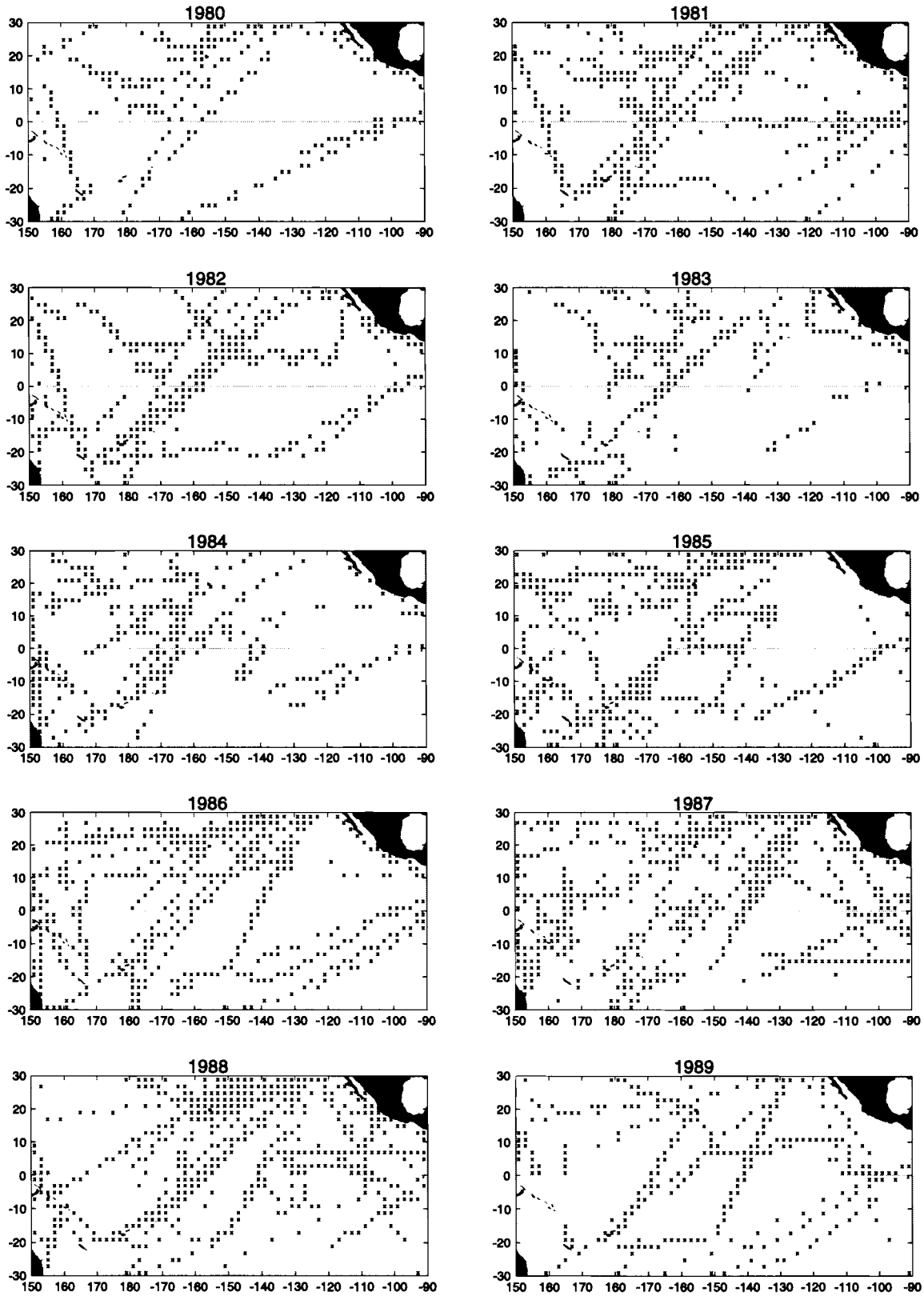

Figure 2c

July COADS Data Distribution

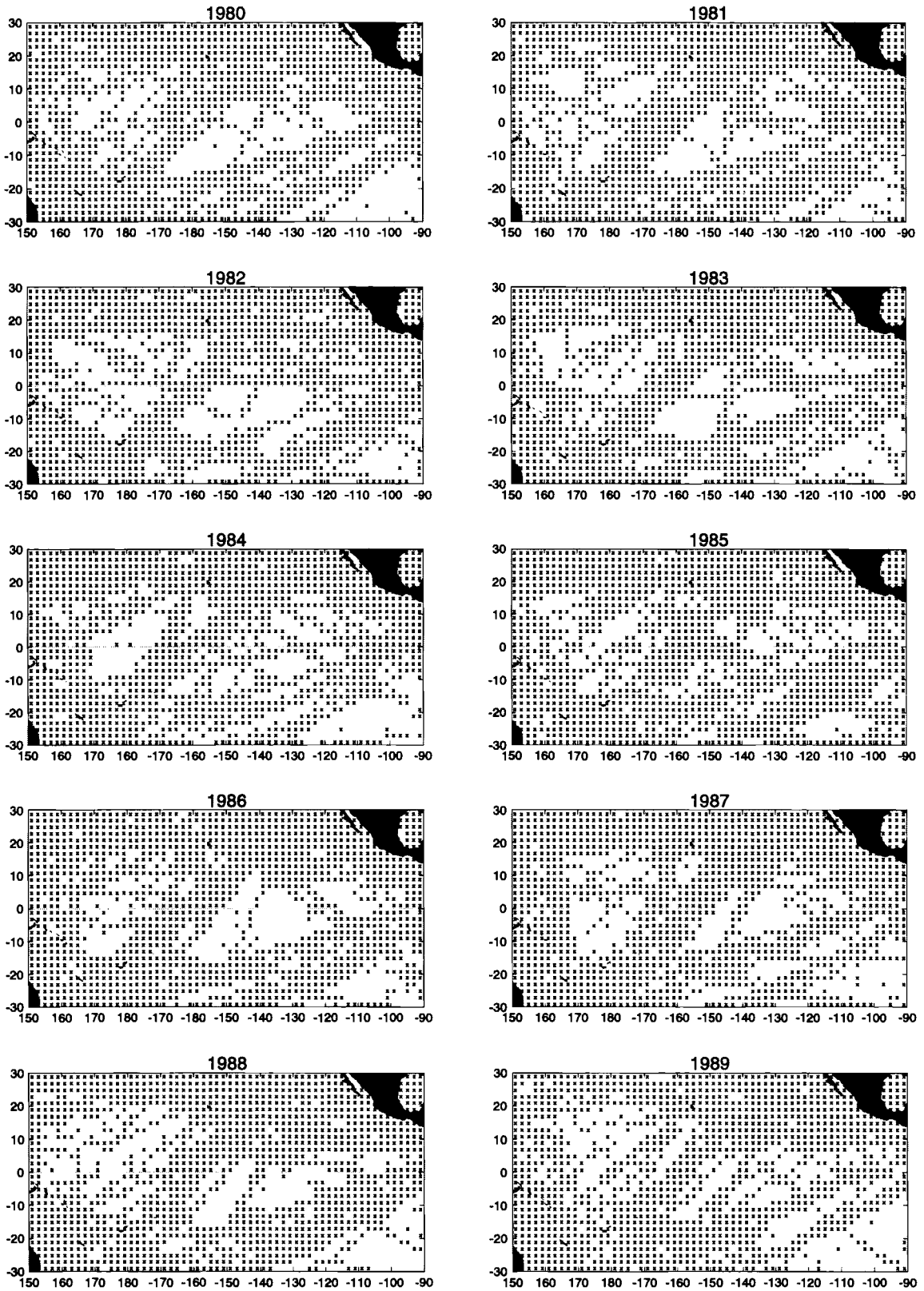

Figure 2d

Model Semivariograms

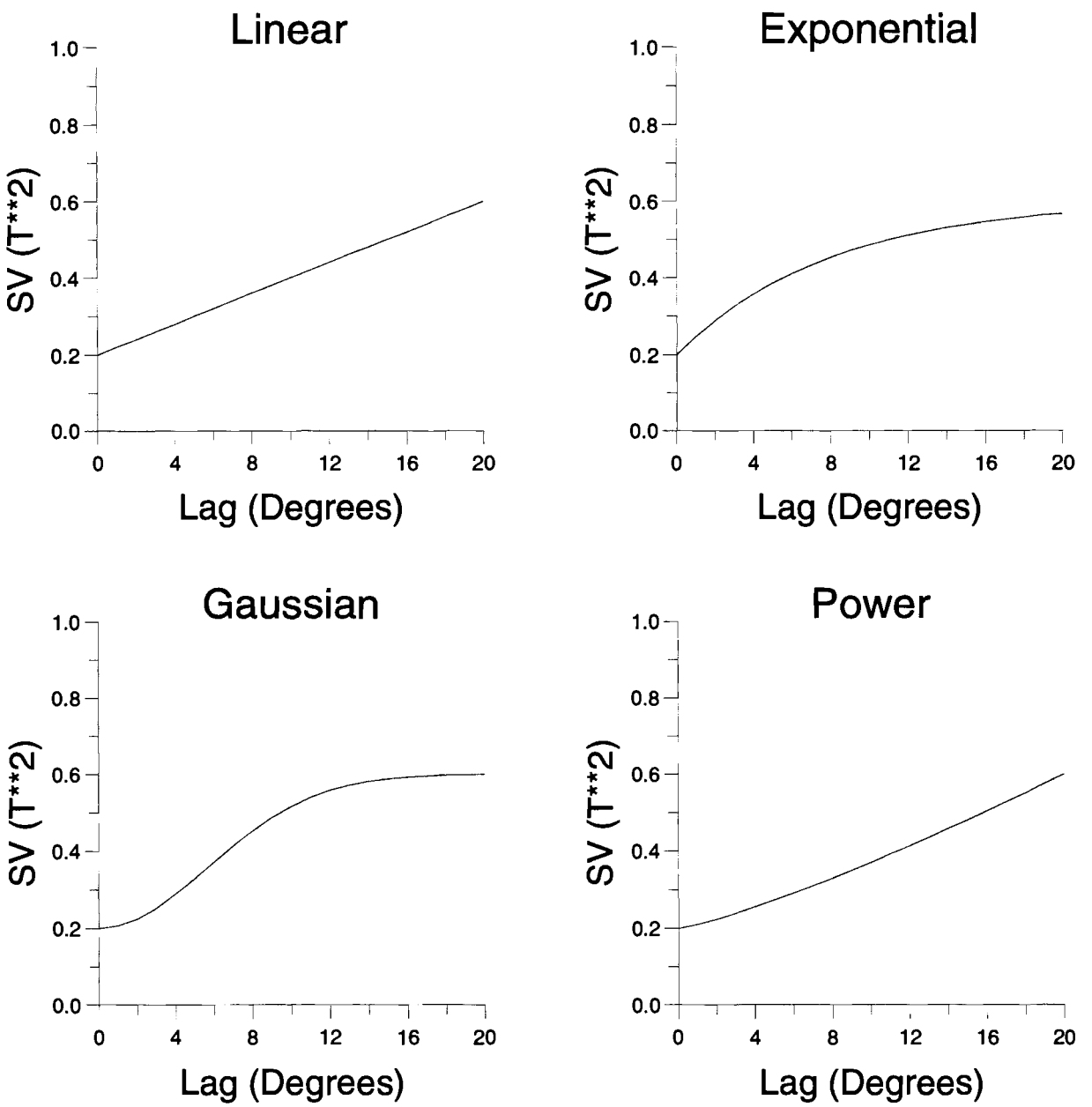

Figure 3

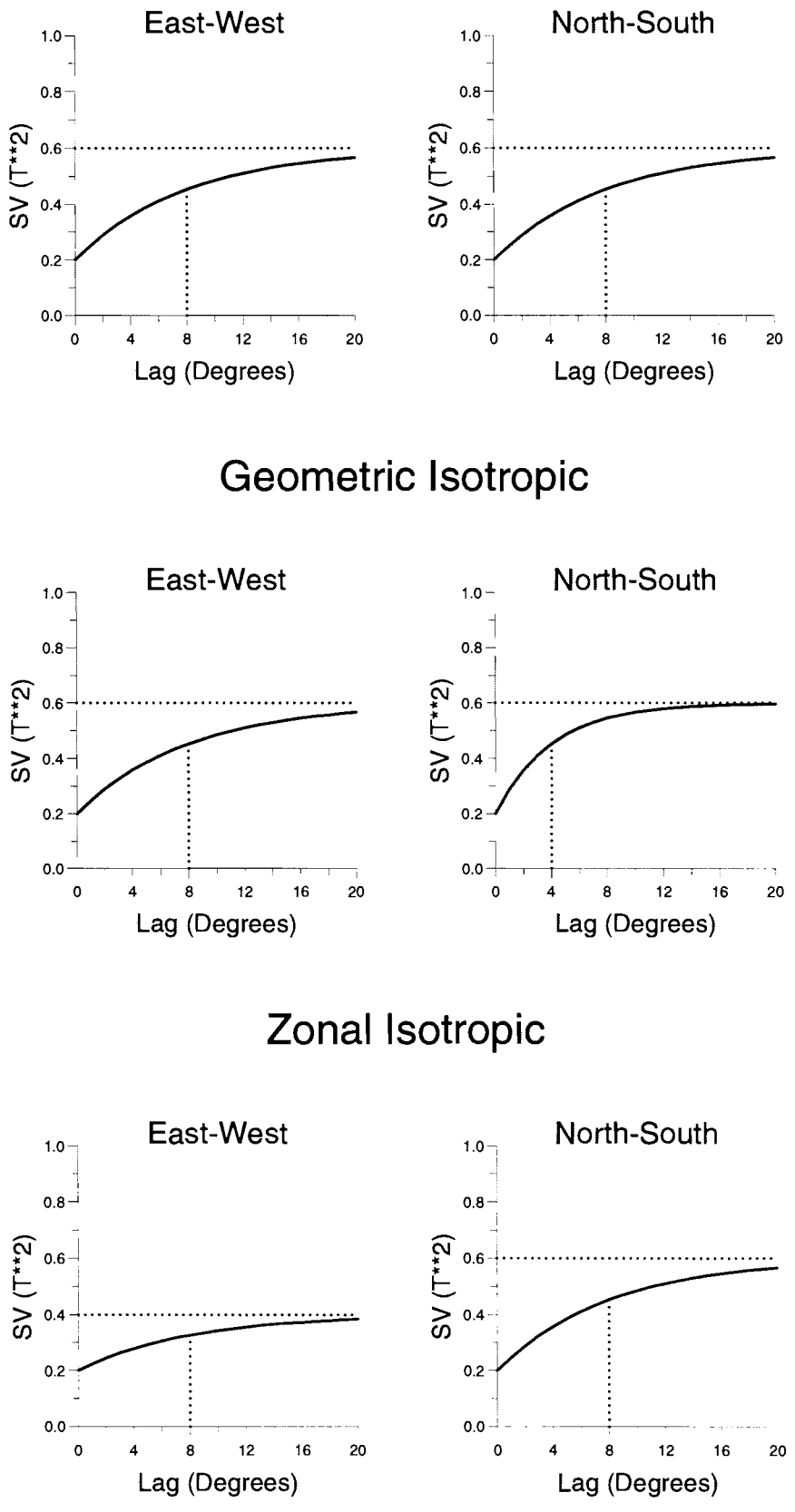
Isotropic
East-West
North-South
SV (T**2)
Lag (Degrees)
Geometric Isotropic
East-West
North-South
SV (T**2)
Lag (Degrees)
Zonal Isotropic
East-West
North-South
SV (T**2)
Lag (Degrees)

Figure 4

Atlantic Semivariograms (SST)

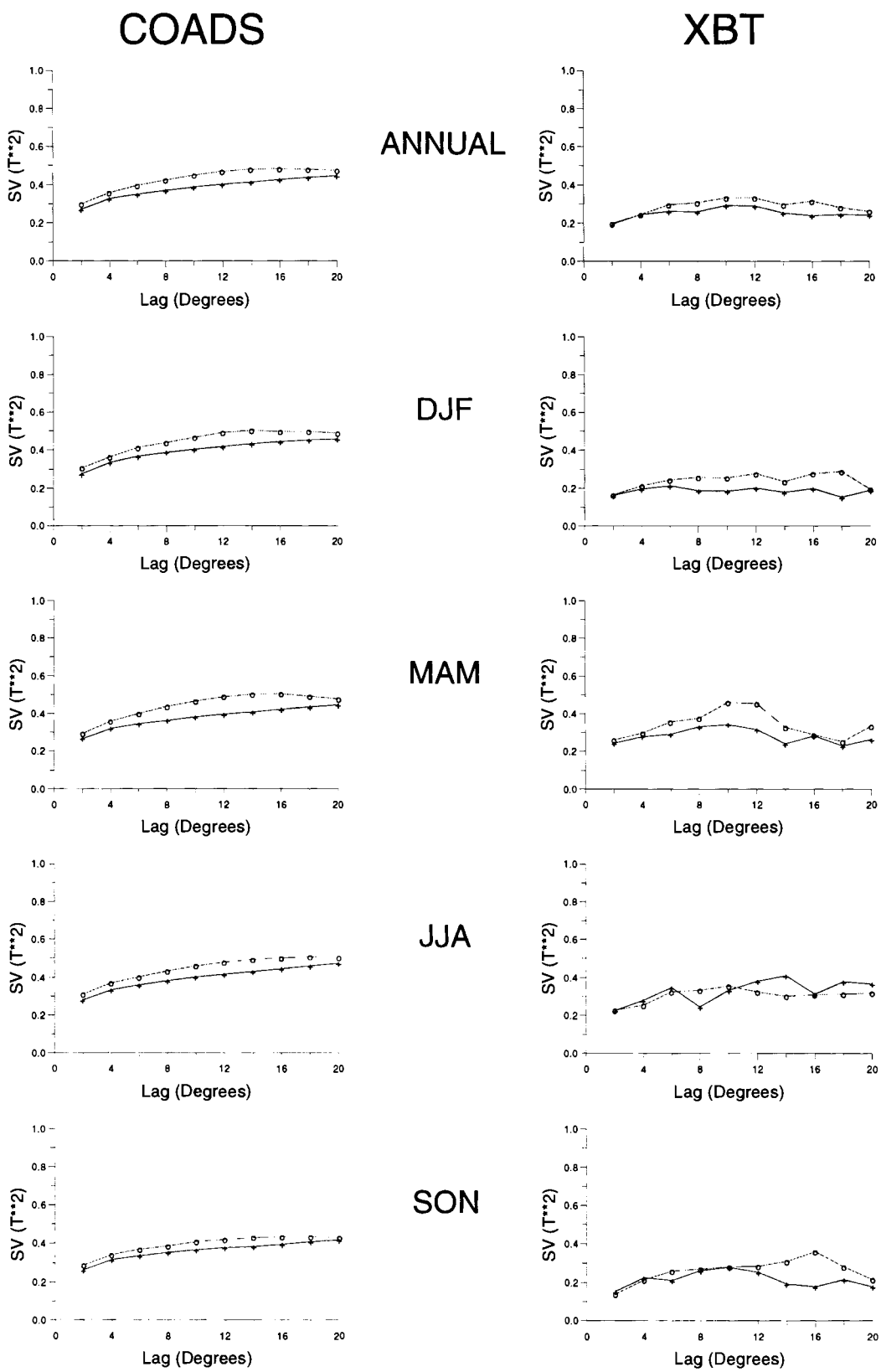

Figure 5

Pacific Semivariograms (SST)

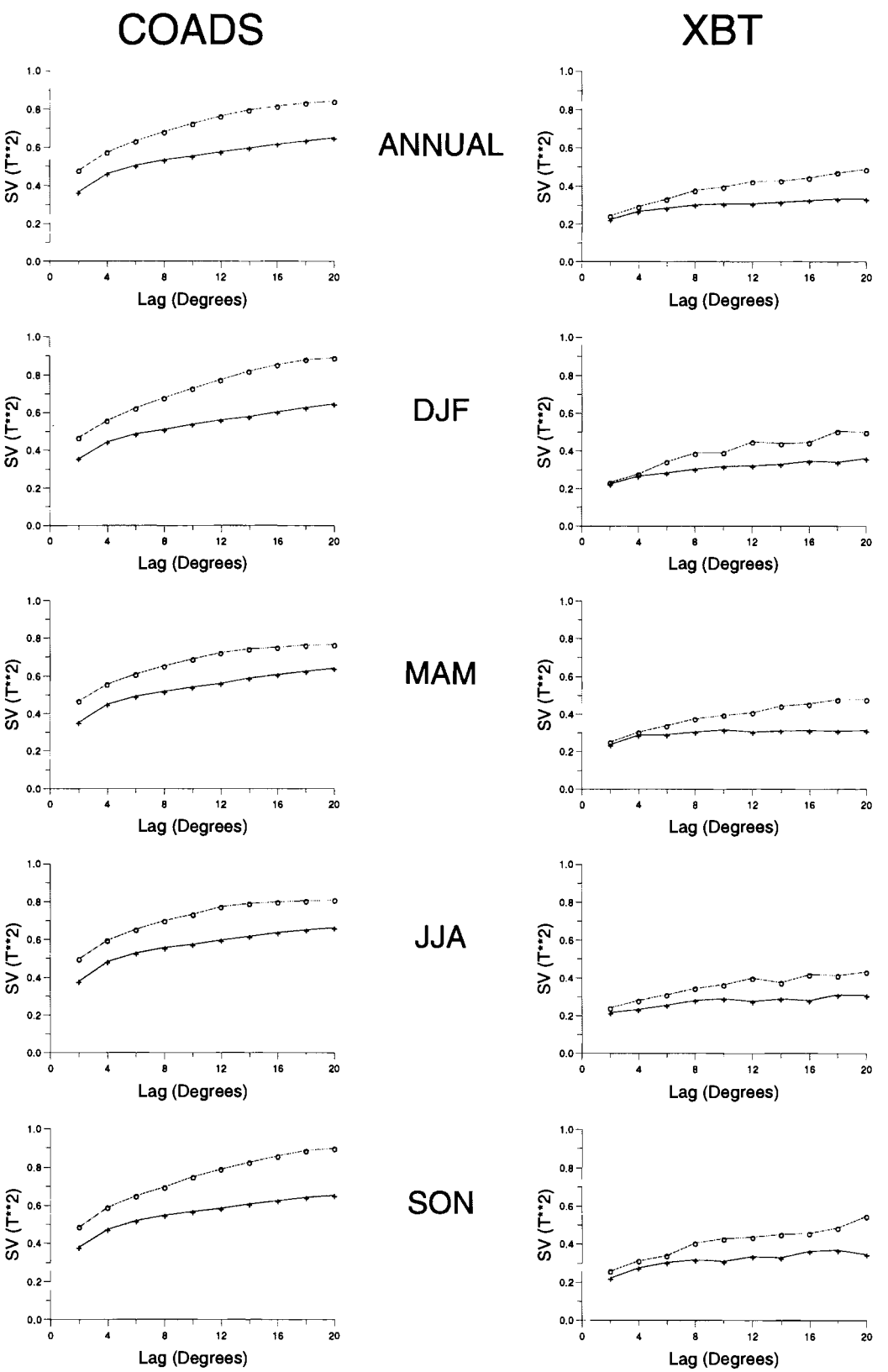

Figure 6a

Pacific Nino 34 Semivariograms (SST)

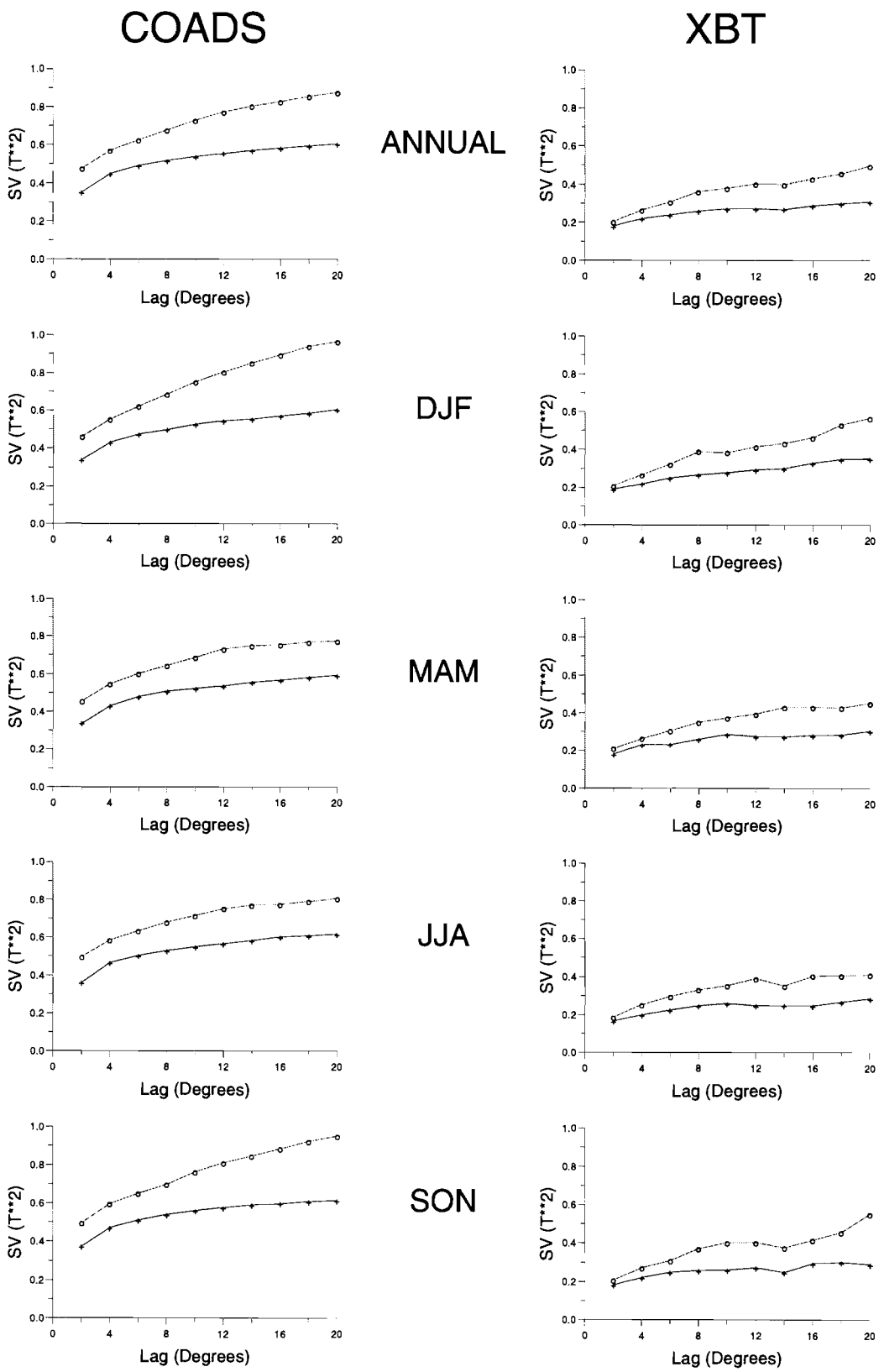

Figure 6b

Pacific XBT Semivariograms (SST)

January

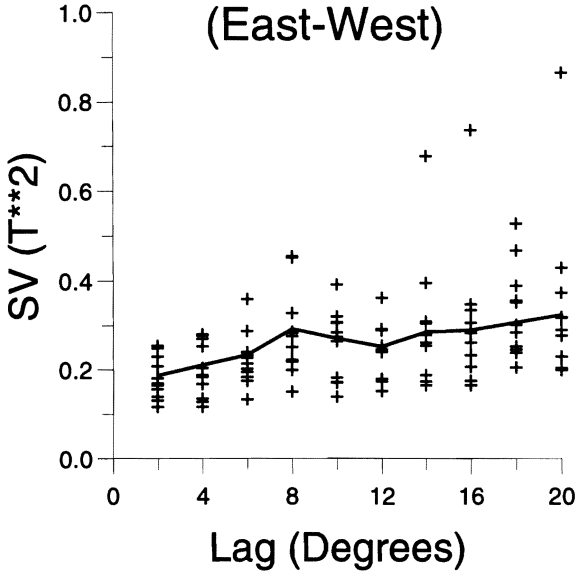

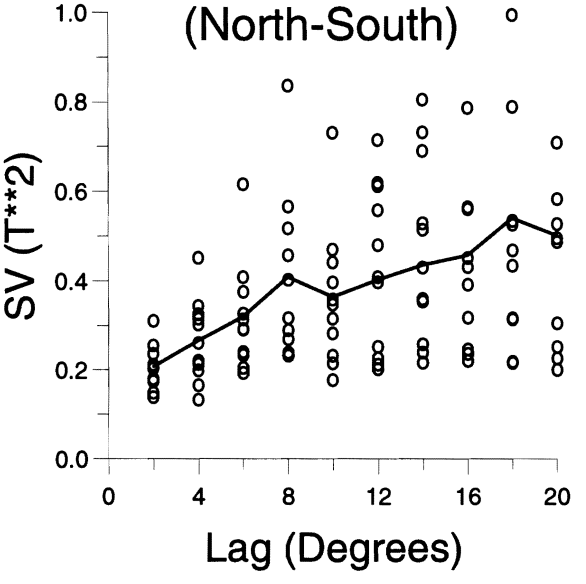

July

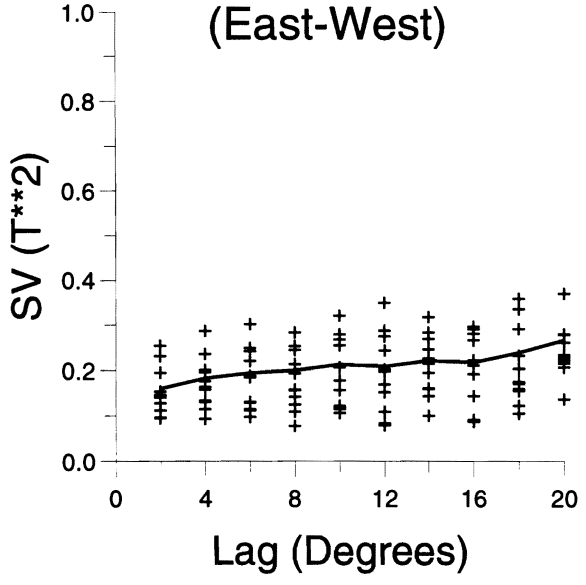

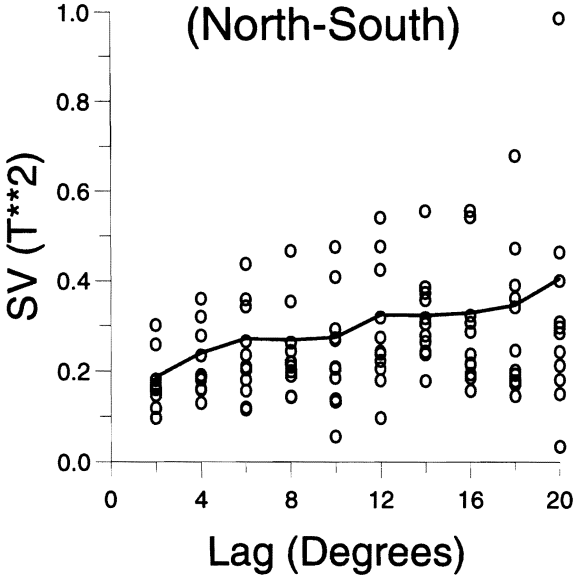

Figure 7

Atlantic Model Semivariograms (SST)

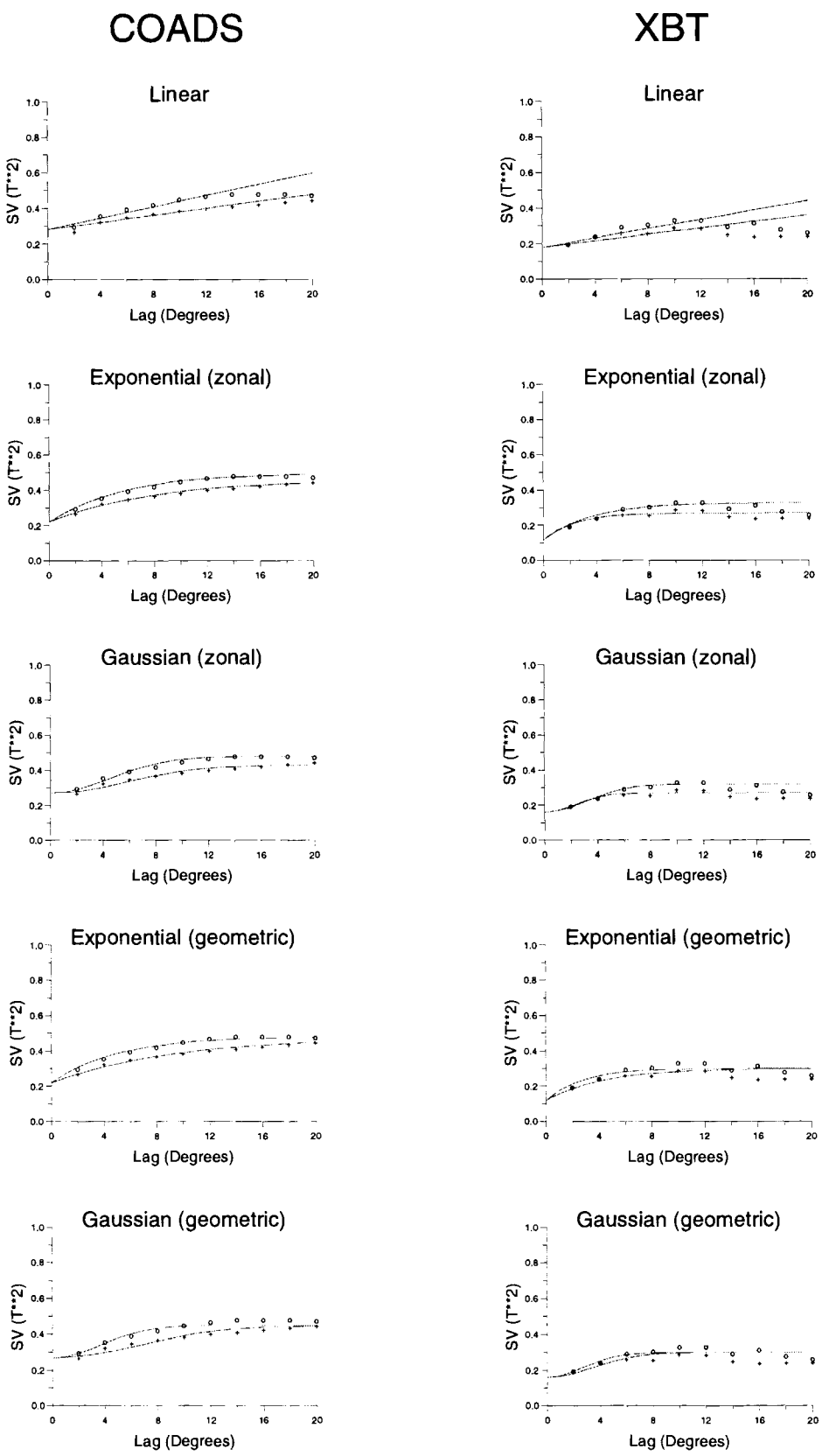

Figure 8

Pacific Model Semivariograms (SST)

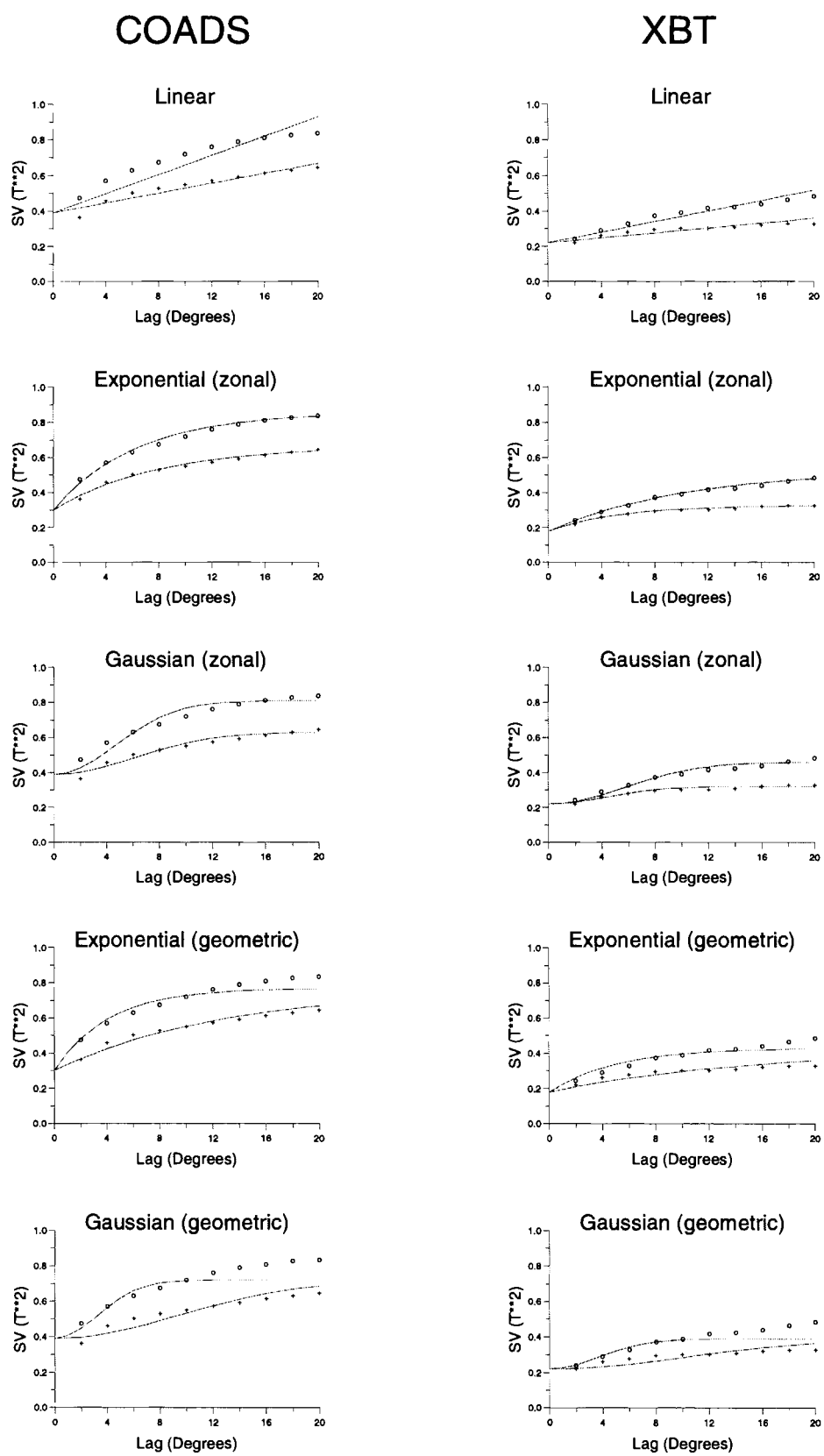

Figure 9

Atlantic XBT Semivariograms

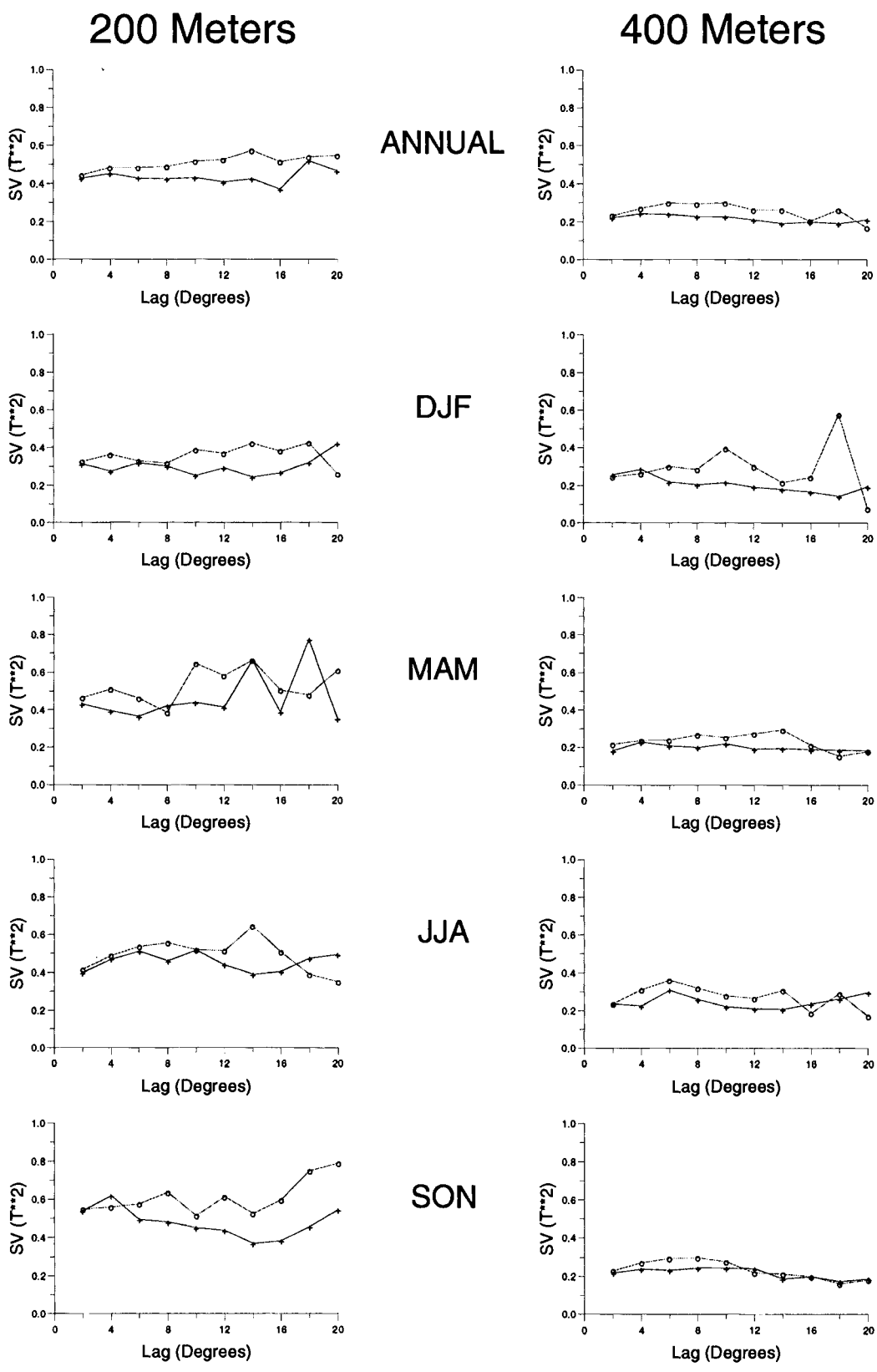

Figure 10

Pacific XBT Semivariograms

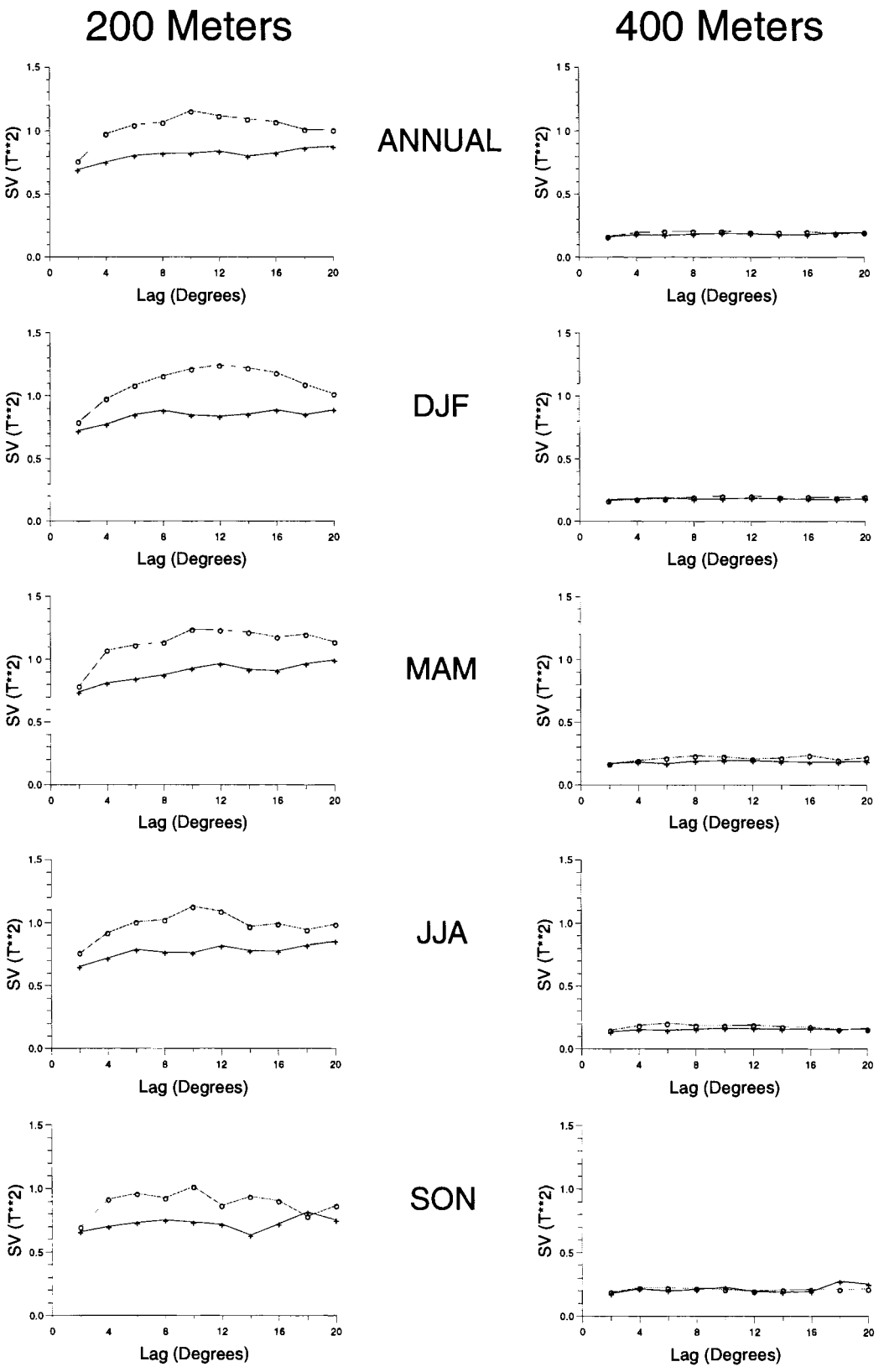

Figure 11

XBT Model Semivariograms

Atlantic

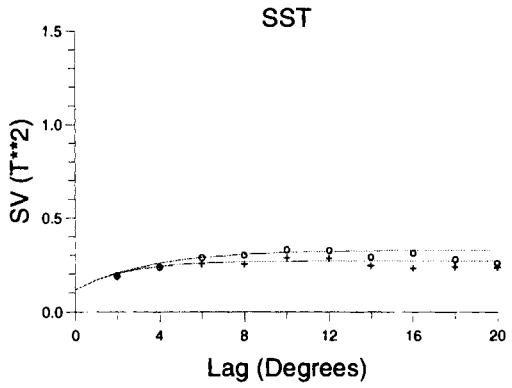

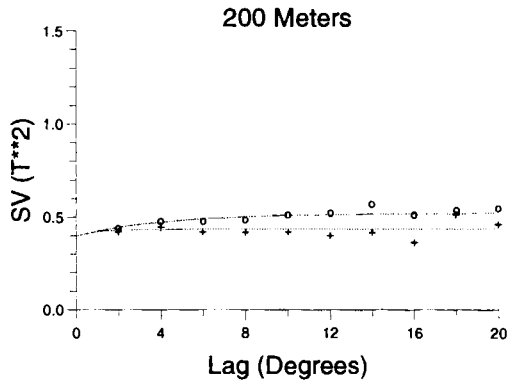

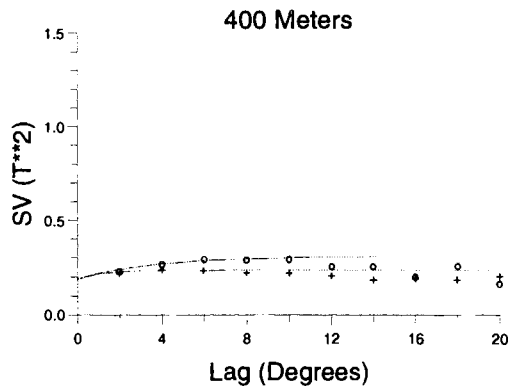

Pacific

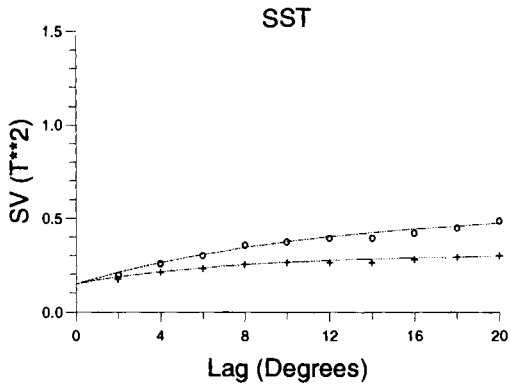

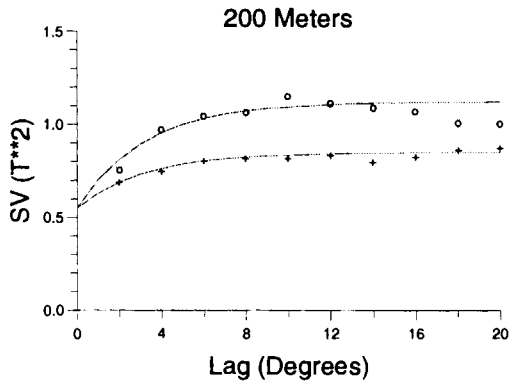

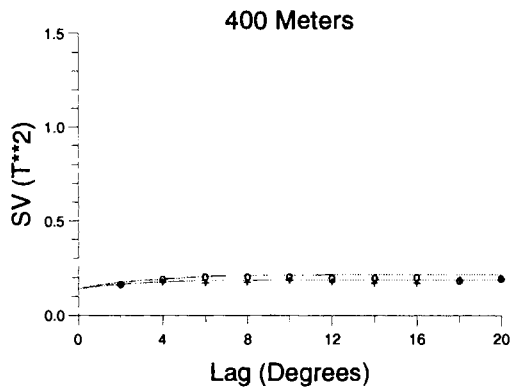

Figure 12

Atlantic Semivariograms

NCEP

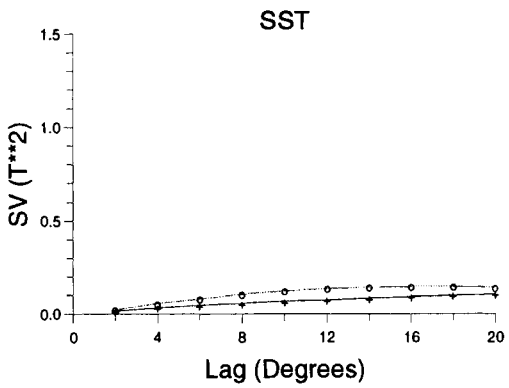

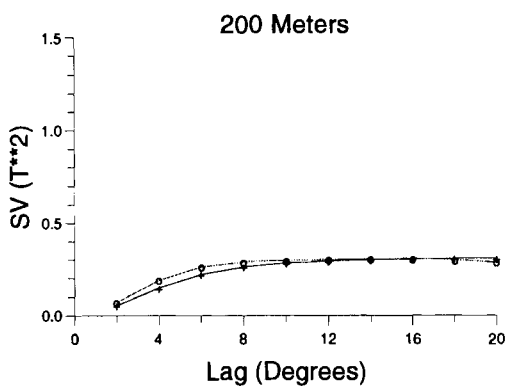

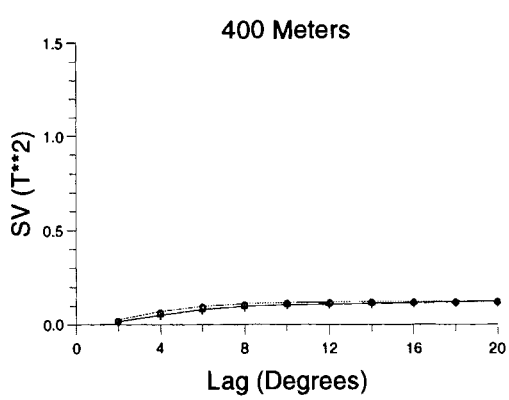

XBT

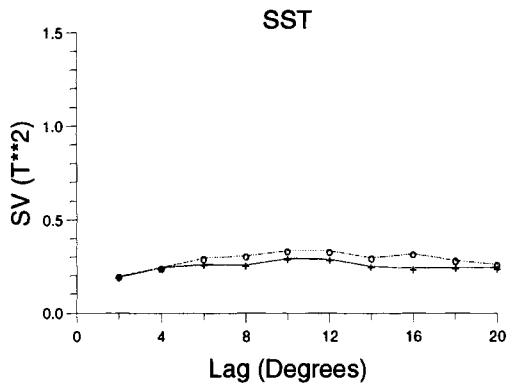

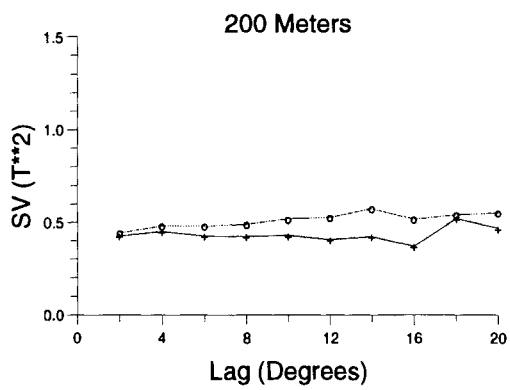

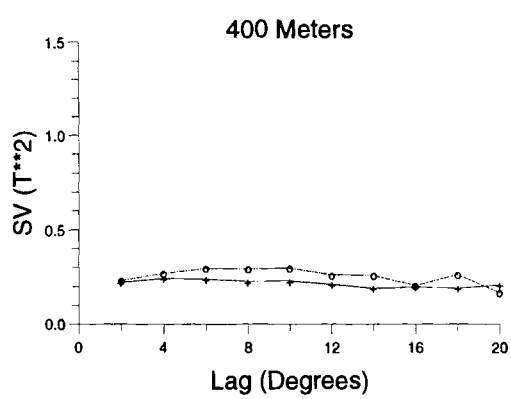

Figure 13

Pacific Semivariograms

NCEP

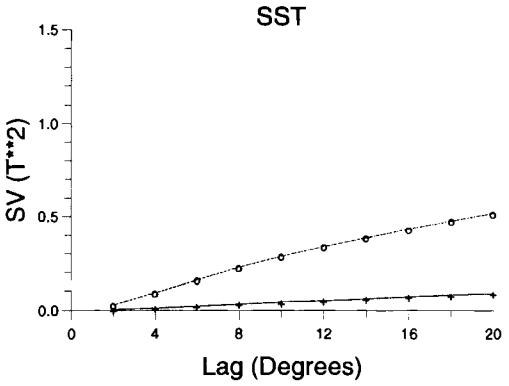

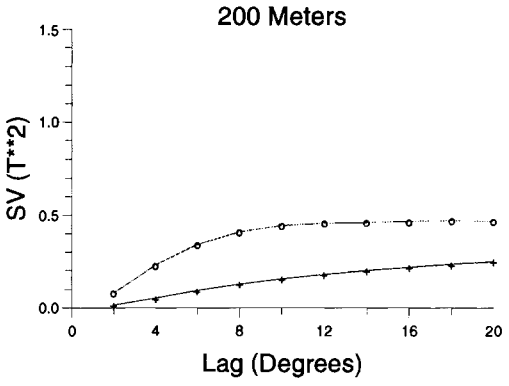

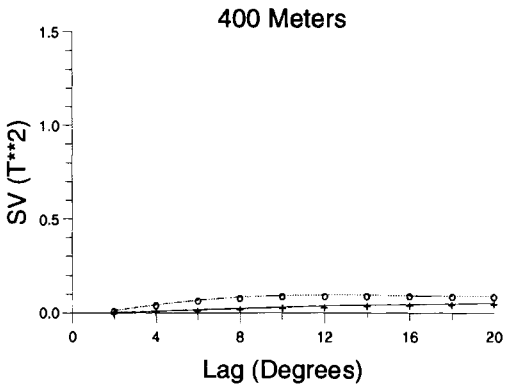

XBT

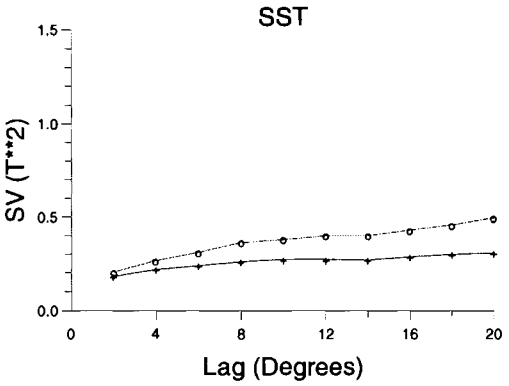

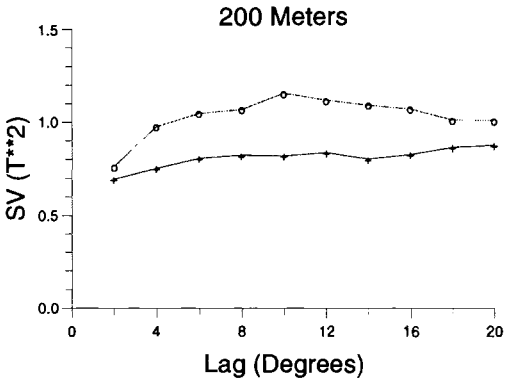

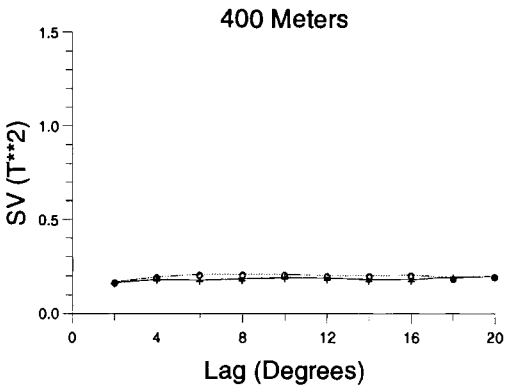

Figure 14

Climatology

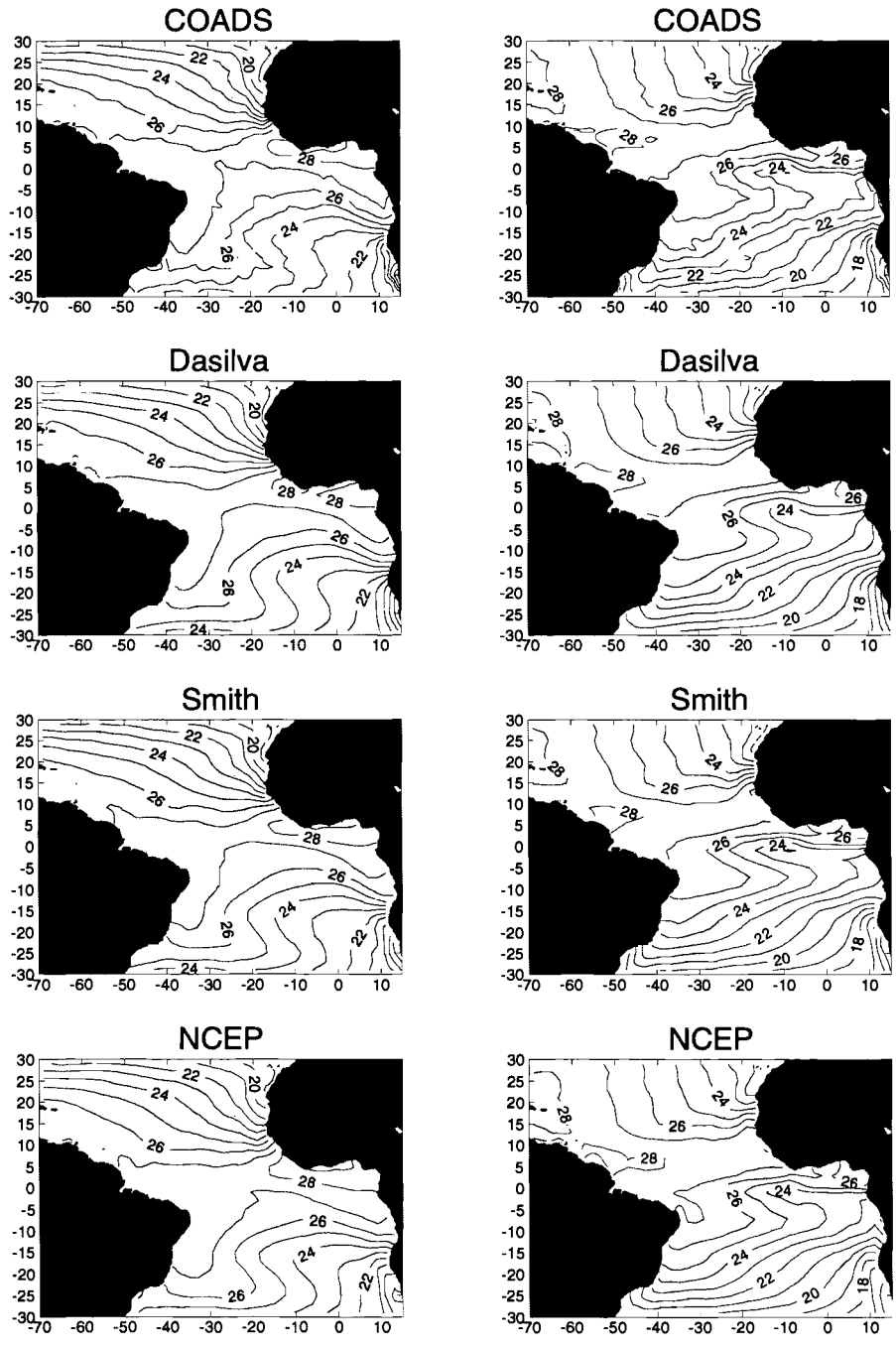

Figure 15

Climatology

January

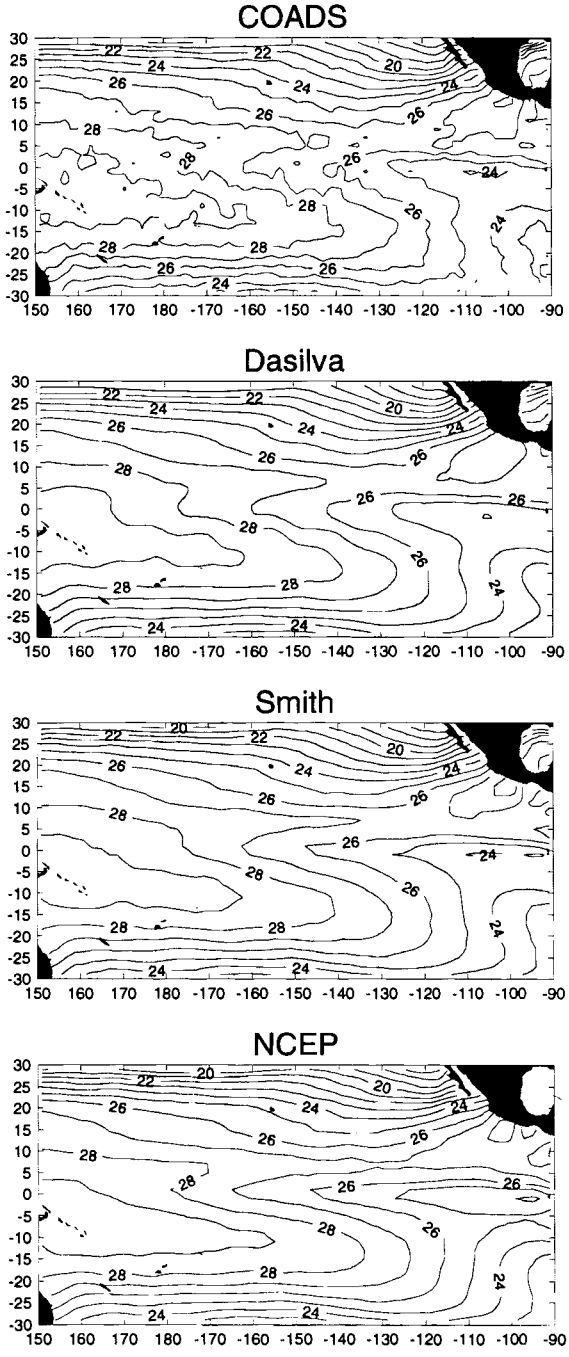

July

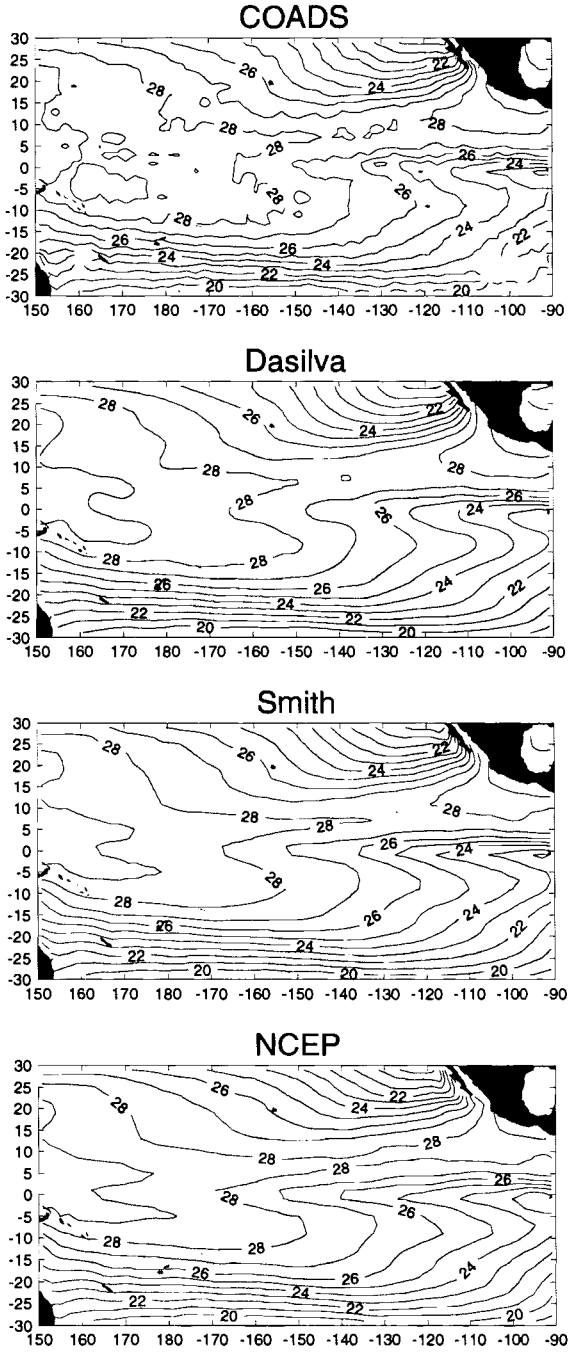

Figure 16

January 1983

Anomaly

Error

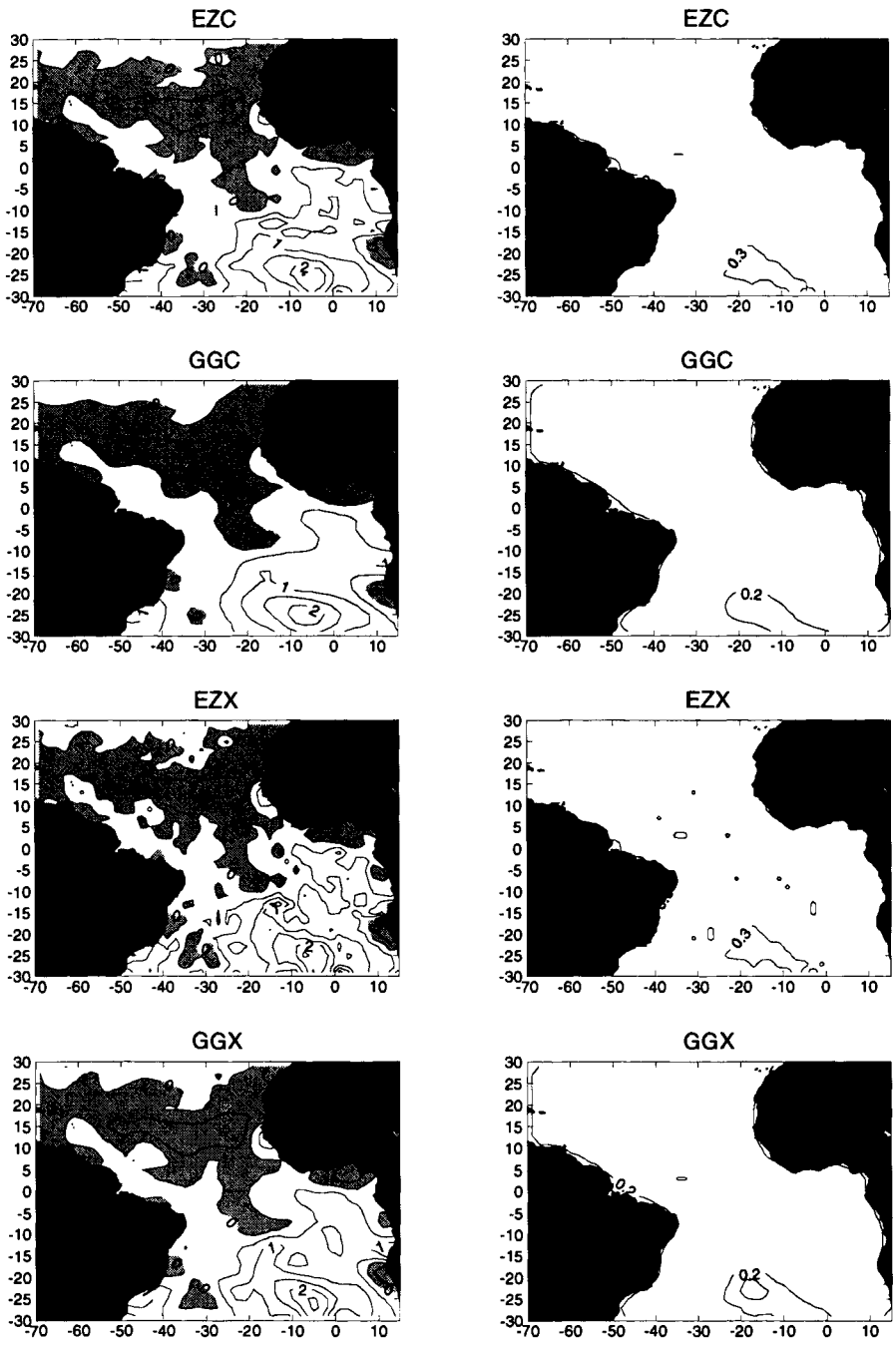

Figure 17a

July 1983

Anomaly

Error

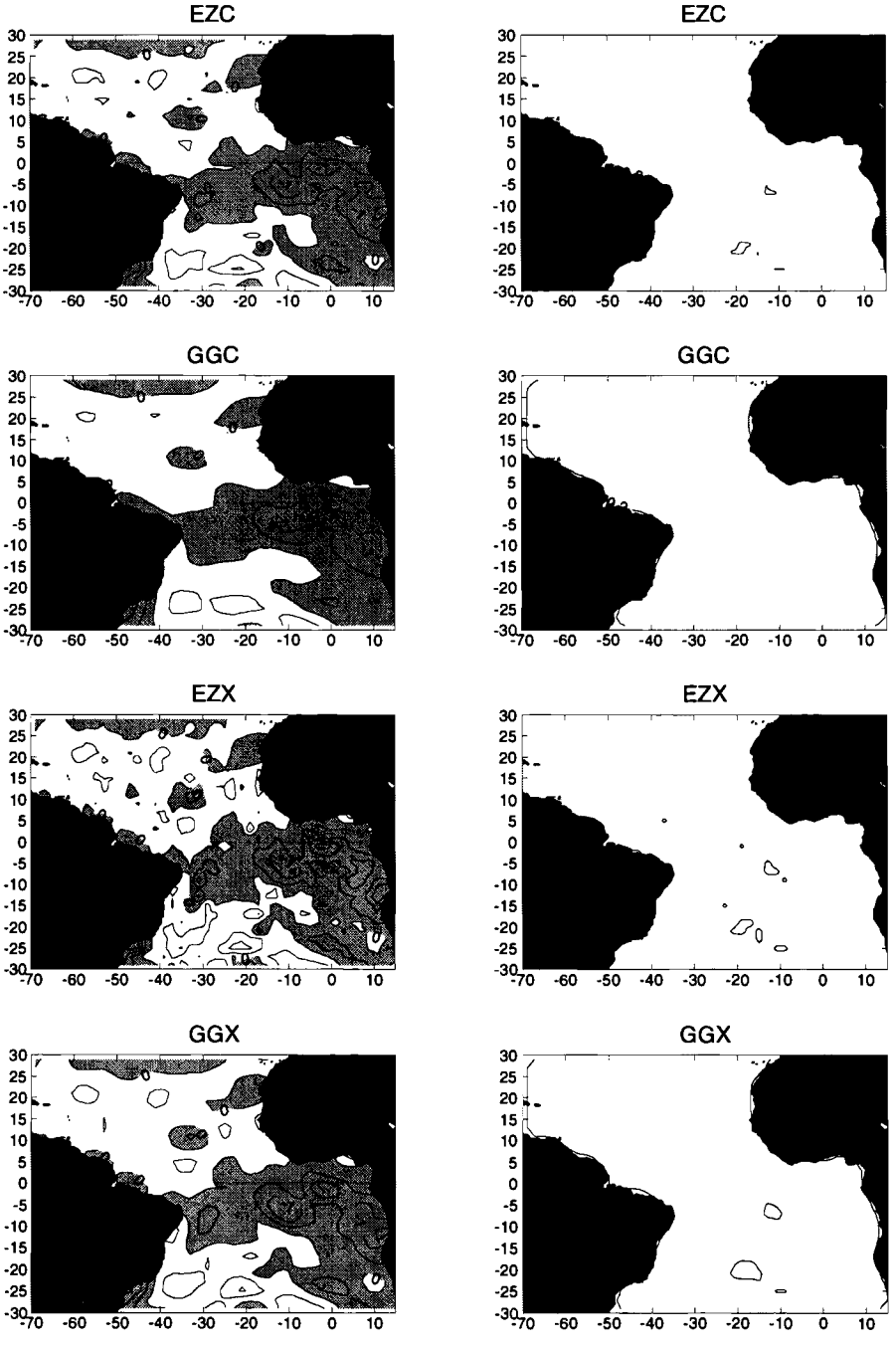

Figure 17b

January 1983

Anomaly

Error

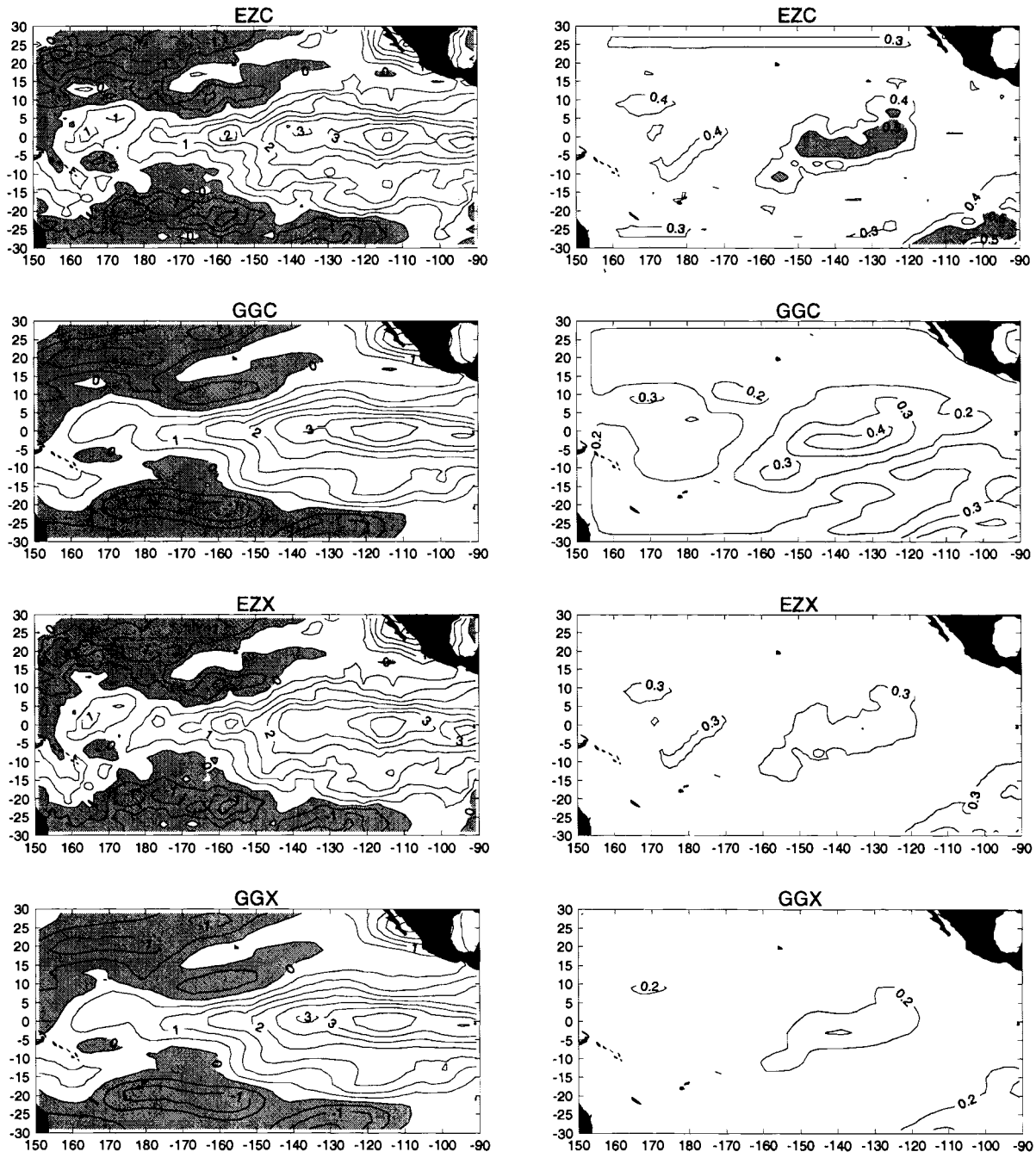

Figure 17c

July 1983

Anomaly

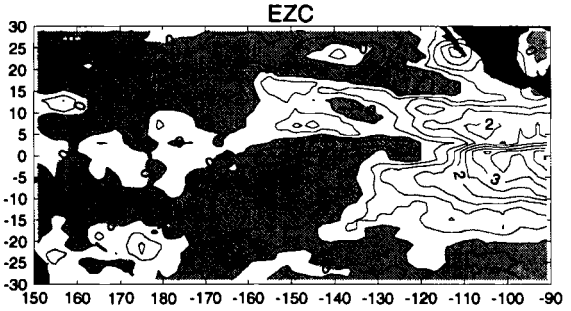

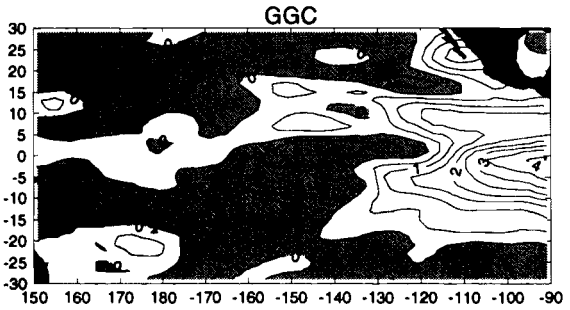

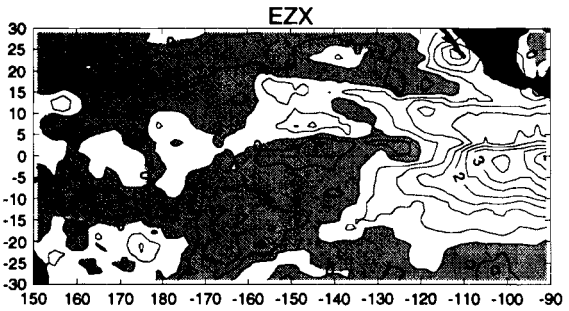

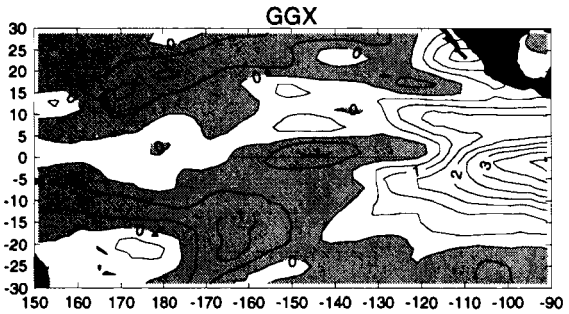

Error

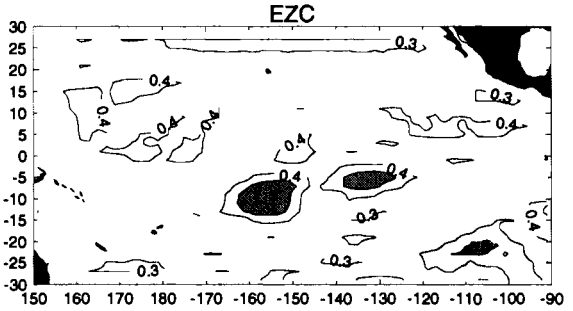

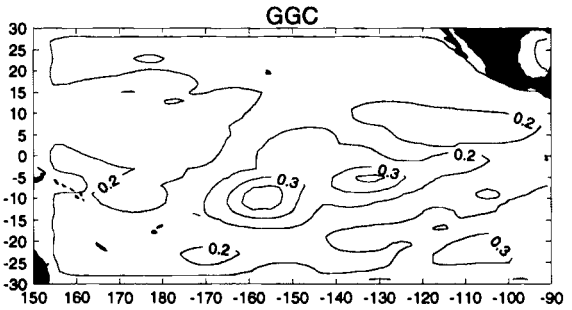

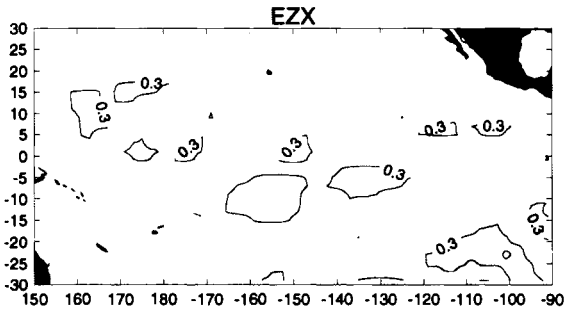

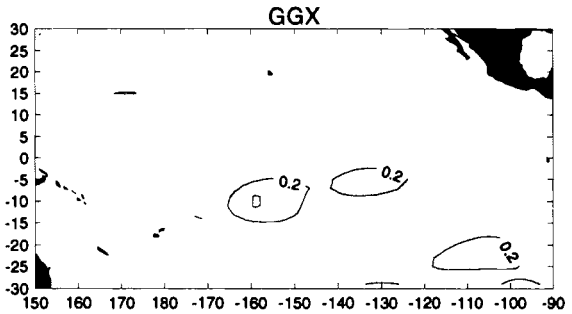

Figure 17d

Atlantic Anomaly (1983)

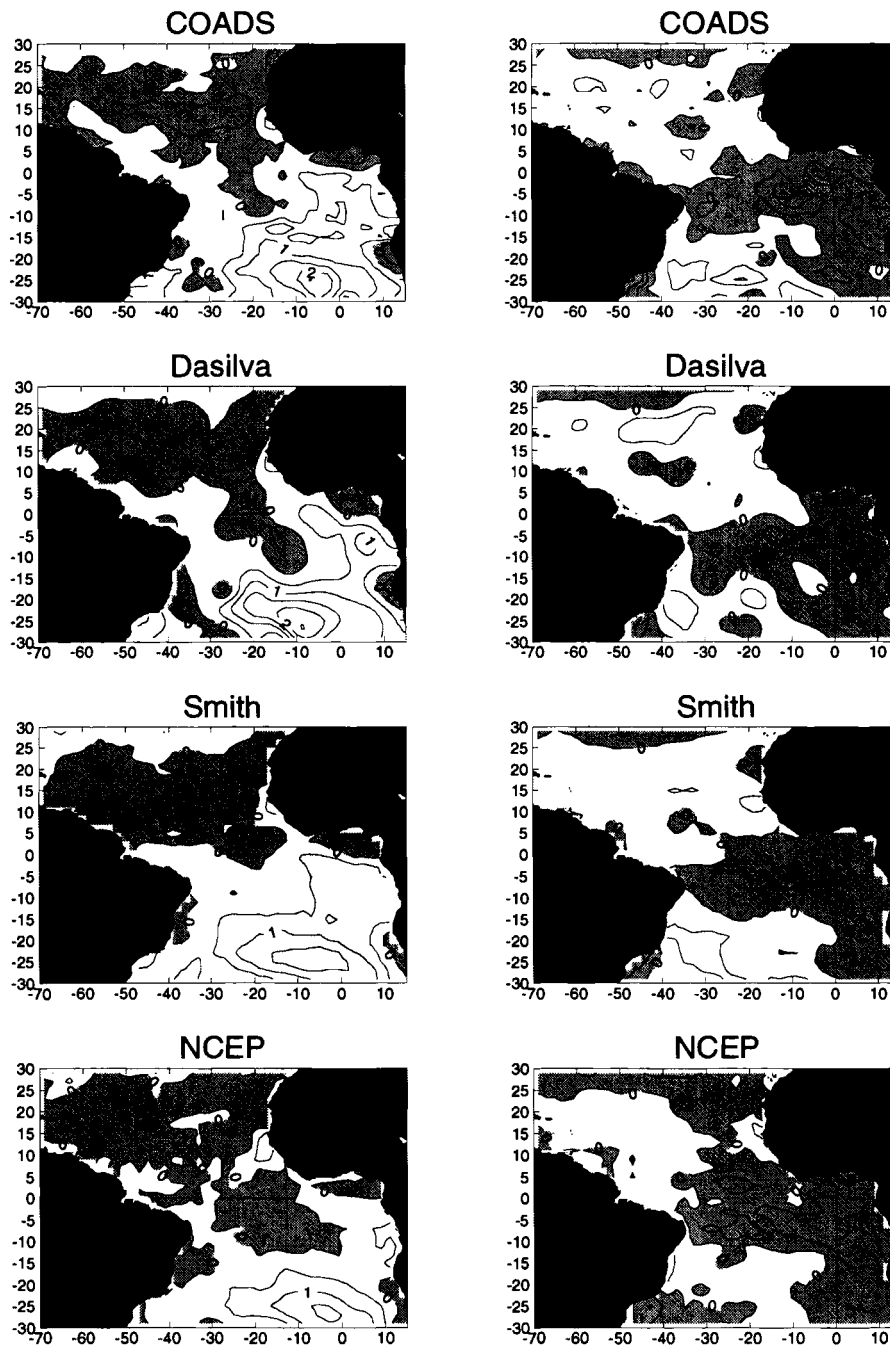

Figure 18a

Atlantic Anomaly (1987)

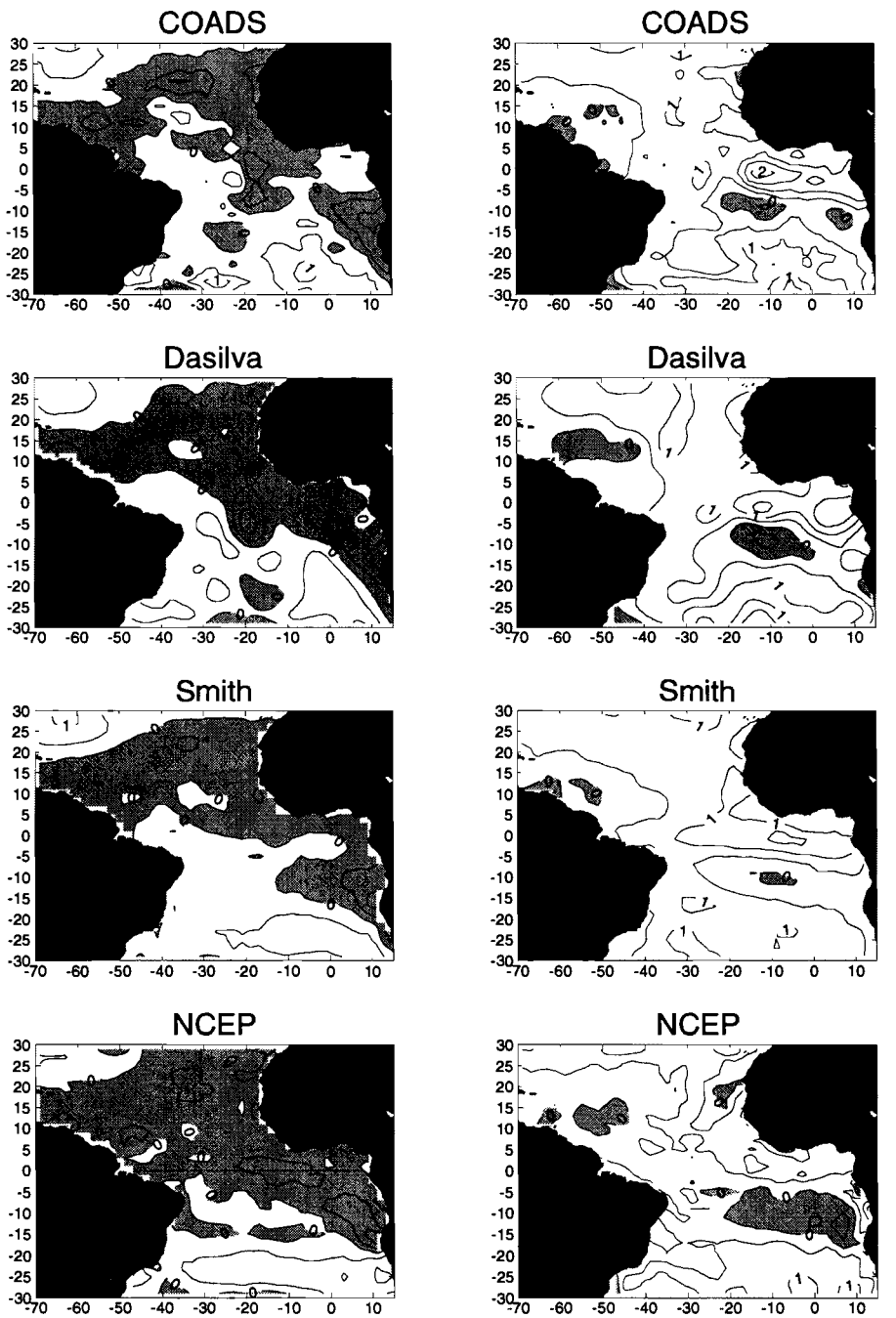

Figure 18b

Pacific Anomaly (1983)

January

July

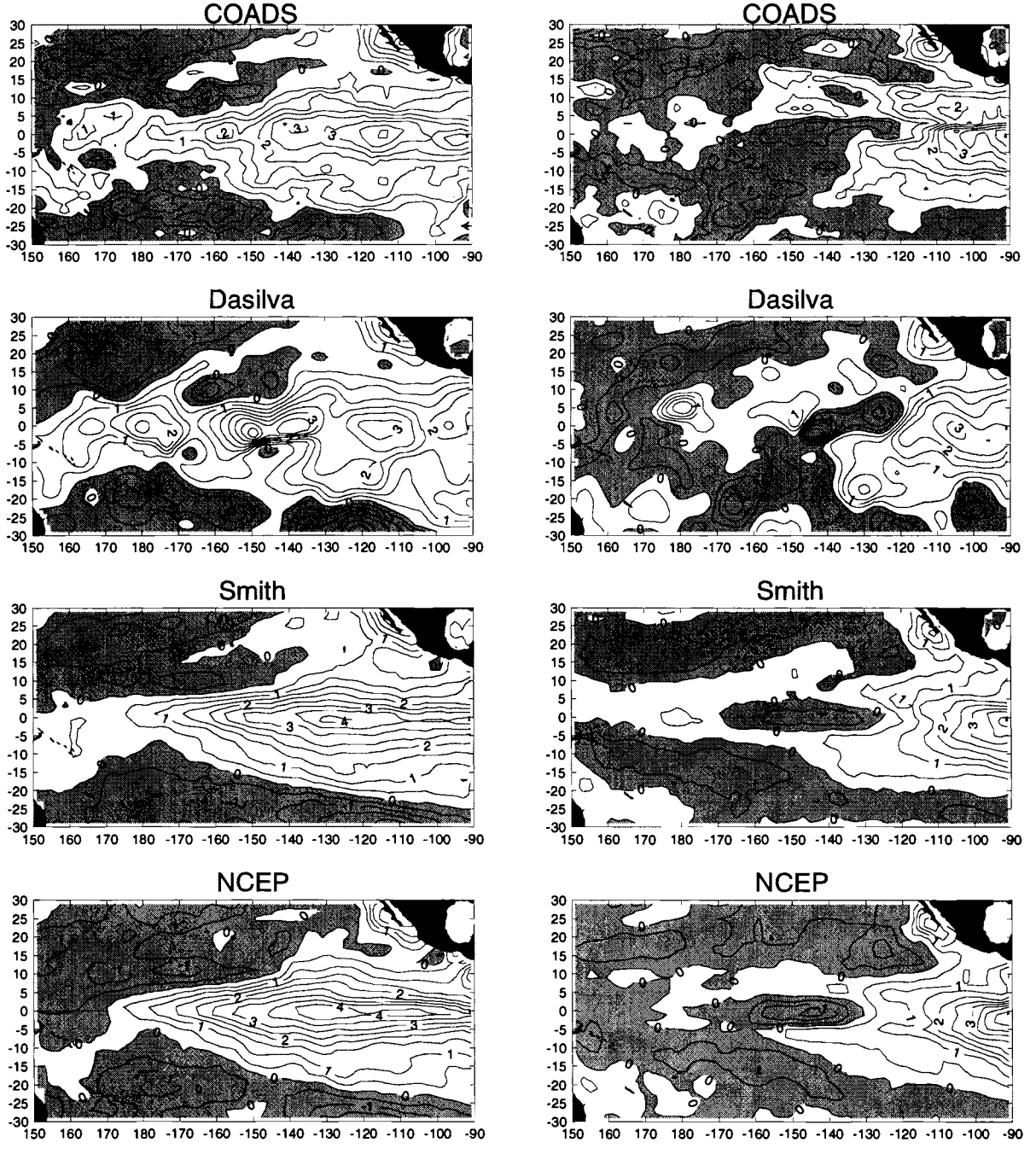

Figure 18c

Pacific Anomaly (1987)

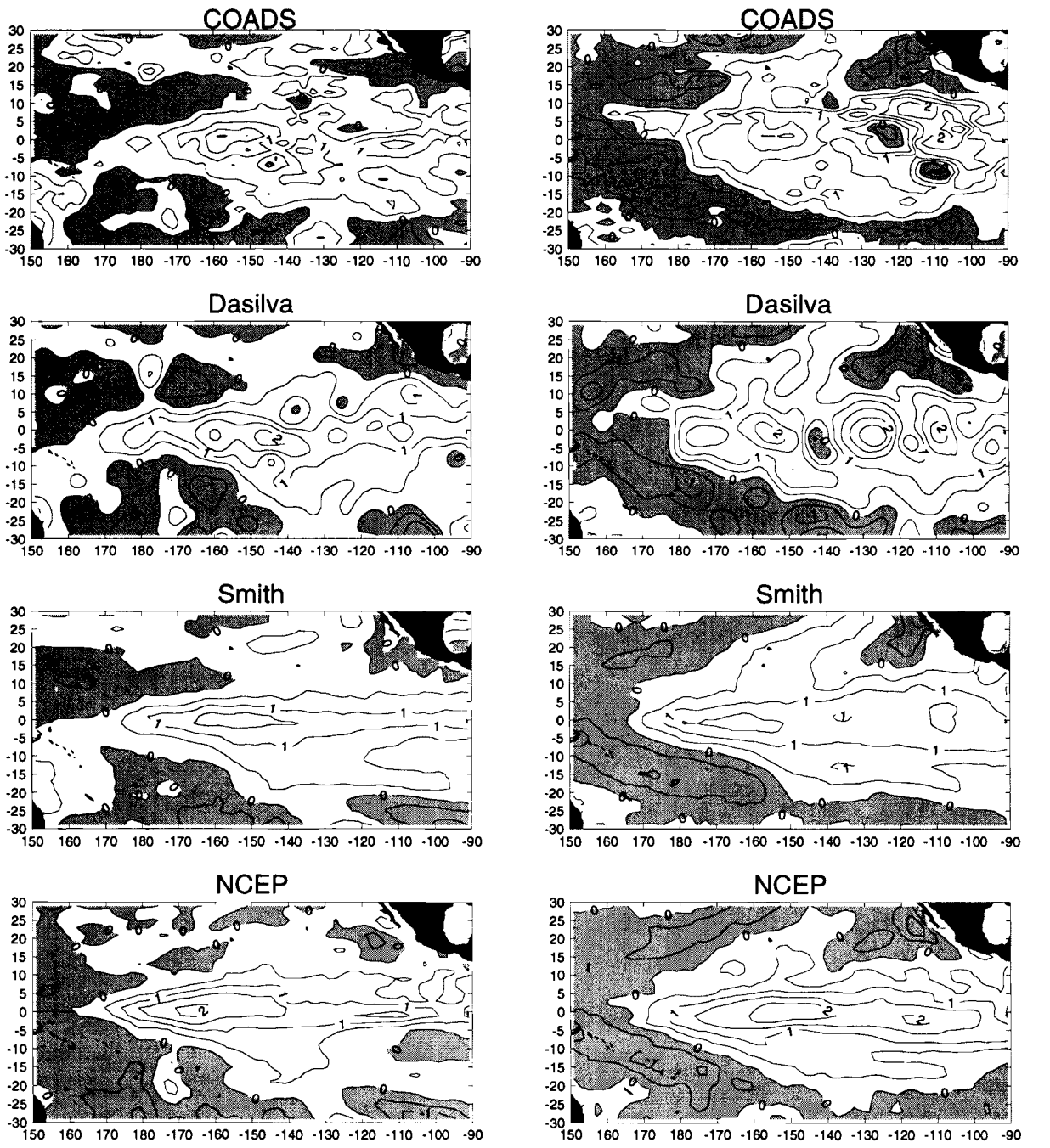

Figure 18d

January (COADS)

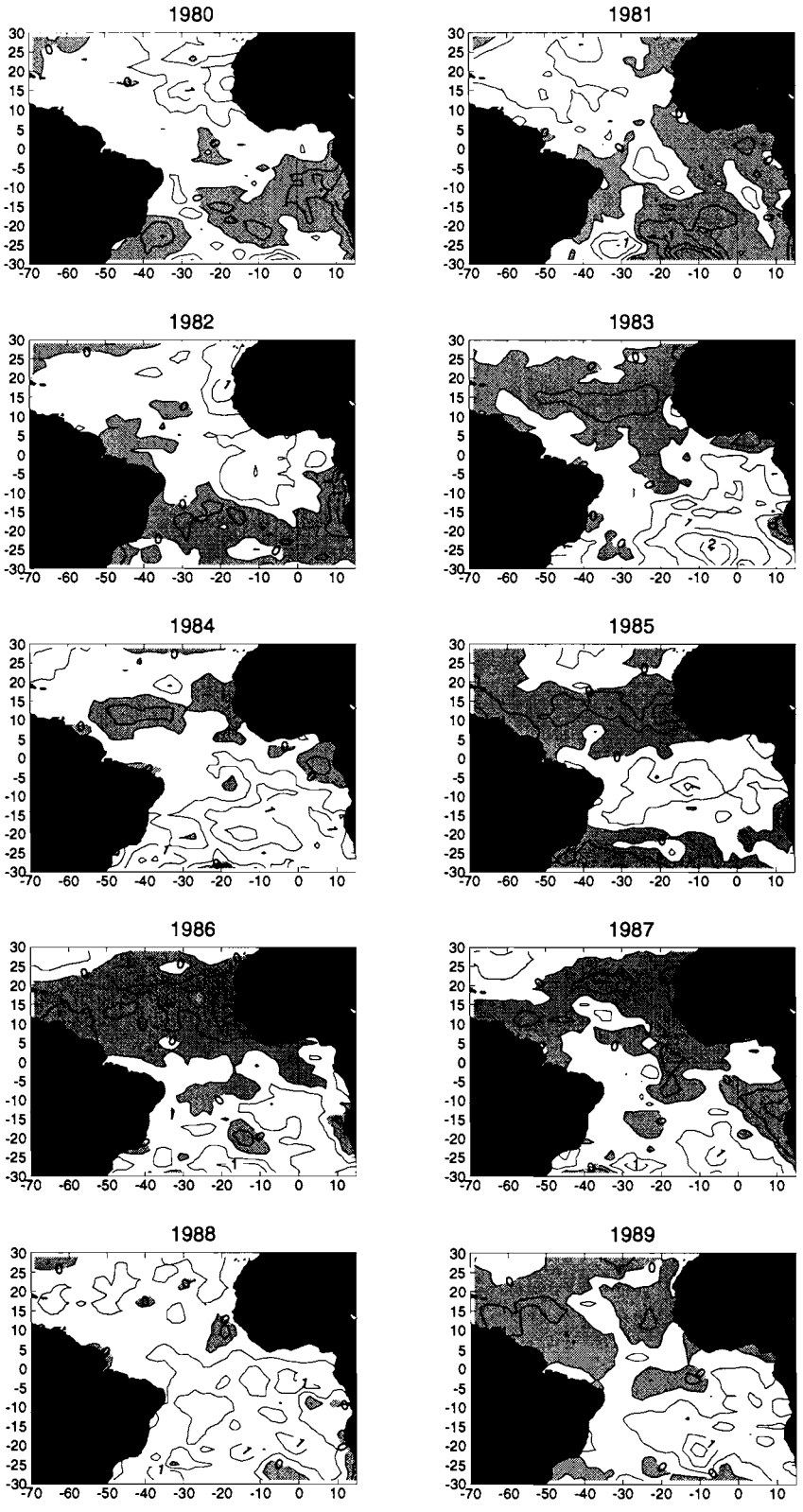

Figure 19a

January (Dasilva)

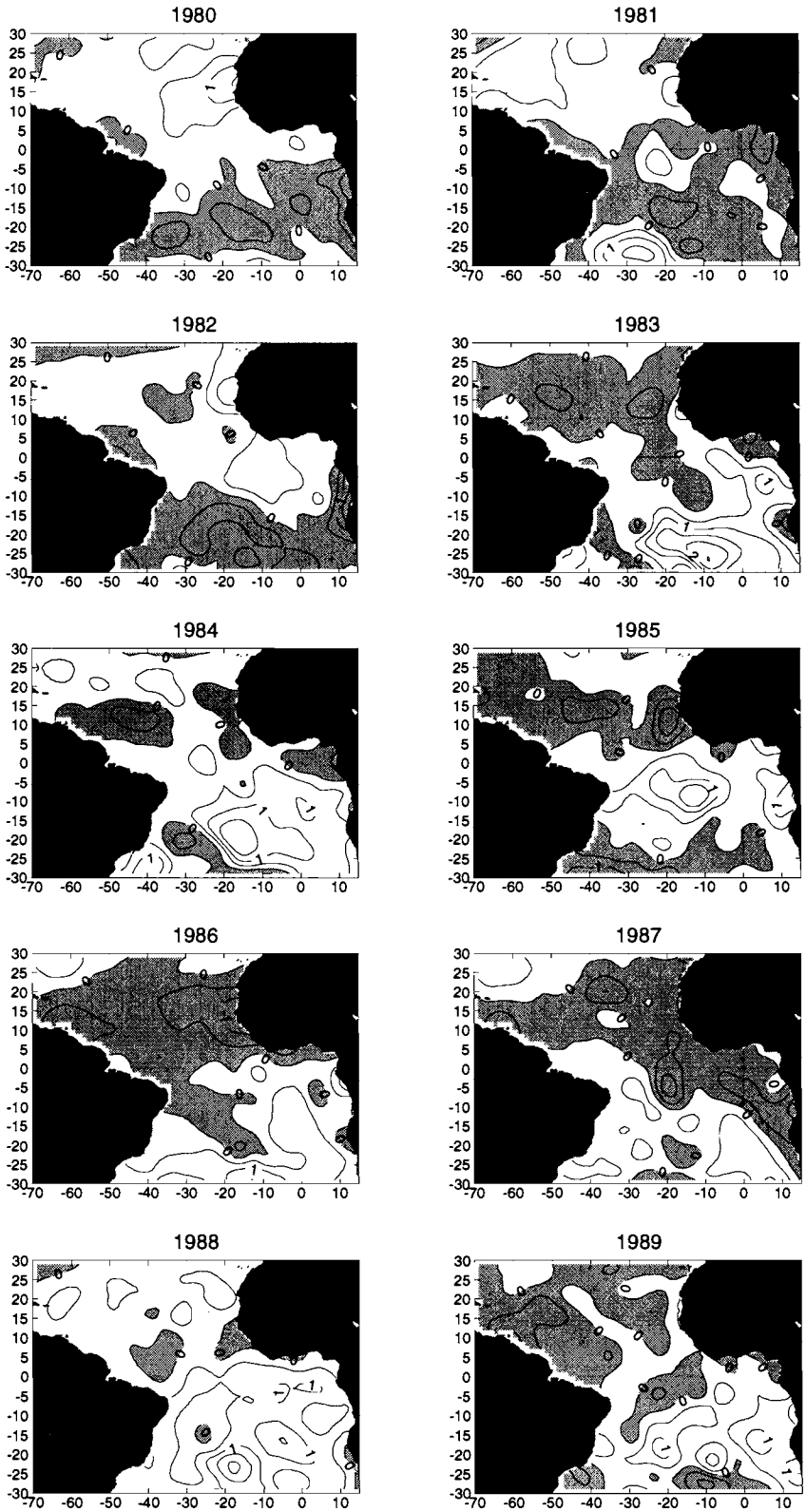

Figure 19b

January (Smith)

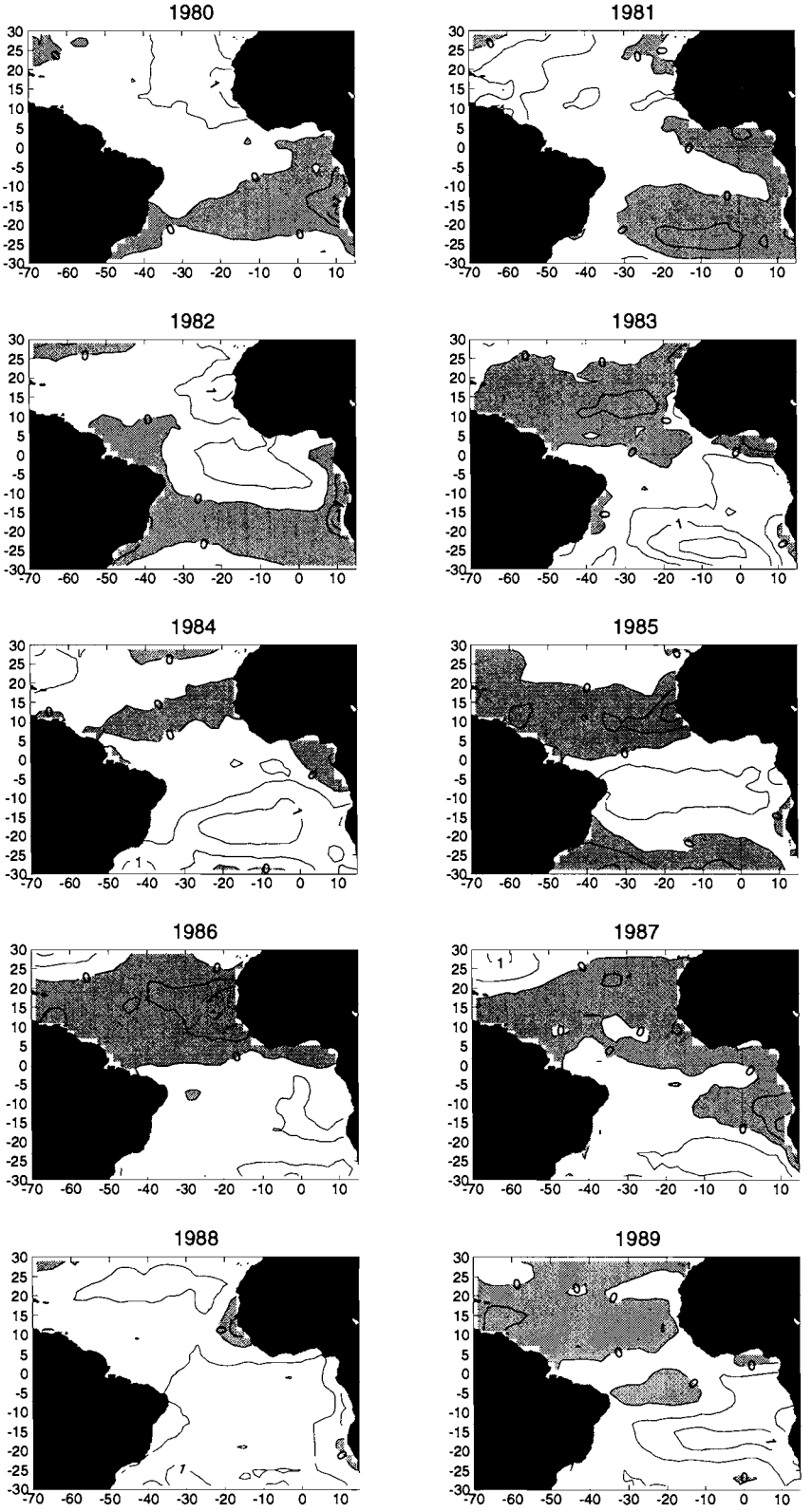

Figure 19c

January (NCEP)

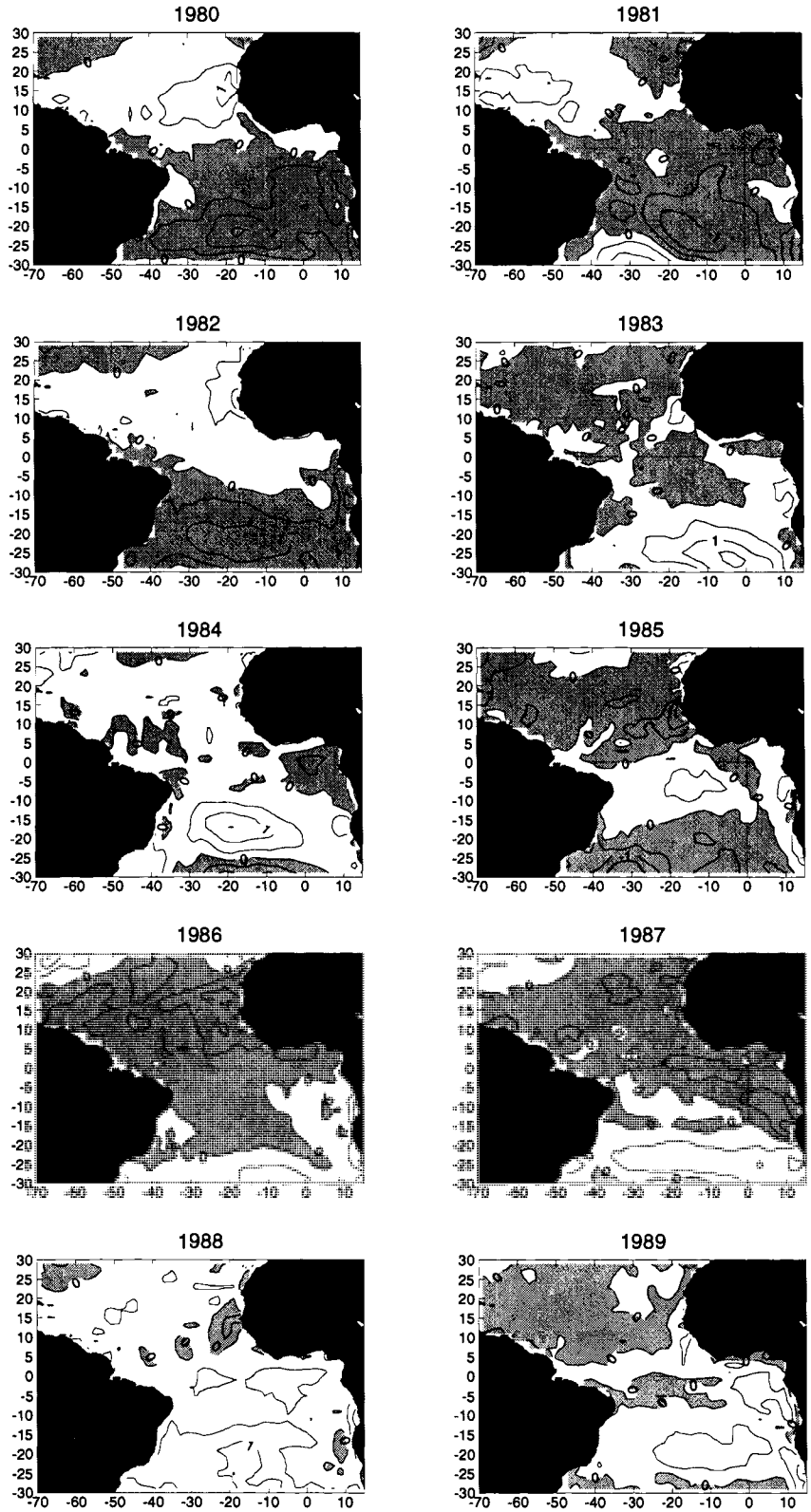

Figure 19d

July (COADS)

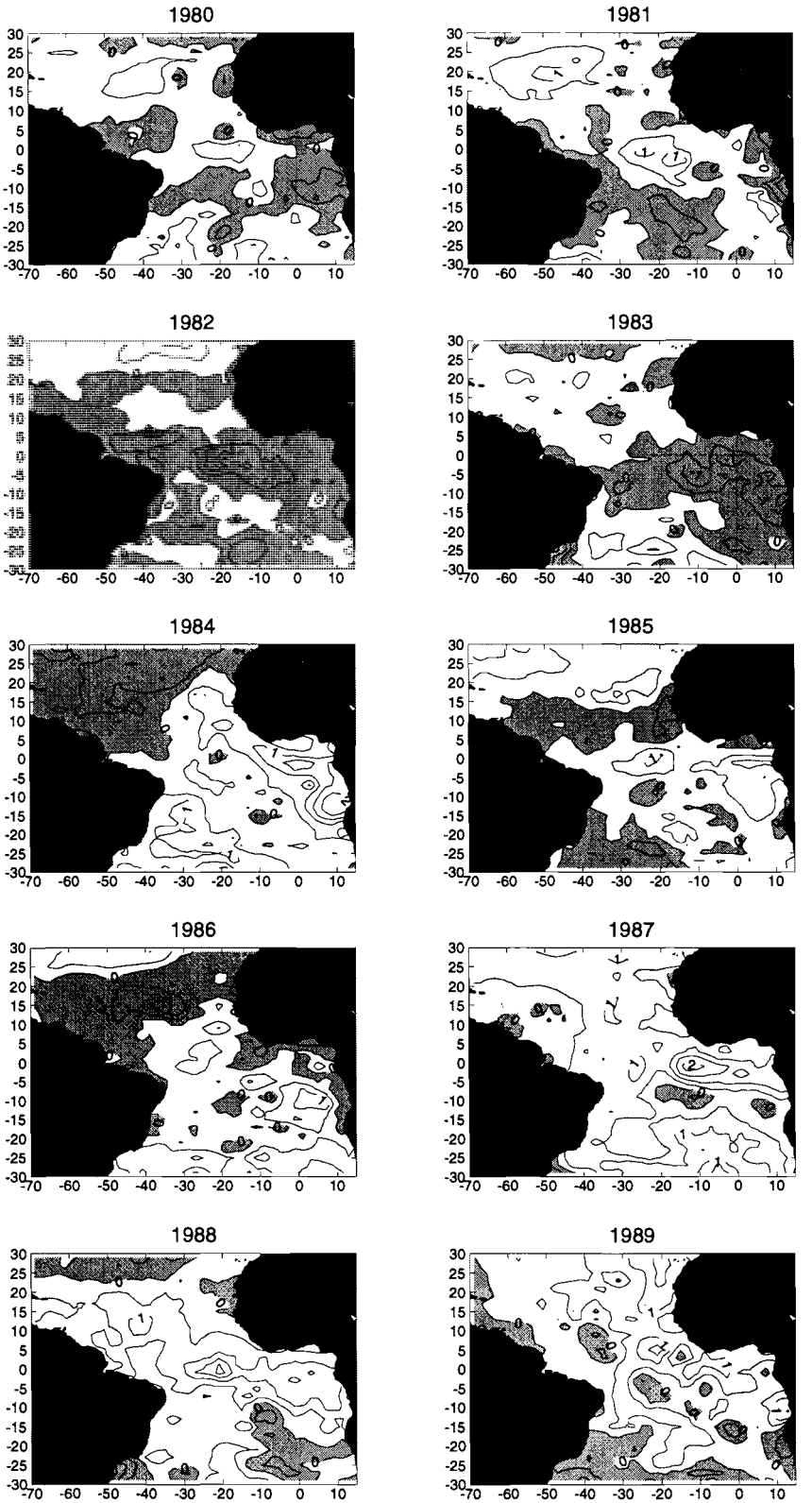

Figure 20a

July (Dasilva)

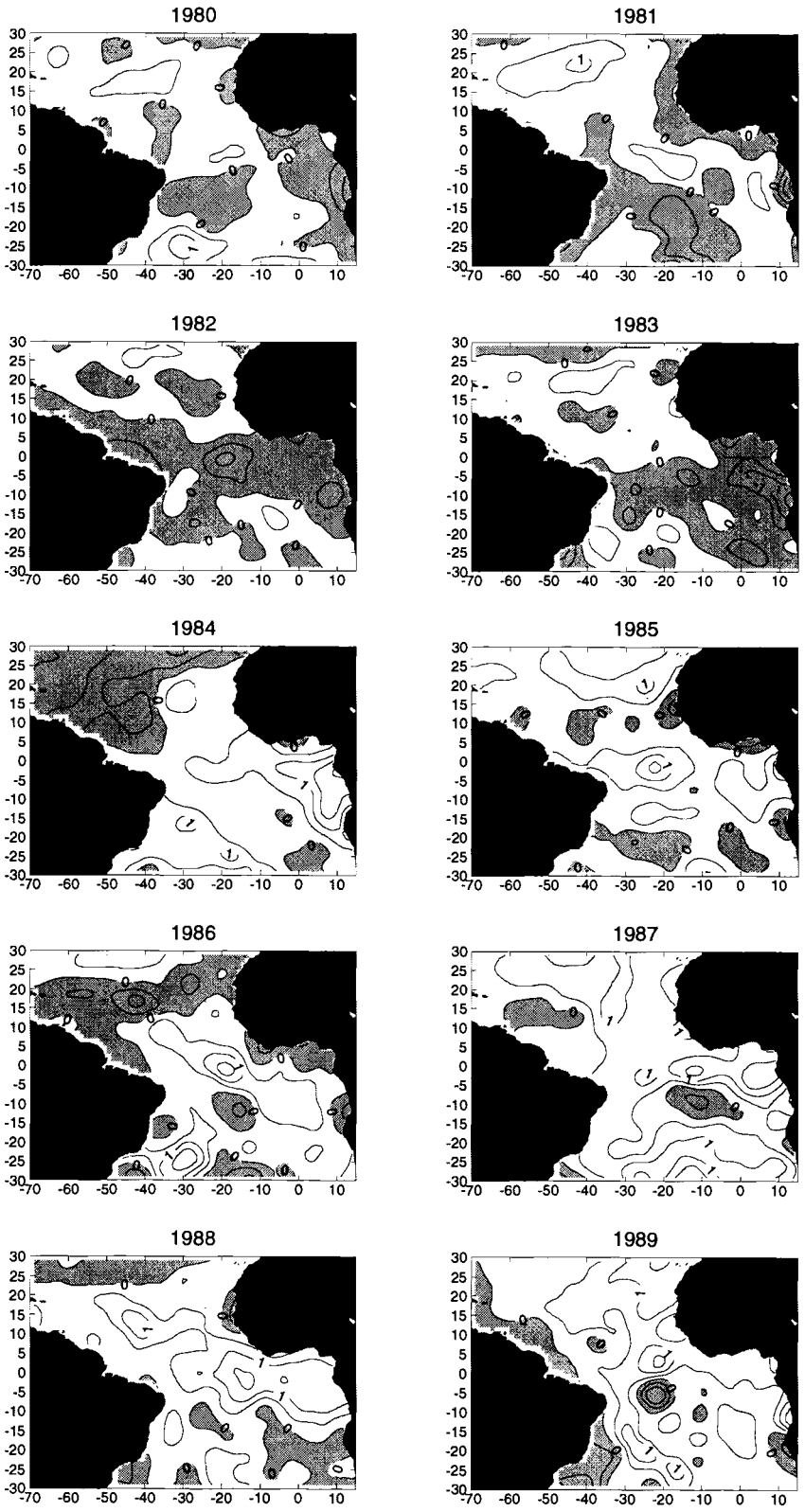

Figure 20b

July (Smith)

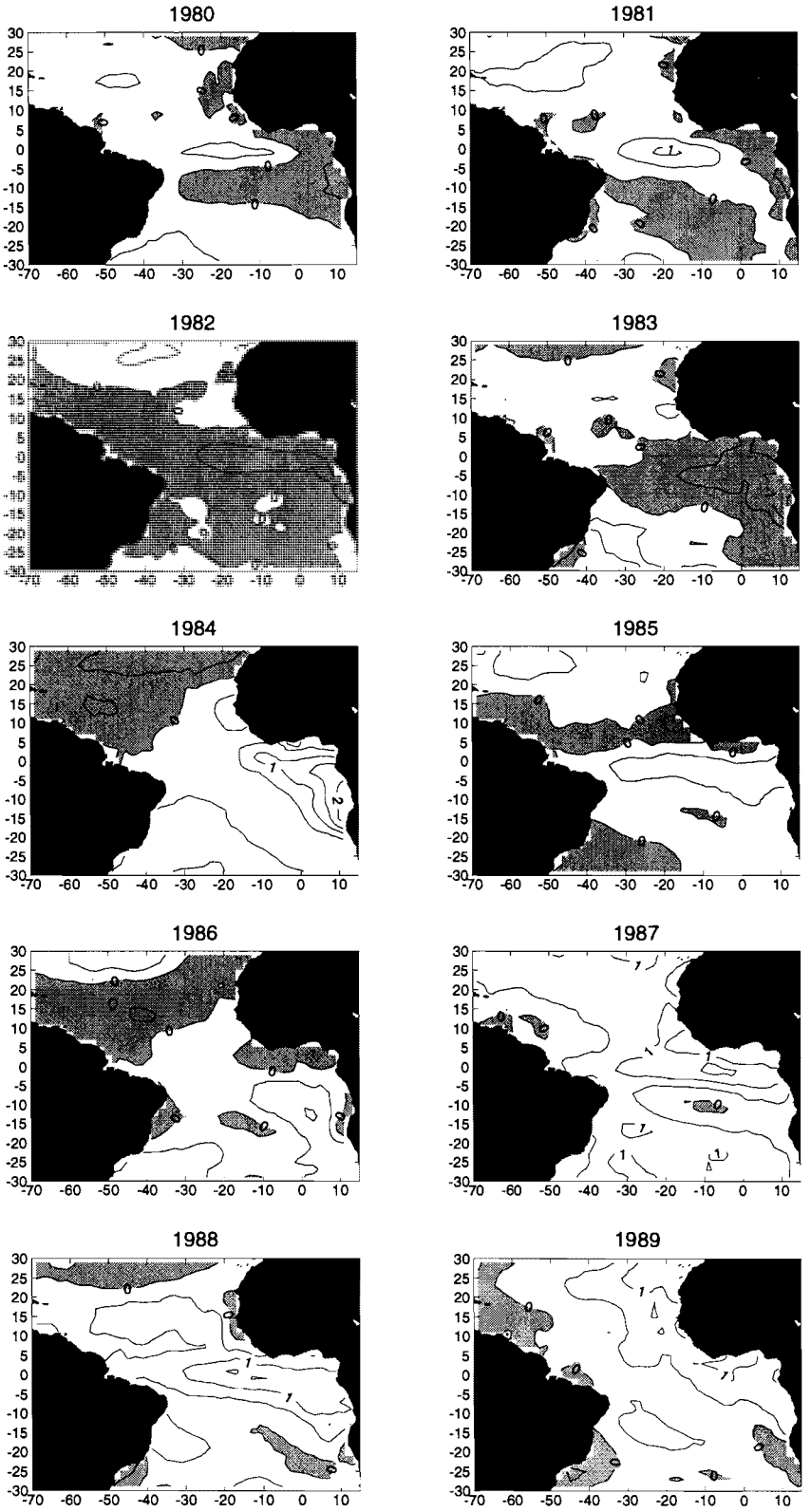

Figure 20c

July (NCEP)

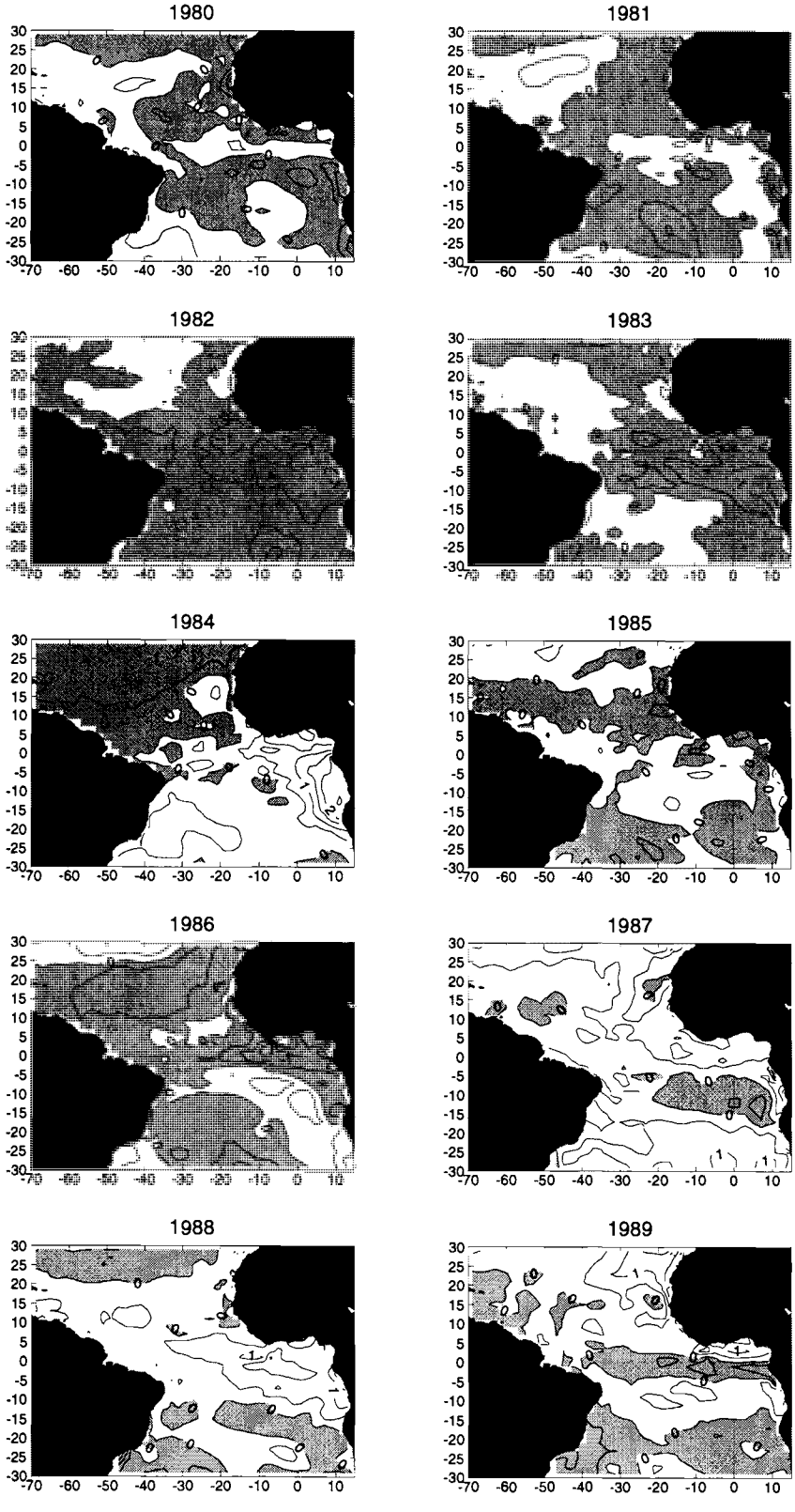

Figure 20d

January (COADS)

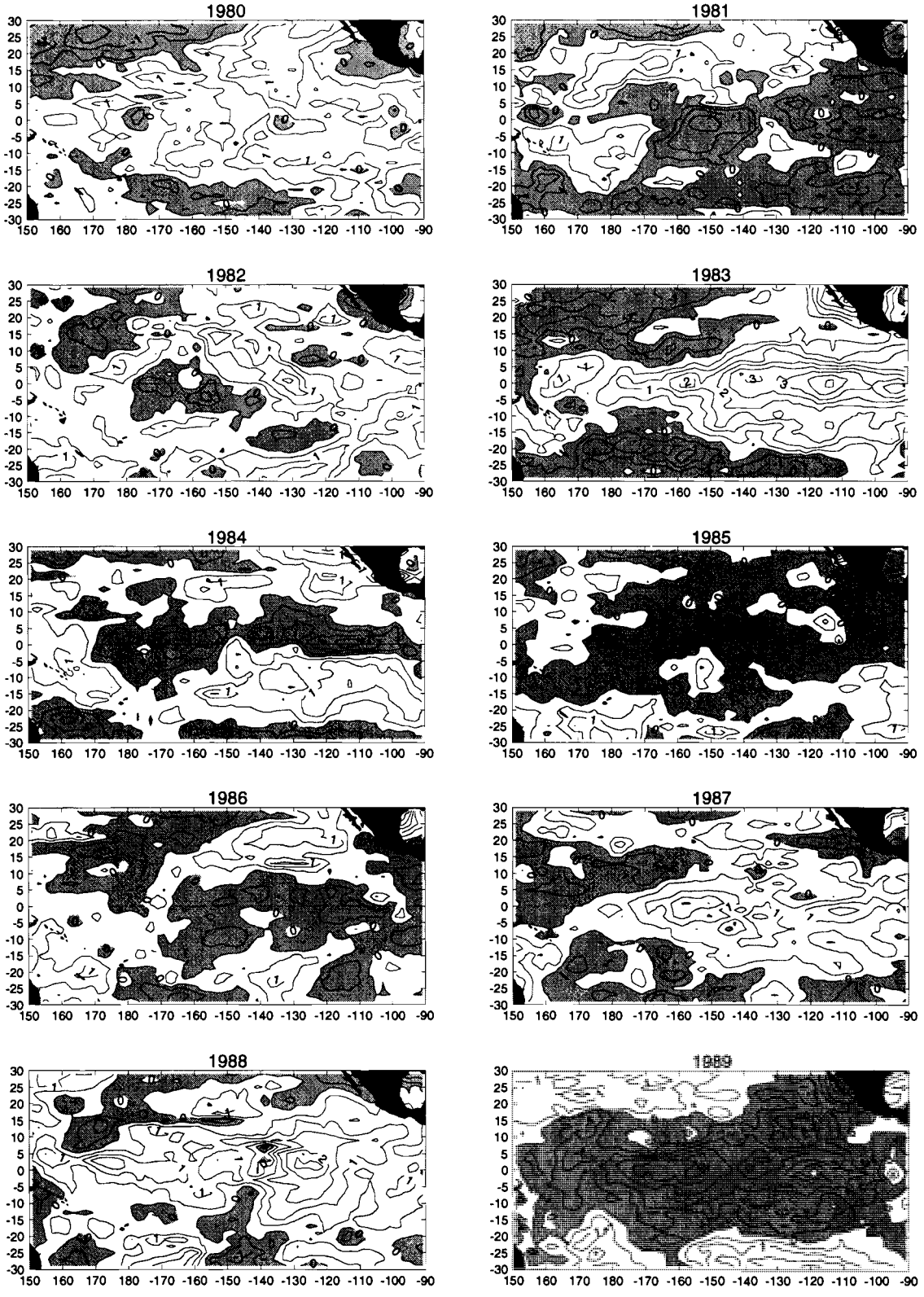

Figure 21a

January (Dasilva)

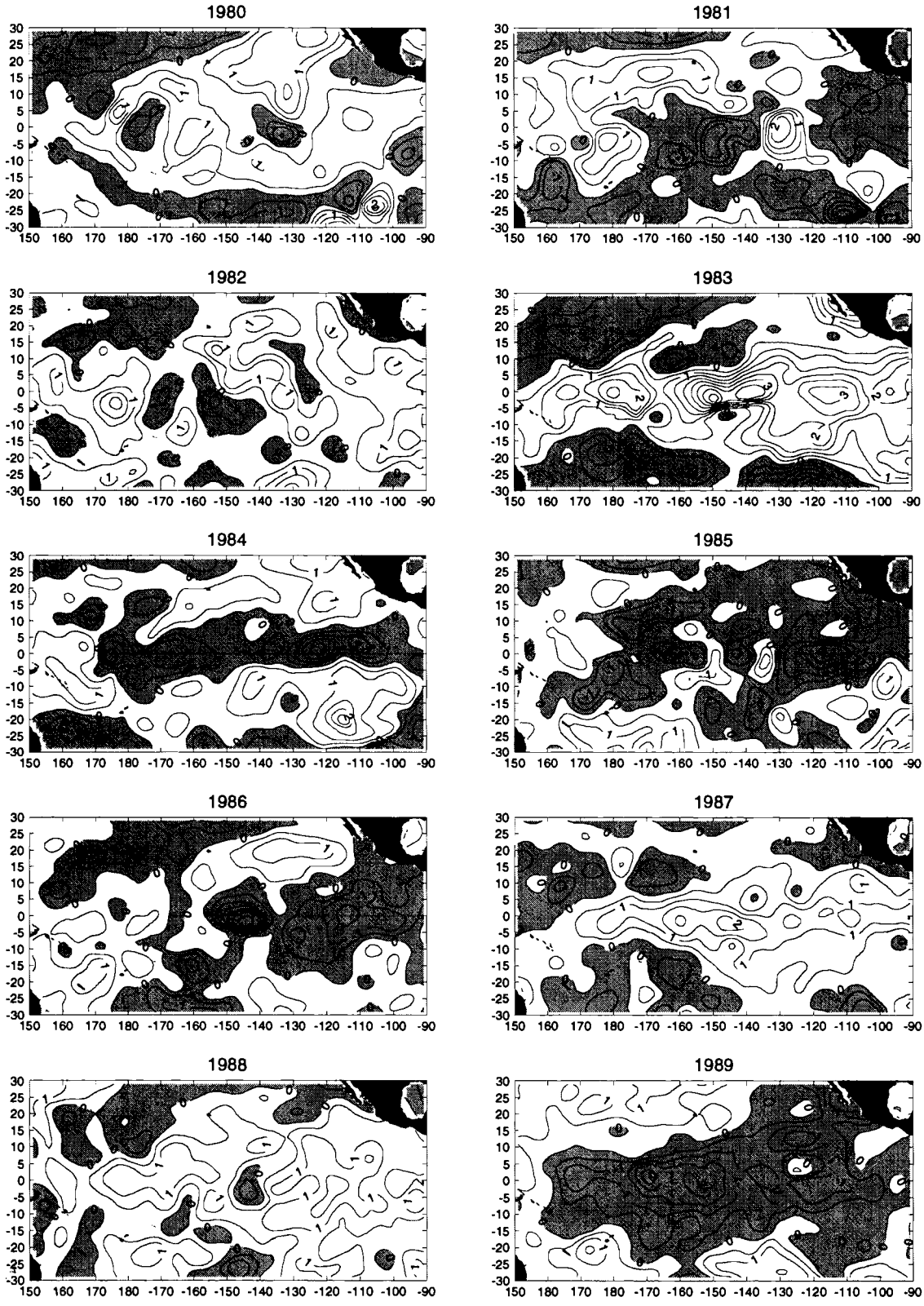

Figure 21b

January (Smith)

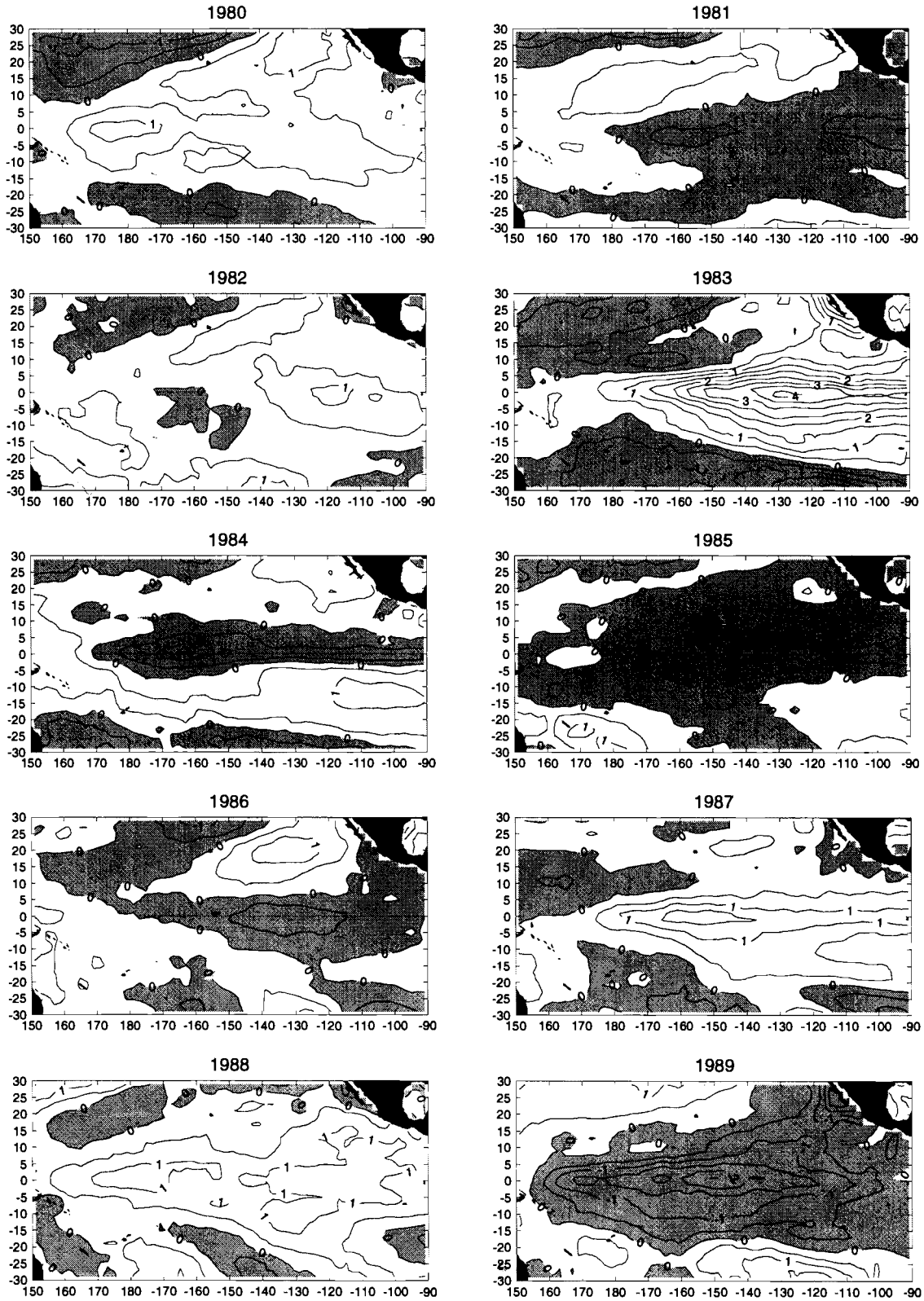

Figure 21c

January (NCEP)

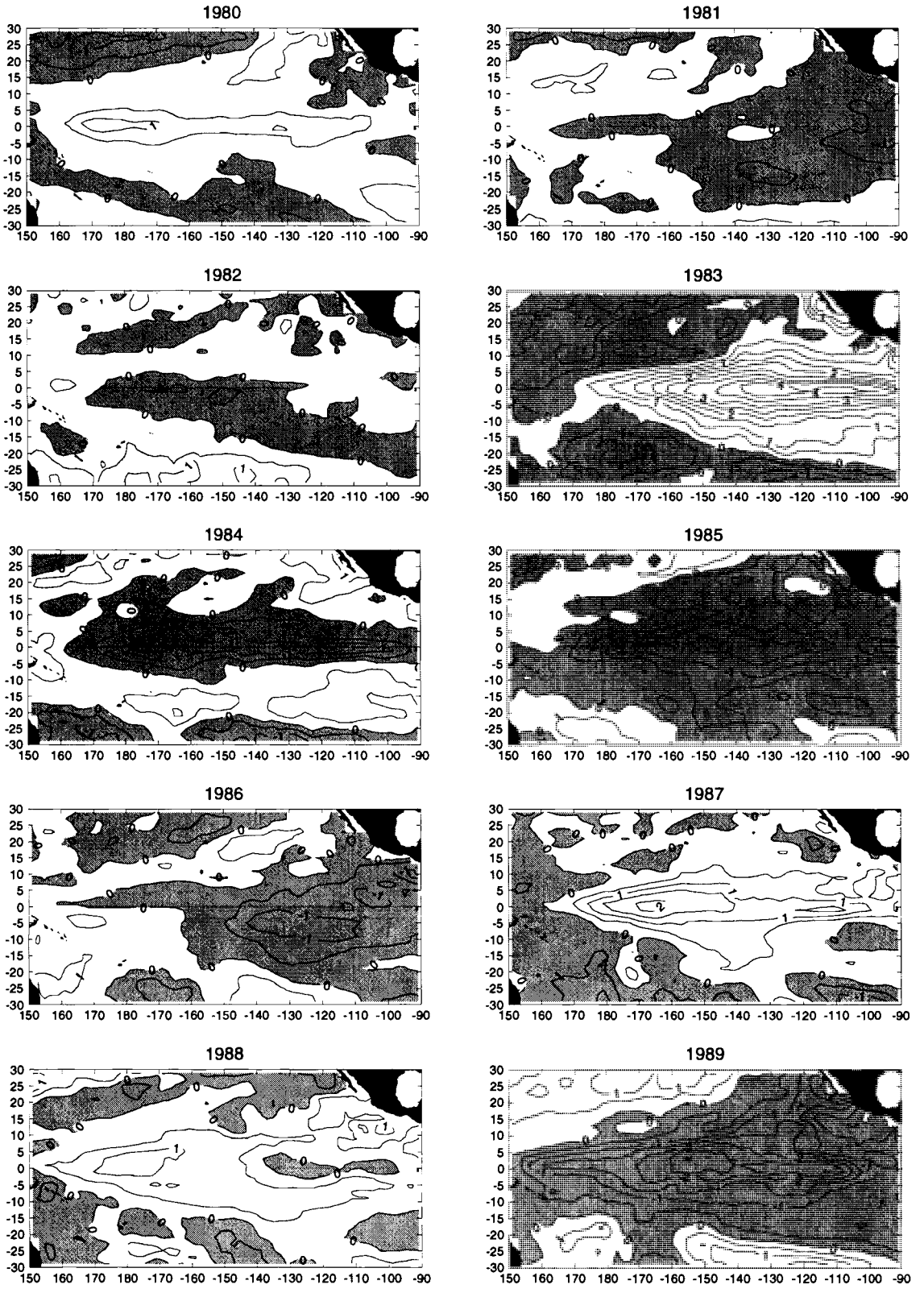

Figure 21d

July (COADS)

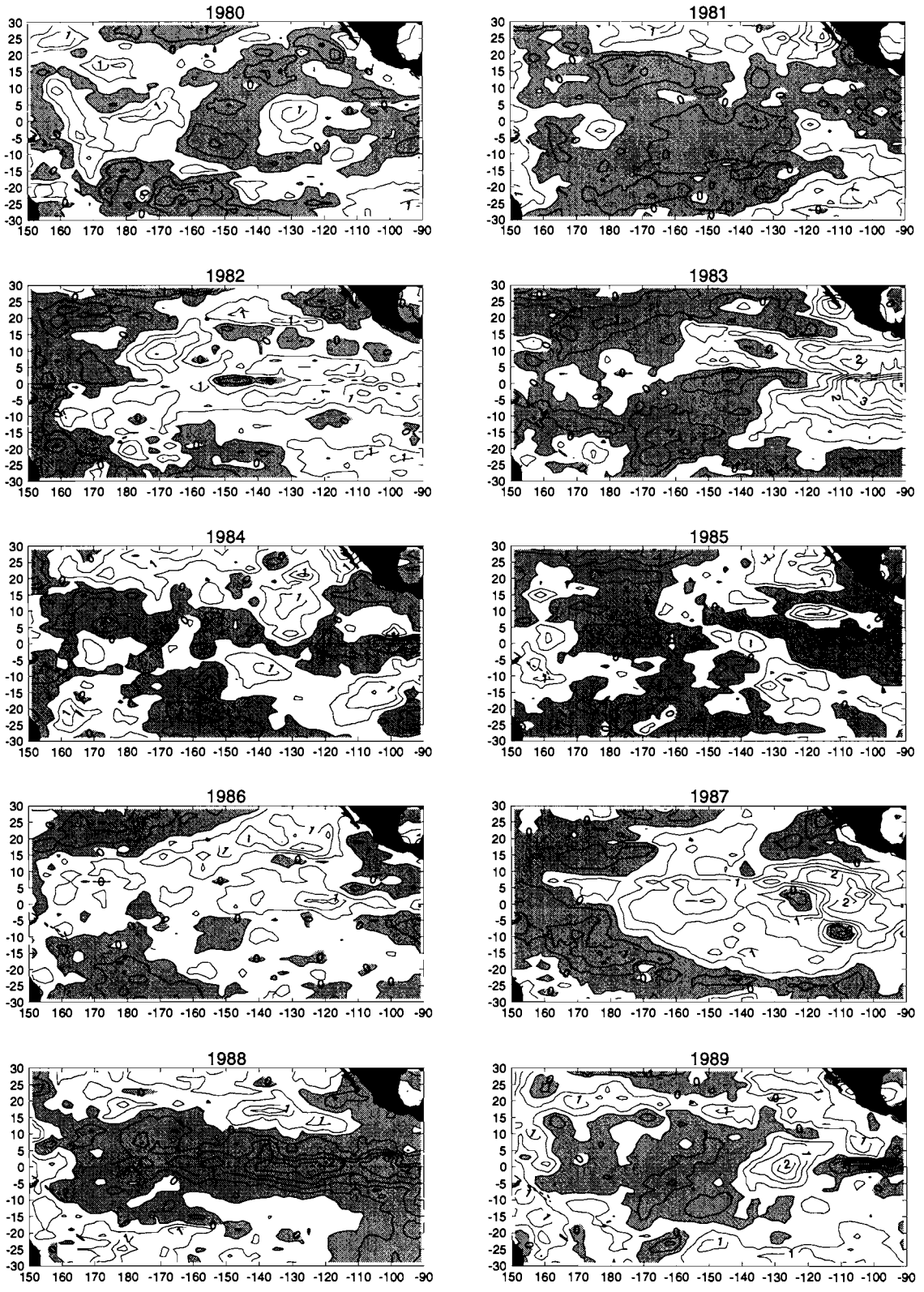

Figure 22a

July (Dasilva)

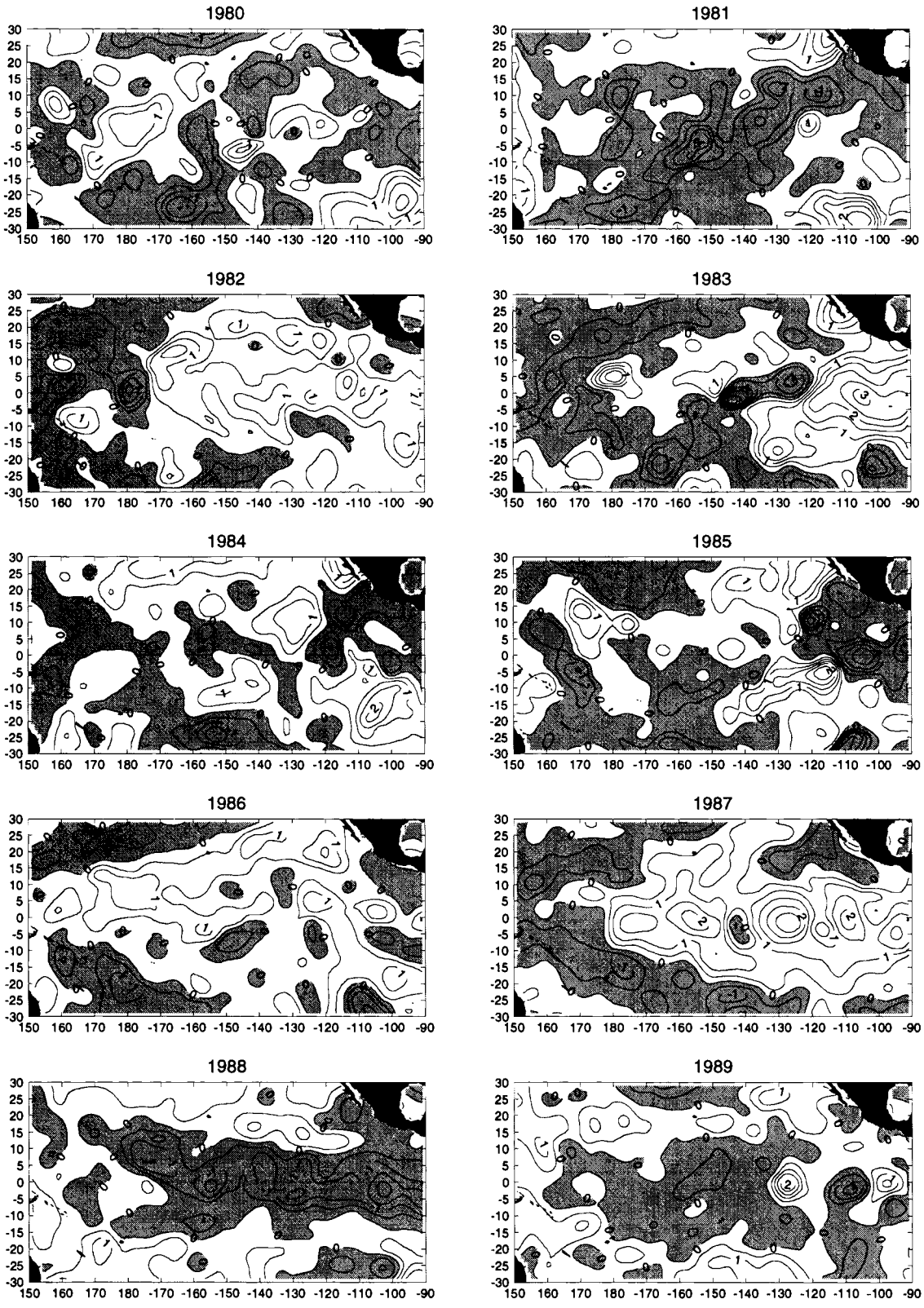

Figure 22b

July (Smith)

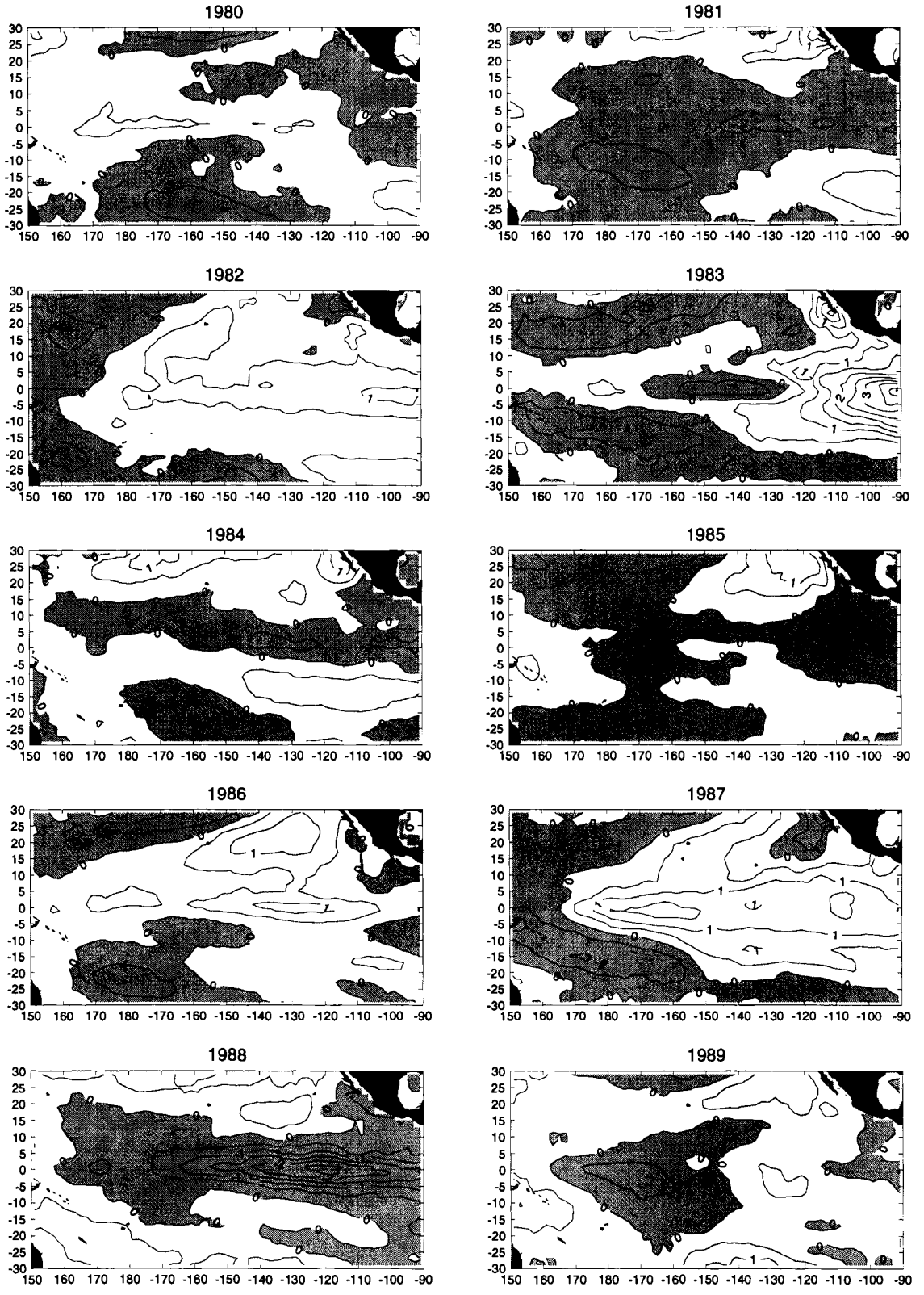

Figure 22c

July (NCEP)

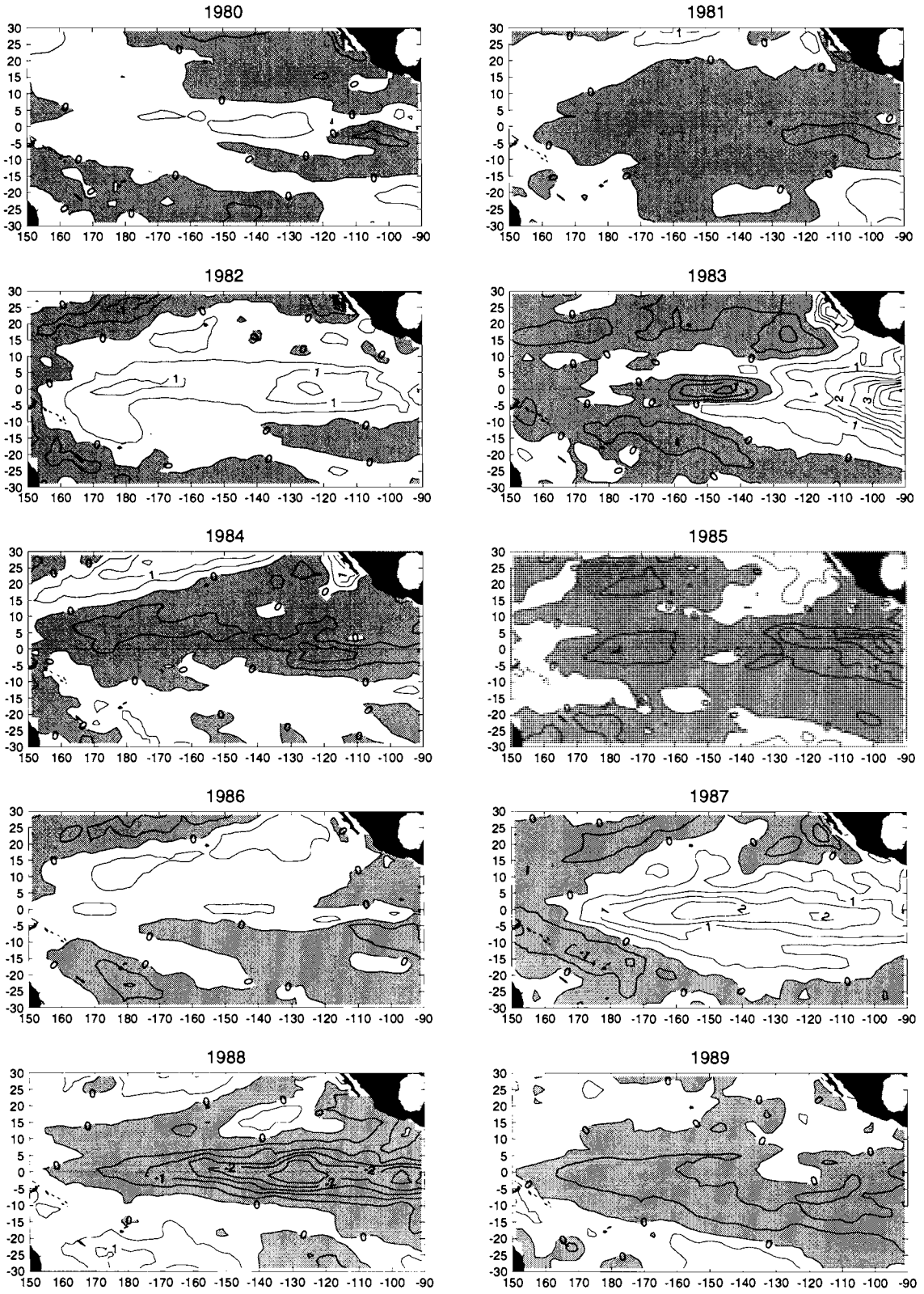

Figure 22d

January (COADS Errors)

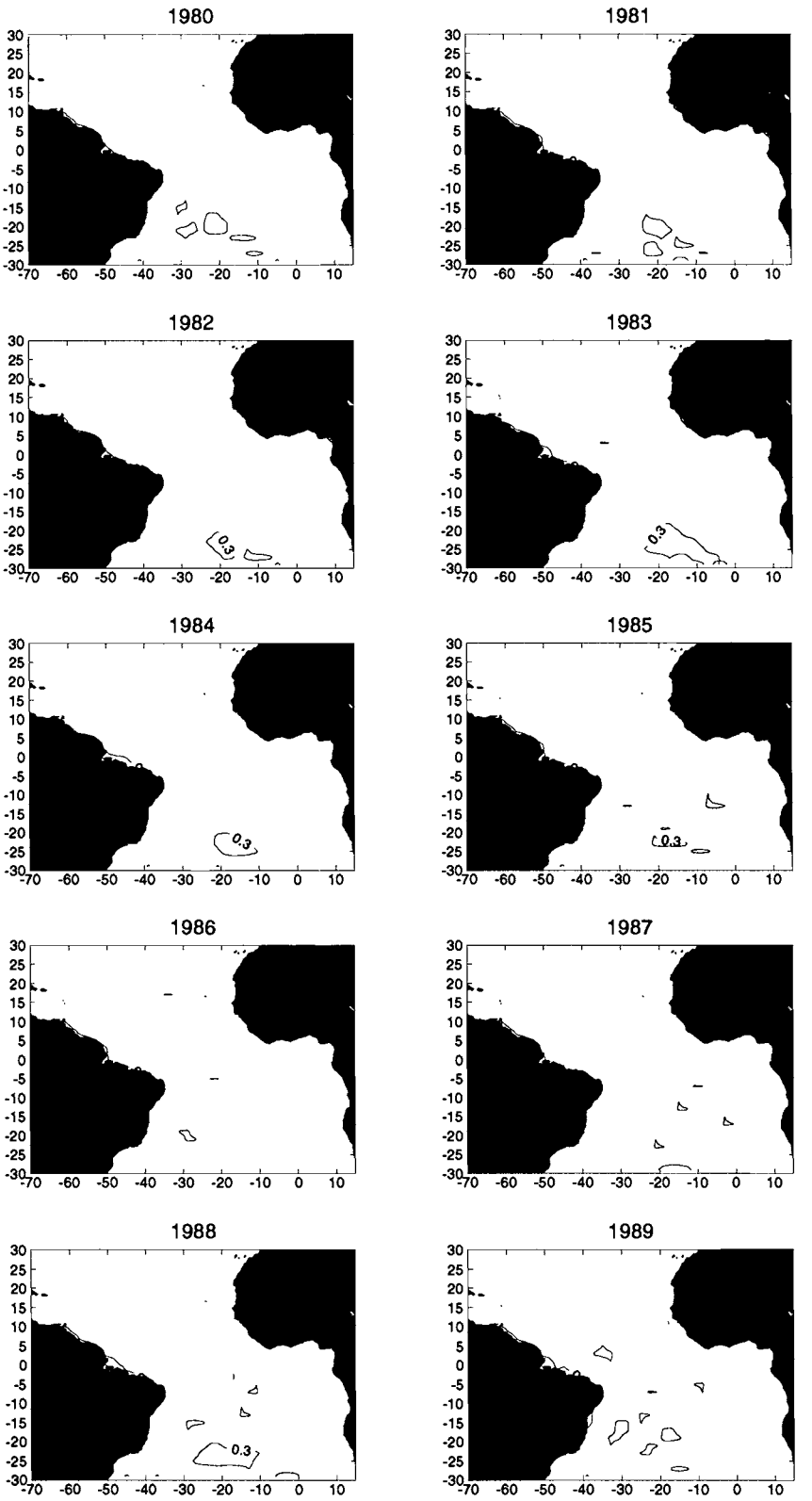

Figure 23a

July (COADS Errors)

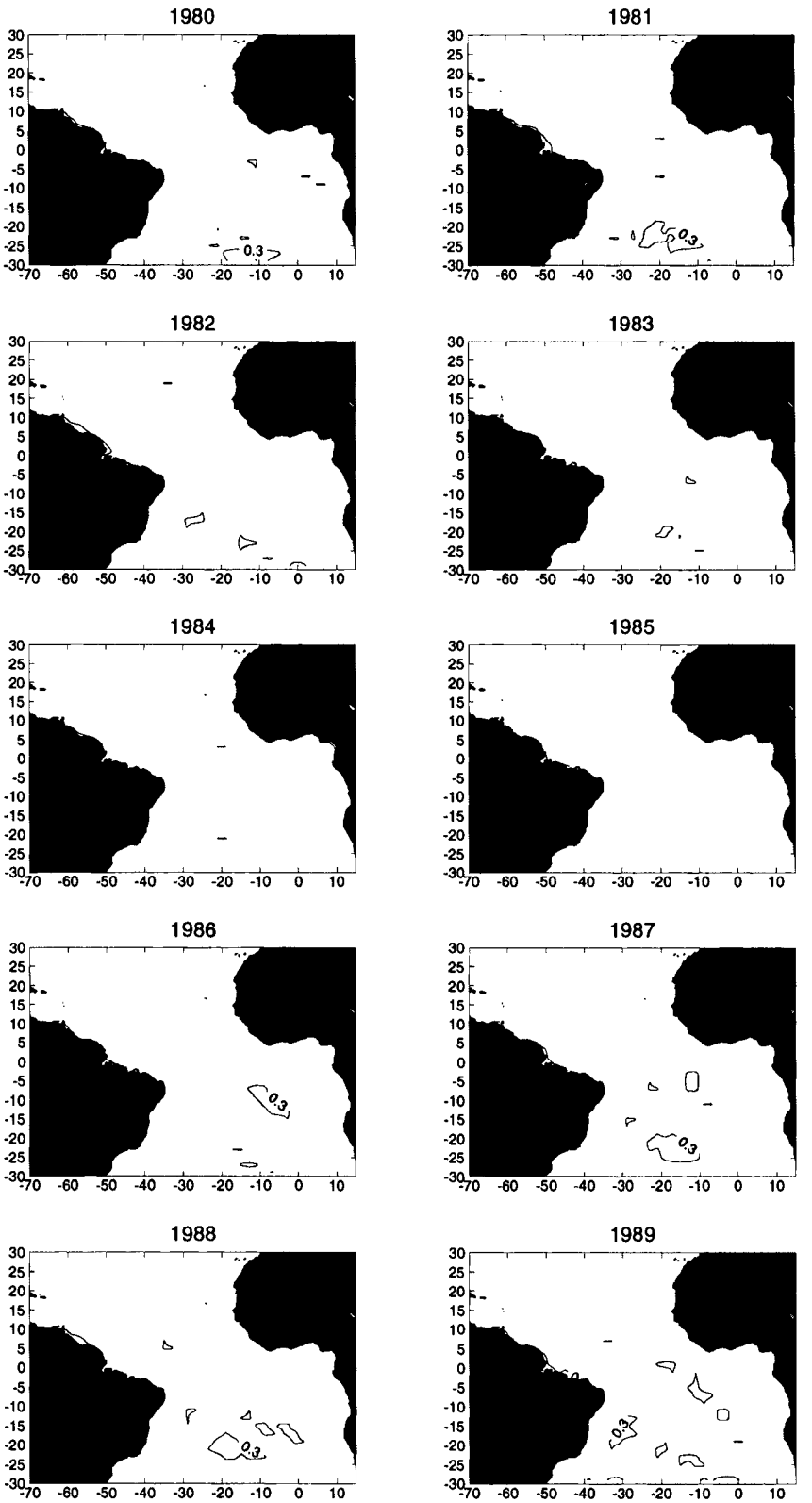

Figure 23b

January (COADS Errors)

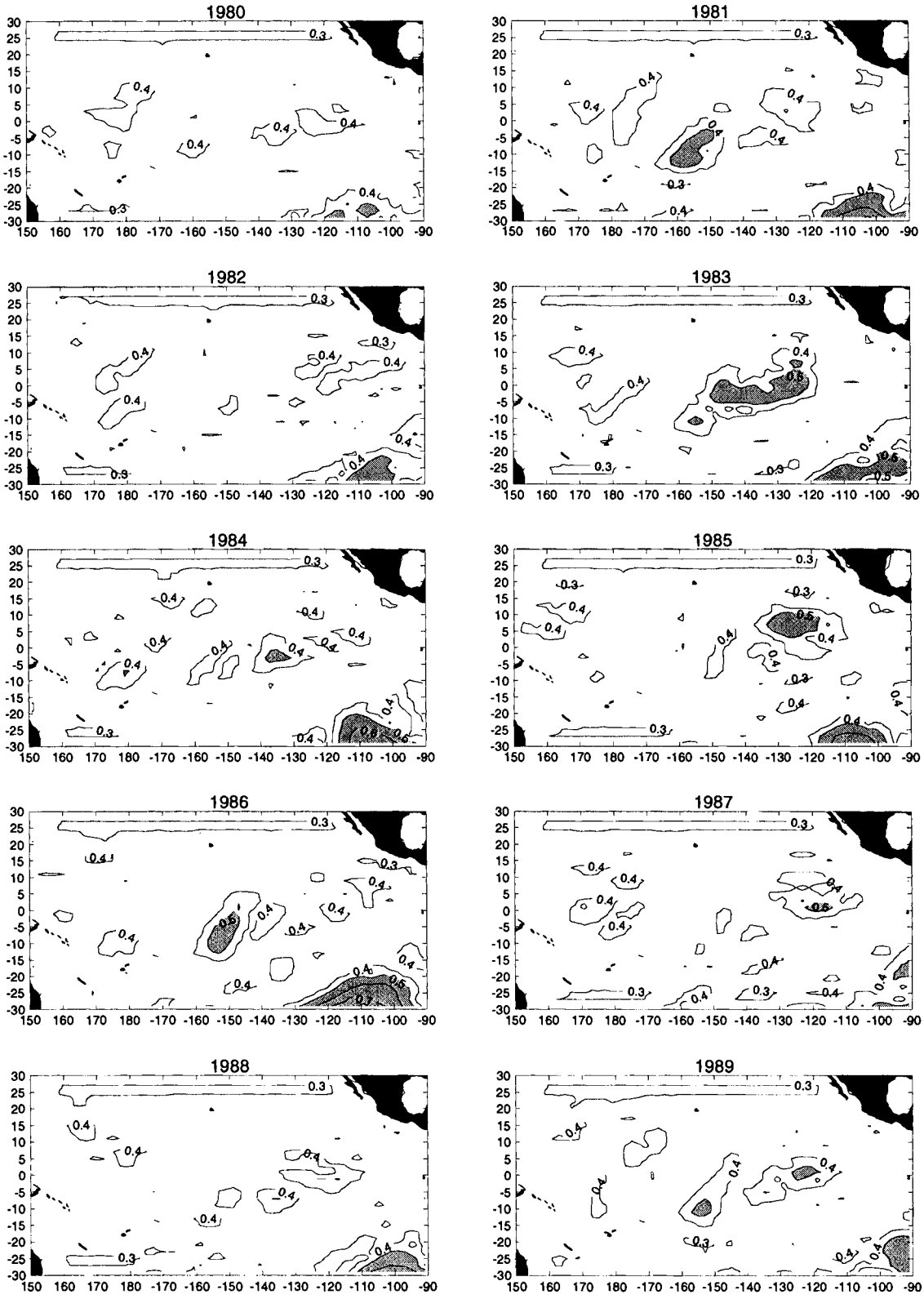

Figure 23c

July (COADS Errors)

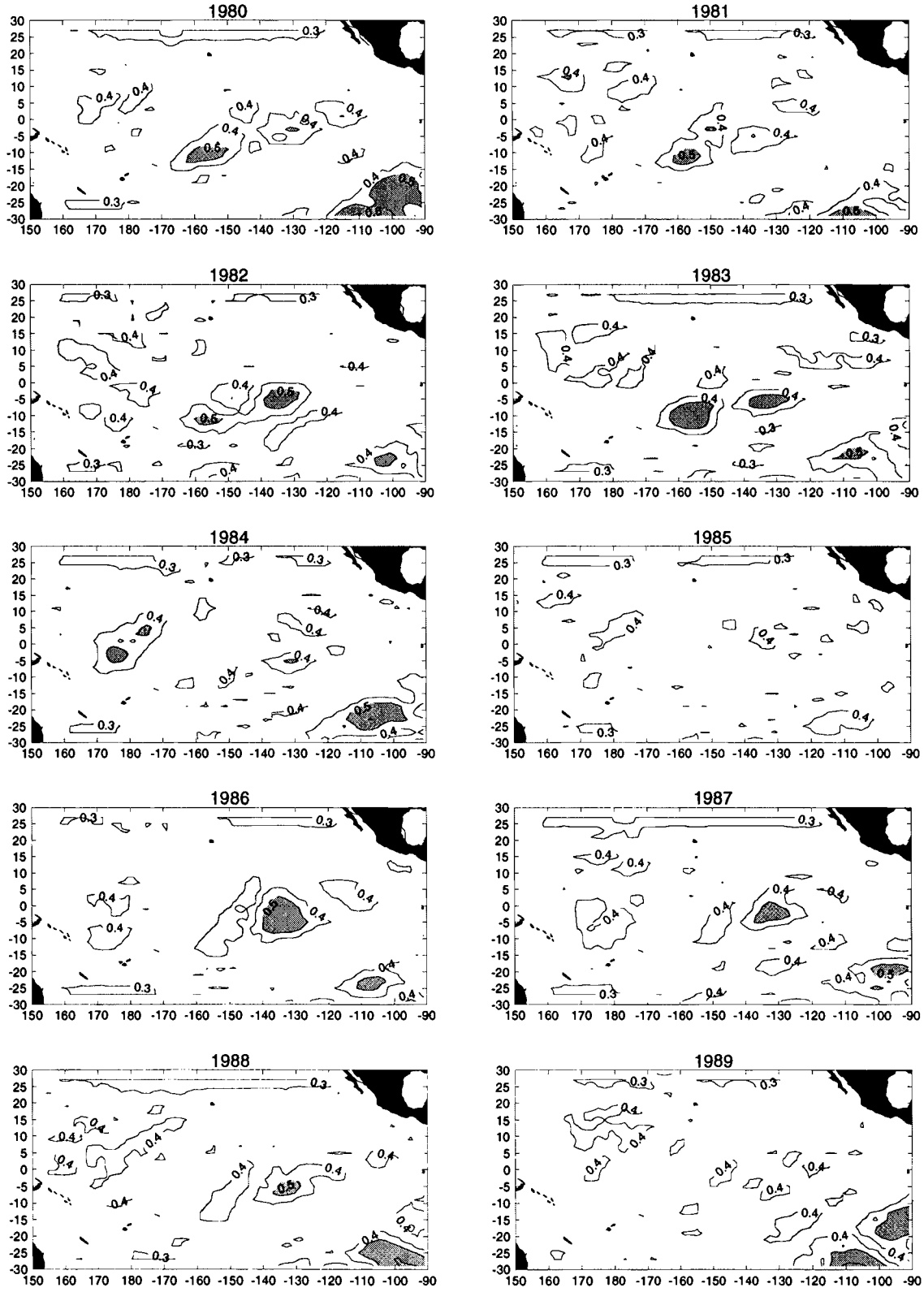

Figure 23d

Atlantic WOCE XBT Lines

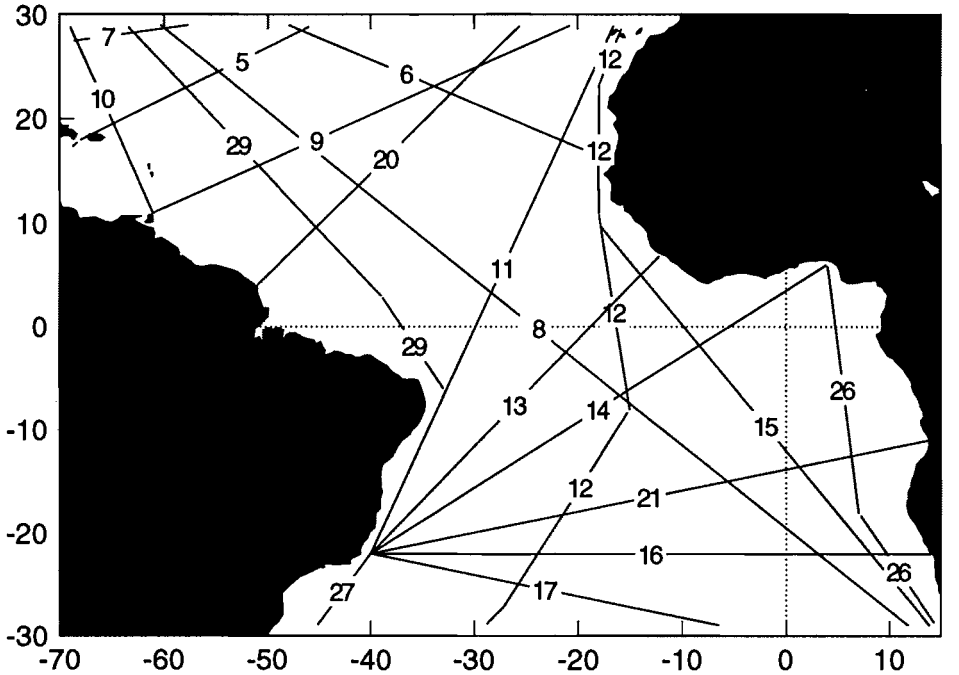

Pacific WOCE XBT Lines

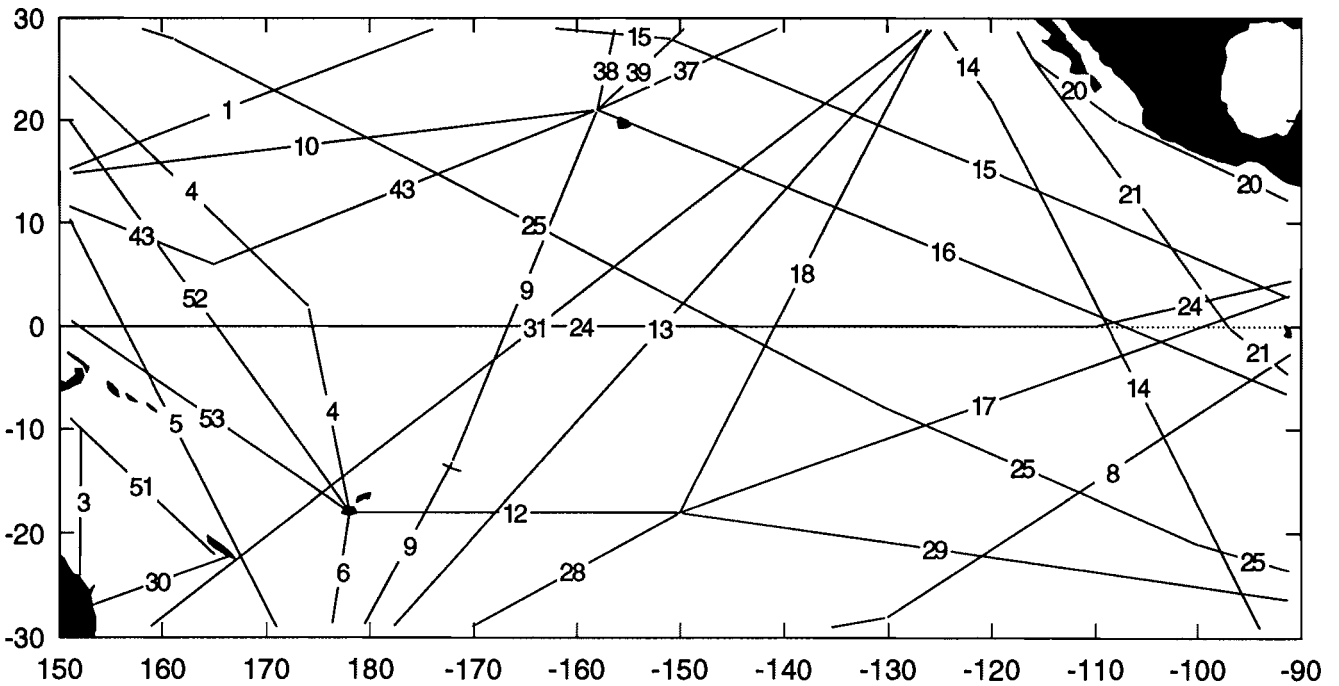

Figure 24

Atlantic WOCE Trackline Errors

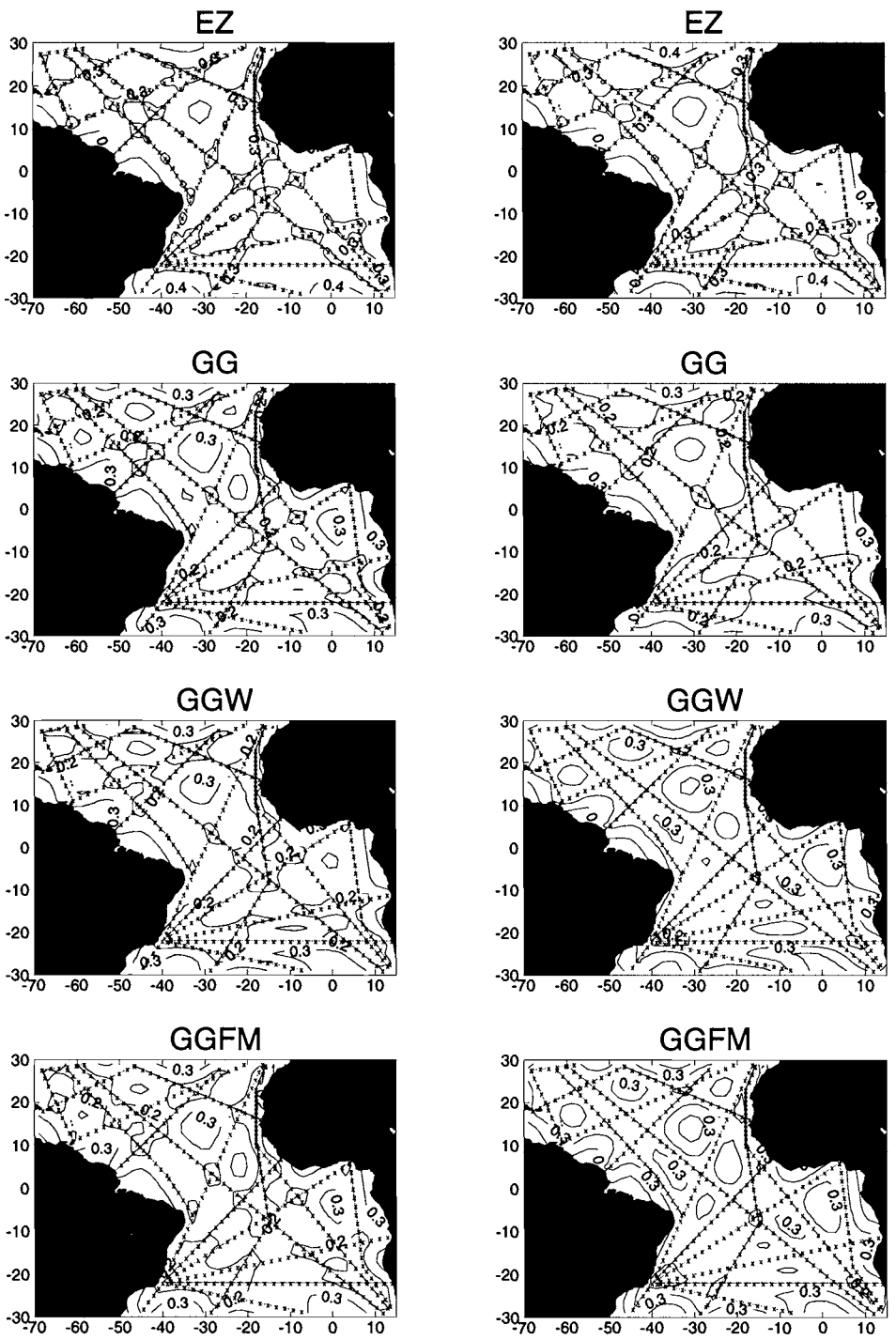

Figure 25

Pacific WOCE Trackline Errors

XBT

COADS

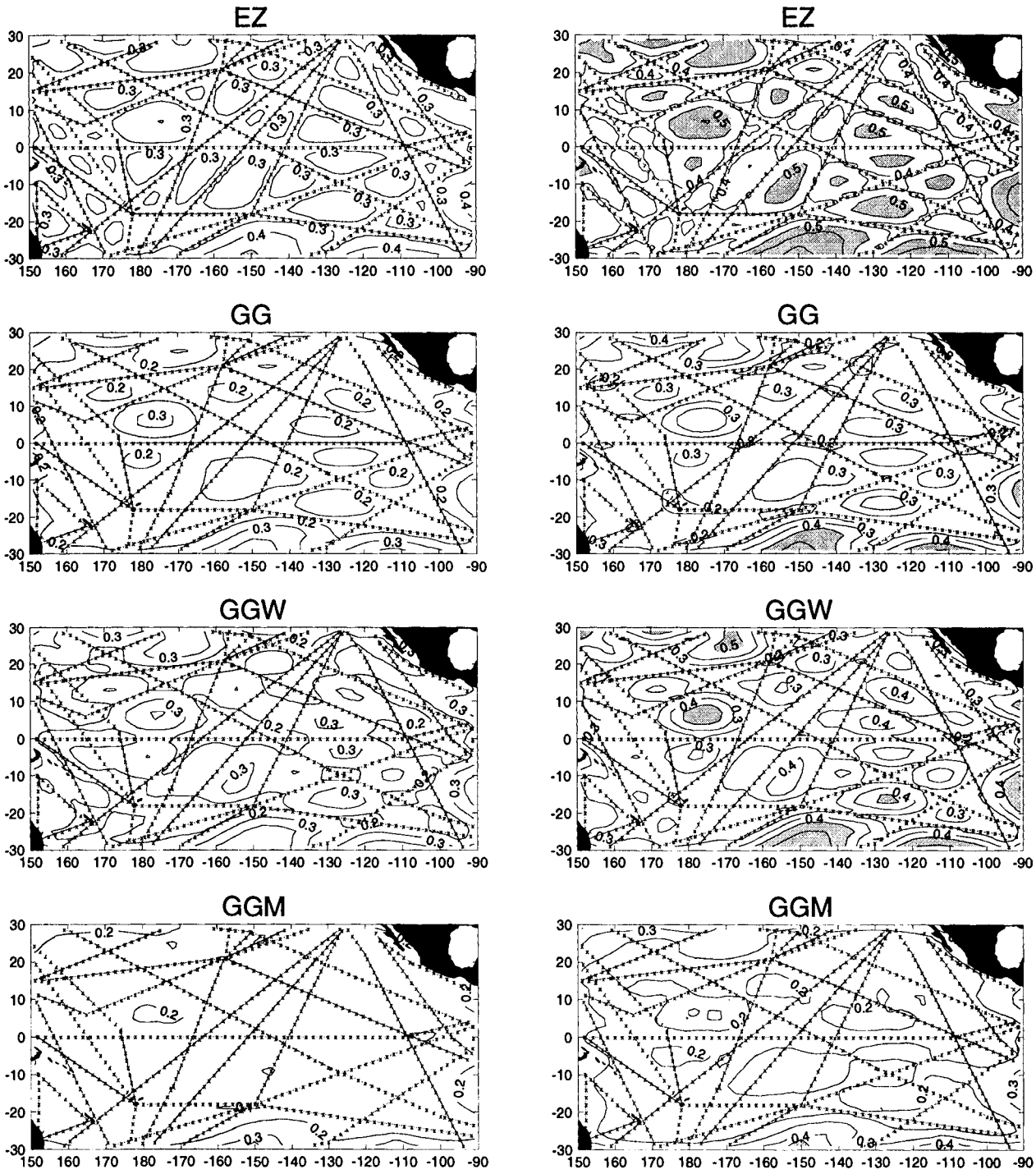

Figure 26